THE CHEMISTRY OF OXO- AND HYDROXO-BRIDGED CHROMIUM(III) DIMERS WITH AROMATIC AMINE LIGANDS

by

BOYD GLENN GAFFORD, B.S.

A DISSERTATION

IN

CHEMISTRY

Submitted to the Graduate Faculty
of Texas Tech University in
Partial Fulfillment of
the Requirements for
the Degree of

DOCTOR OF PHILOSOPHY

Approved

Accepted

August, 1989

ACKNOWLEDGMENTS

The author wishes to express his most sincere gratitude to his advisor, mentor, and friend, Dr. Robert A. Holwerda, for his guidance, wisdom, enthusiasm and encouragement, without which this work would have not been possible. A sincere thanks also goes to Dr. John K. Foley, Dr. Jerry L. Mills, Dr. Edward L. Quitevis and Dr. Bruce R. Whittlesey for their time and effort in committee service.

An expression of gratitude also goes to Dr. Harvey J. Schugar and Joseph A. Potenza for their invaluable $[(tmpa)(SCN)CrOCr(NCS)(tmpa)]SCN_2$ structural determination. The author also wishes to express his gratitude to Dr. Charles F. Campana of Nicolet Instrument Corp. for the $[(tmpa)Cr(OH)_2Cr(tmpa)]Br_4.8H_2O$ structural determination. A sincere thanks also goes to Dr. Charles O'Connor at the University of New Orleans for his collaboration in the magnetic succeptibility temperature dependence of several of our complexes.

The author also wishes to thank all those who supported him during his graduate education, including family, friends, and colleagues. Finally, a deep gratitude is expressed to God, without whose direction and guidance the development of this work would not have been possible.

TABLE OF CONTENTS

LIST OF TABLES

LIST OF FIGURES

CHAPTER I

INTRODUCTION

The chemistry of Cr(III) dimers with a linear oxygen bridge has seen a considerable amount of interest since the discovery of the (μ-oxo)bis{pentaamminechromium(III)} (basic rhodo) dimer by Jorgensen (1882).[1] This interest is due to markedly different substitutional and spectral properties over those of simple Cr(III) monomers, a manifestation of the very different bonding that occurs as a result of the linear Cr-O-Cr unit. For example, the loss of NH_3 in aqueous base from the basic rhodo cation occurs in just minutes,[2] while the loss of NH_3 from $Cr(NH_3)_6^{3+}$ occurs over several days.[3] In addition, the intense transitions in the UV-visible spectrum[4] of the basic rhodo cation are in sharp contrast to the well known, very broad, weak d-d transitions seen in Cr(III) monomeric species.

The unique bonding that results in these properties can be attributed to several atomic orbital overlap combinations, the most important of which is a strong d-p-d π overlap of the Cr-O-Cr unit (of symmetry e_u in D_{4h}) illustrated below:

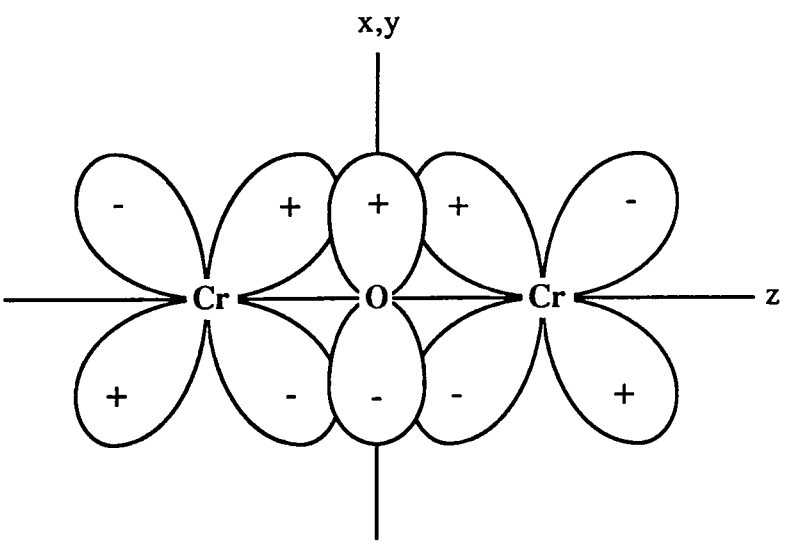

The other significant overlaps that contribute to the unique stability of the linear oxo-bridged dimers are the combination of d_z2 of both chromium centers with the oxygen p_z orbital (of symmetry a_{2u} in D_{4h}), and the combination of d_z2 with the oxygen 1s orbital (of symmetry a_{1g} in D_{4h}).

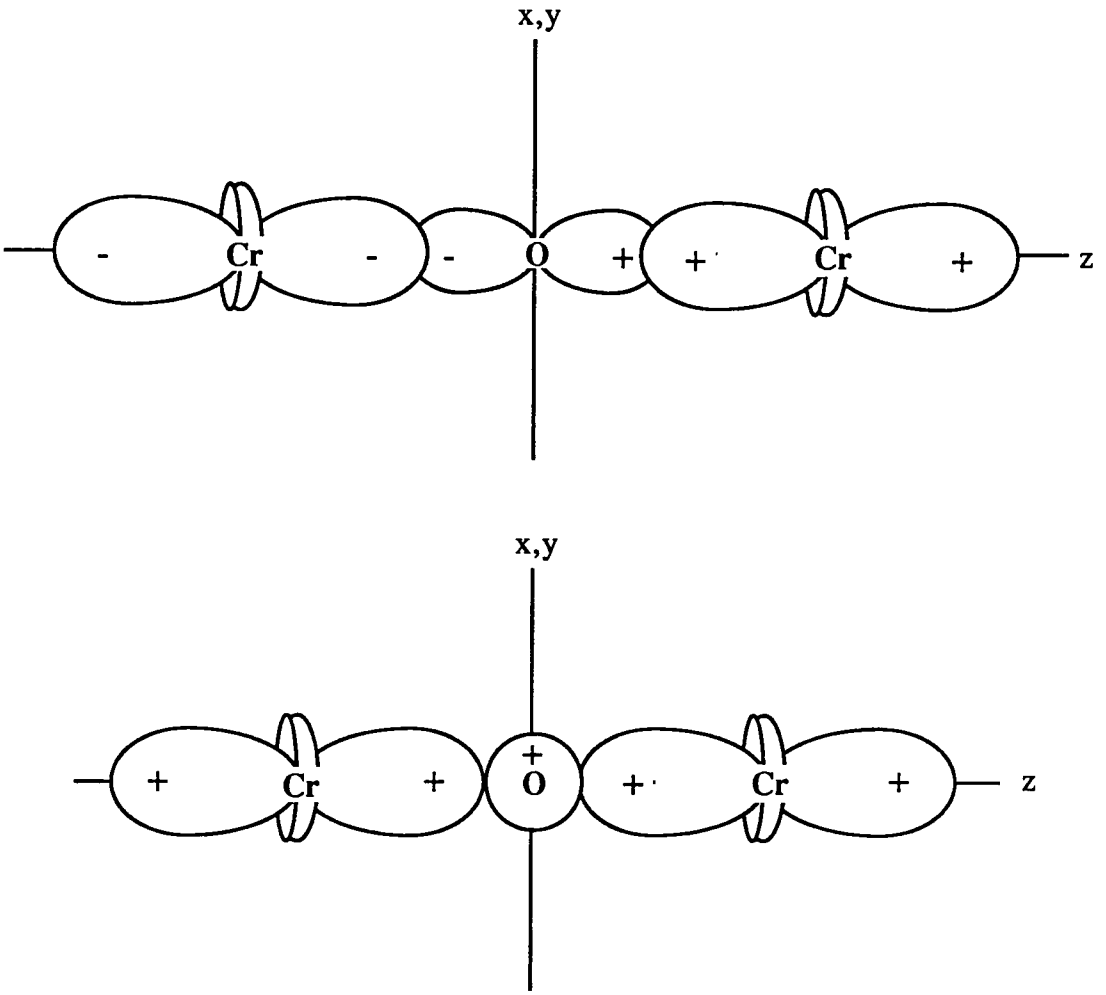

This molecular orbital approch for linear MOM dimers was originally taken by Dunitz and Orgel[5] in the interpretation of the properties of the $Cl_5RuORuCl_5^{4-}$ anion. Their proposed $(e_u)^4(b_{2g})^2(b_{1u})^2(e_g)^4$ electronic configuration and strong d-p-d π overlap argument was successful in explaining the linearity, short Ru-O bond distance, and diamagnetism observed.

To date the greatest body of oxo-bridged dimer work has been concentrated on the spectroscopic and magnetic properties of the basic rhodo ion.[6-11] Interestingly, the

interpretation of its spectroscopic and magnetic properties has come from two very different viewpoints. Magnetic data has been interpreted in terms of Heisenberg exchange between two S = 3/2 ions, with some success being achieved in fitting the magnetic susceptibility temperature dependence to an isotropic model,[6] resulting in a spin-spin coupling constant J of -450 cm^{-1}. However, in the interpretation of the spectral data, the molecular orbital model (Figure 1) derived by Schmidke[12] has provided a means for electronic transition assignments. Electronic transitions between states derived from this model are preferable to the alternative interpretation of simultaneous pair excitations involving ^2E_g and $^2T_{1g}$ states (in O_h) proposed by Gudel and Dubicki.[8]

The substitutional properties of the basic rhodo cation are but one manifestation of the unique bonding found in linear oxo-bridged dimers. Wilmarth, Graff and Gustin[13] established the stoichiometry of the fundamental base hydrolysis reaction as

$$(NH_3)_5CrOCr(NH_3)_5^{4+} + H_2O \longrightarrow (NH_3)_5Cr(OH)Cr(OH)(NH_3)_4^{4+} + NH_3$$

and suggested that the rationale for the weakening and ultimate cleavage of the Cr-N bond was negative charge buildup on chromium mediated by Cr-O-Cr d-p-d π overlap. Schwarzenbach and Magyar[2] attributed the loss of ammonia from the dimer to a weakening of the Cr-N bond due to a trans effect by bridging oxygen. However, Hoppenjans and Hunt[14] showed that the cis-$[(NH_3)_5Cr(OH)Cr(OH)(NH_3)_4]^{4+}$ cation is the only chromium-containing product in the base hydrolysis process, thus ruling out the possibility of a trans effect. Later, a careful kinetic study of this reaction determined the role of hydroxide in the rate law, and an argument consistent with the molecular orbital perspective was presented.[15] Jahn-Teller distortion of a contributing triplet term necessarily involves bending of the Cr-O-Cr unit to lift the degeneracy, and provides the "hidden" driving force for rhodo to erythro conversion.

Interest in the reactivity of linear oxo-bridged Cr(III) dimers experienced a rebirth when the synthesis of the elusive (μ-oxo)bis{pentaaquachromium(III)} dimer (aqua dimer) was discovered through the oxidative elimination of hydroquinone from a hydroxy-hydroquinone-bridged intermediate.[16] This was the first example of an oxo-bridged Cr(III) dimer not derived from the basic rhodo ion. Although the spectral properties of this dimer are remarkably similar to those of the basic rhodo ion, the substitutional properties are not. Indeed, the aqua dimer cleaves to give $Cr(H_2O)_6^{3+}$ in a facile acid hydrolysis reaction which is accelerated by hydrogen ion,[17] anions (including perchlorate ion),[18] and reductants.[19] A completely irreversible reduction wave of the aqua dimer at an $E_{1/2}$ of 0.43 V led to a formulation of the $(e_u^b)^4(b_{2g})^2(b_{1u})^2(e_g)^3$ electronic configuration for the reduction product. The reduction product subsequently undergoes Jahn-Teller distortion involving bending of the Cr-O-Cr unit[19] prior to Cr-O bond cleavage.

The failure to isolate the aqua dimer in the solid state because of its unique reactivity has proven to be a hindrance in obtaining its magnetic properties and a structural analysis by conventional X-ray diffraction methods. Both of these determinations are vital to relating magnetic, redox and substitutional properties to electronic structure, emphasizing the need to isolate a family of the oxo-dimers in the solid state. Unfortunately, to date only three Cr(III)-containing linear oxo-bridged dimers have been synthesized,[20,21,16] each by a different synthetic technique, and only two have been isolated in the solid state.[20,21] It is clear that in order to achieve the objective of relating redox, spectral, magnetic and substitutional properties to electronic structure in these dimers, the development of a general synthetic technique capable of creating a large family in the solid state is of paramount importance. To achieve this goal, the tetradentate tris(2-pyridylmethyl)amine ligand (tmpa) will be used to occupy four coordination positions of $N_4LCrOCrLN_4$, allowing a single degree of freedom in the fifth ligand L. The use of the weakly π-

accepting tmpa ligand over NH_3 or H_2O will also provide a probe into the ordering of the approximately nonbonding e_g, b_{2g} and b_{1u} molecular orbitals.

Objectives

The goals of our research are as follows:

(1) To devise a general synthetic technique capable of generating a large family of linear oxo-bridged Cr(III) dimers with aromatic amine ligands.

(2) To create a family of $N_4LCrOCrLN_4$ dimers, with varying ligand L. A full characterization will include spectral, redox, and magnetic properties along with substitutional reactivity studies.

(3) To relate the properties of each dimer to electronic structure, with emphasis on how the properties change with changing ligand. A molecular orbital model will be tested in the interpretation of these properties.

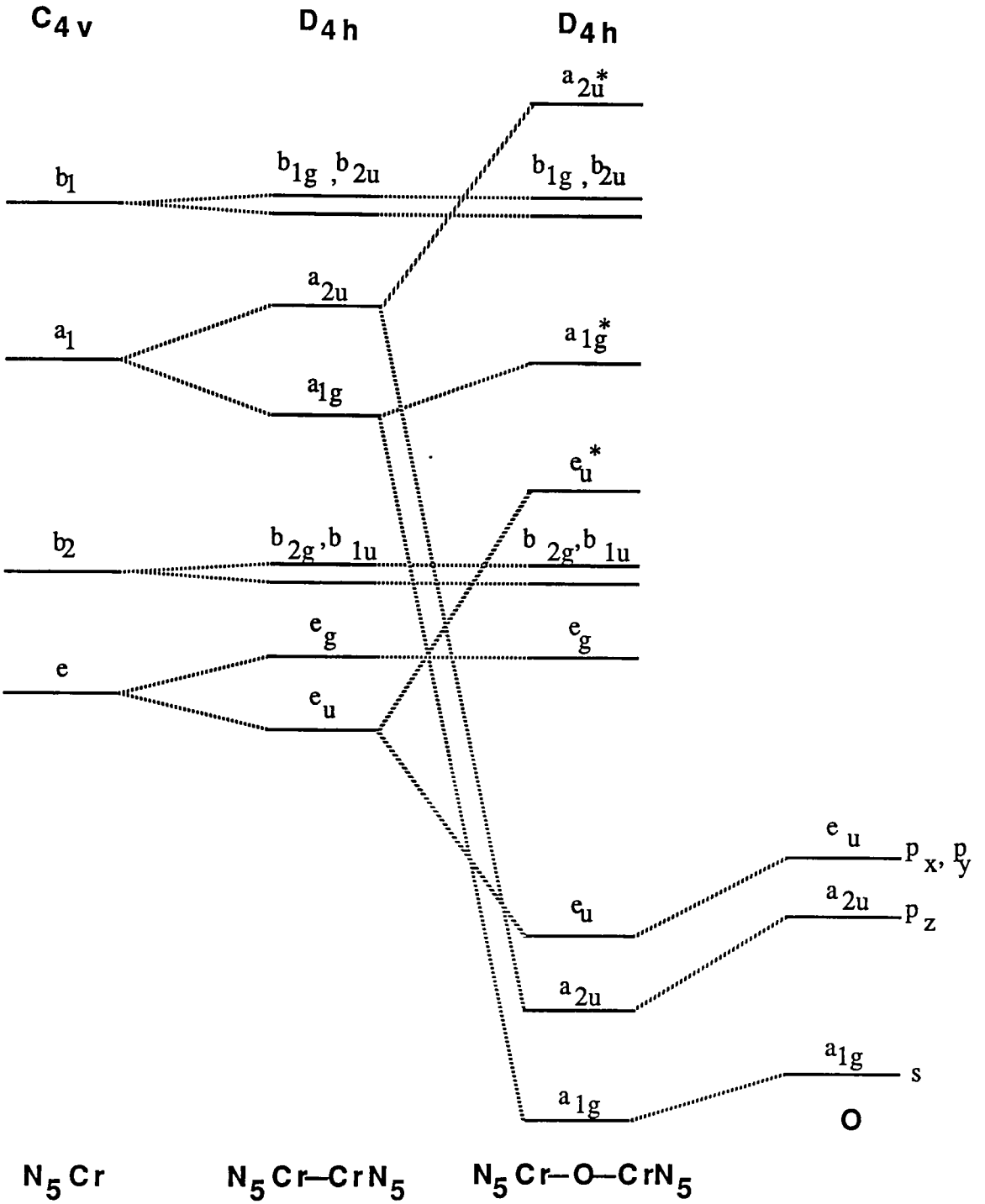

Figure 1. Molecular orbital diagram for $[(NH_3)_5CrOCr(NH_3)_5]^{4+}$. Developed by Schmidtke[12] through angular overlap analysis.

CHAPTER II

EXPERIMENTAL METHOD

Materials and Techniques

Reagent grade chemicals were used throughout. Gold label chromium chunks (Aldrich), 98% 2-picolylchloride hydrochloride (Aldrich), bis(2-pyridylmethyl)amine (Nepara), 2,2'-bipyridine and 1,10-phenanthroline (G. F. Smith) were used as supplied. Solutions for spectroscopic, kinetic and ionization constant determinations were prepared from triply distilled water. Cation exchange chromatography was performed on SP-Sephadex C-25-120 resin (Na^+ form), and eluting solutions were prepared from doubly distilled water. Anaerobic preparations were carried out under chromous-scrubbed nitrogen, using Hamilton gastight syringes fitted with teflon or stainless steel needles for solution transfers.

Solution Preparation

Stock solutions (150 mL) of $Cr(ClO_4)_2$ and $CrBr_2$ were prepared from the anaerobic reactions of excess Cr (8.00 g, 0.154 mol) with 0.300 mol of $HClO_4$ and HBr, respectively, in serum-capped bottles. These solutions were heated under continuous N_2 purge until H_2 evolution was no longer visible, at which time they were cooled to room temperature and standardized by injection into aqueous acidic Fe^{3+}, followed by back titration of the Fe^{2+} formed with $Cr_2O_7^{2-}$ to a diphenylamine sulfonate endpoint. Chromium chunks were treated with concentrated $HClO_4$ immediately prior to use in order to remove the surface oxide layer.

Stock KSCN and NaSCN solutions were prepared with triply distilled water, and standardized with $AgNO_3$ (in 0.100 M HNO_3 / 0.01 M Fe^{3+}) by Volhard titration to an orange-red $FeSCN^{2+}$ endpoint. Standard SCN^- solutions covering a range of 1.0×10^{-4}

to 1.0×10^{-1} M were prepared by successive dilution of a KSCN stock solution, and adjusted to pH 3 at an ionic strength of 0.100 M with $HNO_3/NaNO_3$.

Elemental Analysis

Microanalyses were performed by Desert Analytics (Tucson, Arizona). Chromium(II) and chromium(III) assays were carried out by oxidation to CrO_4^{2-} in aqueous basic peroxide, followed by quantitation of CrO_4^{2-} employing $\varepsilon = 4815\ M^{-1}\ cm^{-1}$ at λ_{max} = 373 nm.

Ligand Synthesis

Tris(2-pyridylmethyl)amine (1)

Tris(2-pyridylmethyl)amine was prepared through an adaptation of the literature method.[22] 2-Picolylchloride hydrochloride (48.4 g, 0.295 mol) was neutralized with 58.9 mL of 5.00 M NaOH (0.295 mol) and then combined with bis(2-pyridylmethyl)amine (58.7 g, 0.295 mol) while stirring. Another 0.295 mol of NaOH was slowly added to the reaction mixture over the period of 1 hour. The resulting brown solution was stirred at ambient temperature for 24 hours and then neutralized with excess concentrated $HClO_4$, generating a tan precipitate of crude $[H_3tmpa](ClO_4)_3$ in 97% yield. Recrystallization and purification were accomplished in one step by preparing a solution 0.1 M in both $[H_3tmpa](ClO_4)_3$ and $[Cr(H_2O)_6](ClO_4)_3$ (to complex with impurities), adjusting the pH to 2.0 with $HClO_4$ and boiling for 15 minutes. The snow-white crystals that formed upon cooling were washed with cold triply distilled water and air-dried. Calculated (Calcd) for $[H_3tmpa](ClO_4)_3$: C, 36.54; H, 3.58; N, 9.47. Found: C, 36.37; H, 3.53; N, 9.27. UV (CH_3CN): λ_{max} 261 nm (e 14,400 $M^{-1}cm^{-1}$), 204 (9600).

Synthesis of Doubly-Bridged Cr(III) Dimers

$[(tmpa)Cr(OH)_2Cr(tmpa)](ClO_4)_4 \cdot 4H_2O$ (2)

$[H_3tmpa](ClO_4)_3$ (1, 14.0 g, 0.0237 mol) was neutralized in 150 mL of vigorously stirred (10 minutes) 2.00 M NaOH. Upon standing for an additional 10 minutes, the upper aqueous phase separated from the light tan tmpa oil, which was quantitatively collected with a syringe and injected into 150 mL of 95% ethanol. Aqueous $Cr(ClO_4)_2$ (0.0237 mol) was injected into this pale yellow ethanolic solution after purging with N_2 for 30 minutes, giving dark brown $Cr(tmpa)(ClO_4)_2$. The reaction mixture was then opened to the air and stirred vigorously, bringing about the rapid deposition of a fine purple powder which was separated from a small amount of red byproduct by filtration. The slightly soluble product was recrystallized by dissolving in 900 mL of boiling 1.0 mM $HClO_4$, followed by the addition of $LiClO_4$ (3.0 g) and slow cooling to room temperature. The resultant large maroon crystals of $[(tmpa)Cr(OH)_2Cr(tmpa)](ClO_4)_4 \cdot 4H_2O$ were washed with triply distilled water and air-dried. Yield: 13.43 g, 95%. Calcd for $[(tmpa)Cr(OH)_2Cr(tmpa)](ClO_4)_4 \cdot 4H_2O$: Cr, 8.75; C, 36.38; H, 3.90; N, 9.43. Found: Cr, 8.73; C, 36.54; H, 3.77; N, 9.27. UV-vis (H_2O): λ_{max} 540 nm (ε 131 $M^{-1}cm^{-1}$), 385 (113), 261 (7850). IR (KBr pellet): 3400 s, 3000 s, 1600 s, 1480 m, 1440 s, 1300 m, 1155 m, 1105 s, 1100 s, 1080 s, 1050 s, 1020 s, 940 w, 890 w, 770 s, 720 w, 650 s cm^{-1}.

$[(tmpa)Cr(OH)_2Cr(tmpa)]Br_4.8H_2O$ (3)

$[(tmpa)Cr(OH)_2Cr(tmpa)]Br_4 \cdot 8H_2O$ was prepared as described above for the perchlorate salt of the diol, using 15.0 g (0.0253 mol) of $[H_3tmpa](ClO_4)_3$, 0.0253 mol of aqueous $CrBr_2$, a 1.0 mM HBr (300 mL) recrystallization medium, and 20.0 g of NaBr added to the hot recrystallization solution before cooling. The crystalline purple product was washed with triply distilled water and air-dried. Yield: 13.8 g, 92%. Calcd for $[(tmpa)Cr(OH)_2Cr(tmpa)]Br_4 \cdot 8H_2O$: Cr, 8.79. Found: Cr, 8.74. UV-vis (H_2O): identical

to 2. IR (KBr pellet): 3400 s, 3000 s, 1600 s, 1480 m, 1440 s, 1300 m, 1155 m, 1105 s, 1080 s, 1050 s, 1030 s, 940 w, 890 w, 770 s, 720 w, 650 s cm^{-1}.

$[(tmpa)Cr(O)(OH)Cr(tmpa)](ClO_4)_3 \cdot H_2O$ (4)

After dissolving 2 (1.00 g) in 400 mL of water, the pH was adjusted to 10.0 by slow addition of 0.1 M NaOH. Solid $LiClO_4$ was then added until precipitation of the brown-green product commenced. The stirred solution was then cooled to 5 °C and digested for 30 minutes, at which time an 87% yield (0.76 g) of the crystalline product was isolated by filtration, washed quickly with cold distilled water and air-dried. Calcd for $[(tmpa)Cr(OH)(O)Cr(tmpa)](ClO_4)_3 \cdot H_2O$: Cr, 10.06; C, 41.81; H, 3.80; N, 10.84. Found: Cr, 10.10; C, 41.65; H, 3.61; N, 10.68. UV-vis (H_2O): λ_{max} 370 nm (ε 900 $M^{-1}cm^{-1}$), 258 (8900). IR (KBr pellet): 3400 s, 1600 s, 1480 m, 1440 s, 1300 m, 1155 m, 1105 s, 1100 s, 1080 s, 1050 s, 1030 s, 940 w, 890 w, 770 s, 720 w, 650 s cm^{-1}. Several attempts to isolate $[(tmpa)Cr(O)_2Cr(tmpa)](ClO_4)_2$ as a pure solid from solutions at pH 12 or above failed because of the facile base hydrolysis reaction of the dioxo dimer.

$[(bpy)_2Cr(OH)_2Cr(bpy)_2](ClO_4)_4 \cdot 2H_2O$ (5)

2,2'-Bipyridine (10.0 g, 0.064 mol) was dissolved in 100 mL of 95% ethanol and purged with N_2 for 30 minutes. A dark purple precipitate and solution were observed upon the anaerobic injection of aqueous $Cr(ClO_4)_2$ (0.032 mol). When this mixture was stirred in the presence of oxygen, the purple intermediate slowly converted to a reddish-tan precipitate of $[(bpy)_2Cr(OH)_2Cr(bpy)_2](ClO_4)_4 \cdot 2H_2O$. The product was recrystallized as above (diol 2), washed with triply distilled water and air-dried. Yield: 14.5 g, 72%. Calcd for $[(bpy)_2Cr(OH)_2Cr(bpy)_2](ClO_4)_4 \cdot 2H_2O$: Cr, 8.69; C, 40.15; H, 3.03; N, 9.36. Found: Cr, 8.31; C, 40.39; H, 2.87; N, 9.41. UV-vis (5.0 mM $HClO_4$ (aq)): λ_{max} 310 nm (ε 20,800 $M^{-1}cm^{-1}$), 392 (344), 416 sh (228), 428 sh (80), 533 (55).

$[(phen)_2Cr(OH)_2Cr(phen)_2](ClO_4)_4 \cdot 3H_2O$ (6)

$Cr(ClO_4)_2$ (0.0253 mol) was injected into an anaerobic solution of 1,10-phenanthroline (10.0 g, 0.0505 mol) dissolved in 100 mL of 95% ethanol, giving a dark brown reaction mixture which deposited a tan precipitate of $[(phen)_2Cr(OH)_2Cr(phen)_2](ClO_4)_4 \cdot 3H_2O$ upon subsequent aerobic stirring. Product workup was identical to that employed for the bpy diol. Yield: 12.2 g, 74 %. Calcd for $[(phen)_2Cr(OH)_2Cr(phen)_2](ClO_4)_4 \cdot 3H_2O$: C, 43.99; H, 2.92; N, 8.55. Found: C, 44.18; H, 2.68; N, 8.55. UV-vis (CH_3CN): λ_{max} 226 nm (ε 58,000 $M^{-1}cm^{-1}$), 276 (40,400), 353 (1740), 538 (55).

Synthesis of Singly-Bridged Cr(III) Dimers

$[(tmpa)(SCN)CrOCr(NCS)(tmpa)](ClO_4)_2 \cdot 0.5\ H_2O$ (7)

2 (1.00 g, 0.841mmol) was dissolved into 200 mL boiling water, and reacted with vigorous stirring with 33.7 mmol of NaSCN (20-fold excess) for 1 hour. A 60% yield of a dark brown-green microcrystalline precipitate was isolated from the hot solution by filtration. The solid was recrystallized by dissolving in 500 mL warm doubly distilled H_2O, followed by slow addition of solid $LiClO_4$ with stirring until precipitation commenced, then cooling and allowing the solid to digest at 5 °C for one hour. The microcrystalline precipitate was washed with cold triply distilled water and air-dried. Calcd for $[(tmpa)(SCN)CrOCr(NCS)(tmpa)](ClO_4)_2 \cdot 0.5H_2O$: Cr, 10.14; C, 44.54; H, 3.64; N, 13.67. Found: Cr, 10.19; C, 44.57; H, 3.39; N, 13.60. UV-vis (CH_3CN): λ_{max} 256 nm (25,000 $M^{-1}cm^{-1}$), 313 (10,800), 355 (14,100), 368, sh (11,200), 398, sh (2,750), 417 (2,740), 457, sh (1,780), 567, plateau (250), and 773 (58).

$[(tmpa)(SCN)Cr(OH)Cr(NCS)(tmpa)](ClO_4)_3 \cdot 6H_2O$ (8)

7 (0.200 g, 0.195 mmol) was dissolved into 200 mL boiling 1.00 M $HClO_4$, and the solution cooled to room temperature. The maroon needles of the singly hydroxy-bridged

dimer that formed in 84% yield were removed from solution by filtration, washed with cold 0.100 M $HClO_4$ and air-dried. Calcd for $[(tmpa)(SCN)Cr(OH)Cr(NCS)(tmpa)](ClO_4)_3 \cdot 6H_2O$: Cr, 8.49; C, 37.28; H, 4.03; N, 11.44. Found: Cr, 8.51; C, 37.19 ; H, 3.22 ; N, 11.29 . UV-visible (H_2O): 262 nm (ϵ 19,400 $M^{-1}cm^{-1}$), 327 (8,700), and 524 (410).

$[(tmpa)(SCN)CrOCr(NCS)(tmpa)]Br_2 \cdot 3H_2O$ (9)

The bromide salt of 7 was prepared by simple ion metathesis using KBr and NaBr. 1.00 g of 7 was stirred rapidly in 500 mL of doubly distilled H_2O and 5.0 g of KBr for 30 minutes at ambient temperature. The colorless supernatant was removed by filtration. Crude 9 was separated from the less soluble $KClO_4$ by washing with small aliquots of H_2O, until the remaining solid showed no brown color. The resulting solution was a dark golden brown. 9 was precipitated from solution by slow addition of solid NaBr with stirring until a cloudiness was observed, followed by cooling to 5 °C and digesting for 2 hours. The solid was reprecipitated twice in this manner. The final dark brown microcrystals were filtered, washed with cold triply distilled H_2O, and air-dried. Chromium assay: Calcd for $[(tmpa)(SCN)CrOCr(NCS)(tmpa)]Br_2 \cdot 3H_2O$: Cr, 10.09. Found: Cr, 10.1. UV-vis (CH_3CN): Identical to 7.

$[(tmpa)(SCN)CrOCr(NCS)(tmpa)](NO_3)_2 \cdot 2H_2O$ (10)

The same procedure used to prepare 9 was followed, with KNO_3 and $NaNO_3$ used in place of the bromide salts. The final dark brown microcrystals were washed with triply distilled water and air-dried. Calcd for $[(tmpa)(SCN)CrOCr(NCS)(tmpa)](NO_3)_2 \cdot 2H_2O$: Cr, 10.64. Found: Cr, 10.6. UV-vis (CH_3CN): Identical to 7.

$[(tmpa)(N_3)CrOCr(N_3)(tmpa)](ClO_4)_2 \cdot 2H_2O$ (11)

2 (1.00 g, 0.841mmol) was ground to a fine powder, dried at 100 °C for 30 minutes and then dissolved in 150 mL of hot CH_3CN. Upon the addition of NaN_3 (1.092 g, 16.8

mmol) and refluxing for 2 hours, the color of the solution changed from purple to deep green. After cooling and filtration of the solution to remove excess NaN_3, ether was added slowly with stirring until a precipitate formed. The green product (73% yield) was collected as usual and air-dried. Calcd for $[(tmpa)(N_3)CrOCr(N_3)(tmpa)](ClO_4)_2 \cdot 2H_2O$: Cr, 10.2; C, 42.41; H, 3.95; N, 19.23. Found: Cr, 10.0; C, 42.65; H, 3.73; N, 18.79. IR: ν_{as} (Cr-O-Cr) = 865 cm^{-1}; ν (NN) = 2061 cm^{-1}.

$[(tmpa)(OCN)CrOCr(NCO)(tmpa)](ClO_4)_2$ (12)

2 (1.00 g, 0.841 mmol) was dissolved in 100 mL of hot acetonitrile, combined with 1.36 g (16.8 mmol) of KOCN, and the mixture refluxed for 2 hours. The brown-green product was precipitated by slow ether addition after removal of excess KOCN by filtration. Crude 12 was then recrystallized three times by dissolving in 700 mL of doubly distilled H_2O, slowly adding solid $LiClO_4$ with stirring until precipitation commenced, and then allowing the solid to digest at 5 °C for 4 hours. The final crop (87% yield) of dark green crystals was washed with water and air-dried. Calcd for $[(tmpa)(OCN)CrOCr(NCO)(tmpa)](ClO_4)_2$: Cr, 10.6; C, 46.40; H, 3.69; N, 14.24. Found: Cr, 10.2; C, 46.32; H, 3.71; N, 14.21. IR: ν_{as} (Cr-O-Cr) = 873 cm^{-1}; ν (CN) = 2210 cm^{-1}.

$[(tmpa)(NC)CrOCr(CN)(tmpa)](ClO_4)_2 \cdot 2H_2O$ (13)

2 (1.00 g, 0.841 mmol) was dissolved in 100 mL of hot CH_3CN, mixed with 0.825 g (16.8 mmol) of NaCN, and the solution was refluxed for 2 hours. Following removal of excess NaCN from the cooled mixture by filtration, the brown-green product was isolated after the addition of 10.0 g of $LiClO_4$, 50 mL of H_2O and slow evaporation of CH_3CN until precipitation was complete. One recrystallization was performed by dissolving the solid in the minimum amount of H_2O at room temperature and then adding $LiClO_4$ with stirring. The 81% final yield of 13 was filtered, washed with water and air-dried. Calcd for

[(tmpa)(NC)CrOCr(CN)(tmpa)]$(ClO_4)_2 \cdot 2H_2O$: Cr, 10.5; C, 46.21; H, 4.08; N, 14.18. Found: Cr, 10.7; C, 46.11; H, 3.64; N, 14.02. IR: ν_{as} (Cr-O-Cr) = 865 cm^{-1}; ν (CN) = 2120 cm^{-1}.

[(tmpa)ClCrOCrCl(tmpa)]$(ClO_4)_2 \cdot 2H_2O$ (14)

2 (1.00 g, 0.841 mmol) was ground to a fine powder, dried at 100 °C for 30 minutes and then combined with 0.983 g (16.8 mmol) of NaCl in 100 mL of hot CH_3CN. After refluxing for 1 hour, the solution was cooled, filtered, and transferred to a large beaker. Ether was slowly added with stirring until a brown-green precipitate was seen. The product (95% yield) was isolated by filtration, washed with ether and air-dried. Recrystallization from water was not feasible because 14 rapidly decays to 2 in this solvent. Calcd for [Cl(tmpa)CrOCr(tmpa)Cl]$(ClO_4)_2 \cdot 2H_2O$: Cr, 10.3; C, 42.96; H, 4.00; N, 11.13. Found: Cr, 10.4; C, 42.76; H, 3.60; N, 10.96. IR: ν_{as} (Cr-O-Cr) = 844 cm^{-1}.

$[(bpy)_2(SCN)CrOCr(NCS)(bpy)_2](ClO_4)_2 \cdot H_2O$ (15)

5 (4.00 g, 3.34 mmol) was dissolved in 300 mL of boiling water and then combined with 10.8 g (134 mmol) of NaSCN. The color of the solution changed from red-brown to dark chocolate brown within 30 seconds, when crystalline 15 began to form. The reaction mixture was allowed to boil for an additional 10 minutes, at which time the solid was isolated by filtering the hot solution, washed with water and air-dried. The dark chocolate brown microcrystals (58% yield) showed no change in %Cr upon recrystallization from water. Calcd for $[(bpy)_2(SCN)CrOCr(NCS)(bpy)_2](ClO_4)_2 \cdot H_2O$: Cr, 9.6; C, 46.80; H, 3.18; N, 12.99. Found: Cr, 9.6; C, 46.81; H, 2.91; N, 12.83. IR: ν_{as} (Cr-O-Cr) = 856 cm^{-1}; ν(CN) = 2066 cm^{-1}. UV-vis (CH_3CN): λ_{max} (ε_{max}) 301 nm (52,300 $M^{-1}cm^{-1}$).

$[(bpy)_2(N_3)CrOCr(N_3)(bpy)_2](ClO_4)_2 \cdot H_2O$ (16)

5 (1.00 g, 0.836 mmol) was mixed with 2.17 g (33.4 mmol) of NaN_3 in 100 mL of boiling water. After several minutes, the color of the solution changed from red to dark

brown, but, unlike the preparation of 15, no precipitate emerged. $LiClO_4$ (5.0 g) was then added to the hot solution, inducing the precipitation of the chocolate brown product within 2-3 minutes. 16 was isolated by filtration of the hot solution, washed with water and air-dried. The crude product was recrystallized by dissolving in 200 mL of acetone, adding 2.00 g $LiClO_4$ dissolved in 20 mL of H_2O, followed by slow evaporation. The crystals (23% yield) that formed upon reducing the solution volume to 30 mL were washed with water and air-dried. Calcd for $[(bpy)_2(N_3)CrOCr(N_3)(bpy)_2](ClO_4)_2 \cdot H_2O$: Cr, 9.9; C, 45.94; H, 3.28; N, 18.75. Found: Cr, 9.9; C, 46.58; H, 3.03; N, 18.79. IR: ν_{as} (Cr-O-Cr) = 836 cm^{-1}; ν(NN) = 2059 cm^{-1}. λ_{max} (ε_{max}) 300 nm (56,000 $M^{-1}cm^{-1}$).

Synthesis of Oxo-, Carboxylato-Bridged Cr(III) Dimers

$[(tmpa)Cr(O)(CH_3COO)Cr(tmpa)](ClO_4)_3$ (17)

2 (1.00 g, 0.841 mmol) was dissolved into 100 mL of CH_3CN, and heated until dissolution was complete. After 2.29 g (16.8 mmol) of CH_3COONa was added, the solution was refluxed for one hour. Excess solid CH_3COONa was removed by filtration, and the solution evaporated to 50 mL. Fifty mL water and 1.0 g of $LiClO_4$ was added and the solution was allowed to evaporate until a dark green solid had formed, leaving a virtually colorless supernatant. The solid was isolated by filtration, and recrystallized once by dissolving into 700 mL H_2O, slowly adding solid $LiClO_4$ until precipitation was initiated, then cooling to 5 °C and digesting with stirring for one hour. The solid was filtered, washed twice with cold triply distilled water and air-dried. Yield: 0.81 g, 91%. Calcd for $[(tmpa)Cr(O)(CH_3COO)Cr(tmpa)](ClO_4)_3$: Cr, 9.83; C, 43.14; H, 3.72; N, 10.59. Found: Cr, 9.72; C, 43.09; H, 3.61; N, 10.44. UV-vis (CH_3CN): λ_{max} 562nm (ε 200$M^{-1}cm^{-1}$), 419 (1,780), 388 (2,070), 372 (2,890), 336 (4,090), 256 (20,600). IR: ν_{as} (CO) = 1549 cm^{-1}; ν_s(CO) = 1443 cm^{-1}.

[(tmpa)Cr(O)(HCOO)Cr(tmpa)]$(ClO_4)_3$ (18)

2 (1.00 g, 0.841 mmol) was dissolved into 100 mL of CH_3CN, and heated until dissolution was complete. Then 1.144 g (16.8 mmol) of HCOONa was added, and the solution refluxed for one hour. The excess solid HCOONa was filtered off, 100 mL water and 20.0 g of $LiClO_4$ was added, and the solution was allowed to evaporate until a deep green solid had formed. The solid was isolated by filtration, and recrystallized once as in the preparation of 17. The recrystallized solid was filtered, washed with cold triply distilled water and air-dried. Yield: 0.84 g, 96 %. Calcd for [(tmpa)Cr(O)(HCOO)Cr(tmpa)]$(ClO_4)_3$: Cr, 9.96; C, 42.56; H, 3.57; N, 10.73. Found: Cr, 9.94; C, 42.46; H, 3.54; N, 10.80. UV-vis (CH_3CN): λ_{max} 563 nm (ε 217 $M^{-1}cm^{-1}$), 419 (2,050), 388 (2,240) (sh), 372 (3,600), 256 (21,900). IR: ν_{as} (CO) = 1561 cm^{-1}; ν_s(CO) = 1369 cm^{-1}.

[(tmpa)Cr(O)(C_6H_5COO)Cr(tmpa)]$(ClO_4)_3 \cdot 2H_2O$ (19)

2 (1.00 g, 0.841 mmol) was dissolved into 100 mL of CH_3CN, and heated until dissolution was complete. Then 0.485 g (3.37 mmol) of C_6H_5COONa was added and the solution was refluxed for 30 minutes. Excess solid C_6H_5COONa was removed by filtration, 100 mL water and 20.0 g of $LiClO_4$ were added, and the solution was allowed to evaporate until the dark green solid had formed. The solid was recovered, recrystallized, washed, and dried as usual. Yield: 0.87 g, 93 %. Calcd for [(tmpa)Cr(O)(C_6H_5COO)Cr(tmpa)]$(ClO_4)_3 \cdot 2H_2O$: Cr, 8.99; C, 44.67; H, 3.92; N, 9.69. Found: Cr, 9.01; C, 44.81; H, 3.62; N, 9.76. UV-vis (CH_3CN): λ_{max} 566 nm (ε 225 $M^{-1}cm^{-1}$), 419 (2,330), 388 (2,540) (sh), 371 (3,450), 337 (5,440), 251 (35,200). IR: ν_{as} (CO) = 1527 cm^{-1}; ν_s(CO) = 1413 cm^{-1}.

Synthesis of Cr(III) Monomers

$[Cr(tmpa)(SCN)_2](ClO_4)$ (20)

Method A. A solution of 2 (1.00 g, 0.841 mmol) mixed with 1.68 mmol of NaOH in 200 mL of water was boiled for 10 minutes, resulting in the quantitative formation of blue $[Cr(tmpa)(OH)_2]^+$. After converting the dihydroxo monomer to red $[Cr(tmpa)(OH_2)_2]^{3+}$ through the addition of 1.75 mL of 11.45 M $HClO_4$, NaSCN (5.46 g, 67.4 mmol) was added and the solution was boiled with stirring for 60 minutes. The brick red precipitate that formed upon cooling to room temperature was washed with triply distilled water and air-dried. Yield: 0.890 g, 95%. Calcd for $[(tmpa)Cr(NCS)_2](ClO_4)$: Cr, 9.32. Found: Cr, 9.25. UV-vis (CH_3CN): λ_{max} 515 nm (ε 210 $M^{-1}cm^{-1}$), 348 (8700), 324 sh (6100), 261 (12,300). IR (KBr pellet): 3400 m, 2020 s, 1600 m, 1480 w, 1440 m, 1280 w, 1300 w, 1100 s, 1030 m, 900 w, 770 m, 740 w, 650 w cm^{-1}.

Method B. 2 (1.00 g, 0.841 mmol) was allowed to react with NaSCN (5.46 g, 67.4 mmol) at pH 1.5 ($HClO_4$) for 2 hours in 500 mL of boiling water, with an accompanying color change from purple to bright red and reduction of the solution volume to 300 mL. Upon cooling to room temperature, a 75% yield (0.700 g) of the product crystallized and was recovered as in method A. Calcd for $[(tmpa)Cr(NCS)_2](ClO_4)$: Cr, 9.32; C, 43.05; H, 3.25; N, 15.06. Found: Cr, 9.27; C, 43.08; H, 3.43; N, 15.49. UV-vis (CH_3CN) and IR (KBr pellet): identical to product from method A.

$[Cr(tmpa)Cl_2](ClO_4)\cdot 2.5\ H_2O$ (21)

2 (1.00 g, 0.841 mmol) was converted to $Cr(tmpa)(OH_2)_2^{3+}$ in 100 mL of water as before, followed by saturation of the solution with NaCl and heating at 60 °C for 3 hours. The large dark red crystals that formed upon overnight refrigeration of the product solution (70% yield) were washed with cold triply distilled water and air-dried. Calcd for $[Cr(tmpa)Cl_2](ClO_4)\cdot 2.5\ H_2O$: Cr, 9.3; C, 40.06; H, 3.92; N, 10.38. Found: Cr, 9.4; C,

40.02; H, 3.67; N, 10.26. UV-vis (H_2O): λ_{max} (ε_{max}) 395 nm (127 $M^{-1}cm^{-1}$), 539 (122).

Ionization Constant Determinations

A 367 nm spectrophotometric titration[23] was performed to determine the first (K_{a1}) and second (K_{a2}) ionization constants of the $[(tmpa)Cr(OH)_2Cr(tmpa)]^{4+}$ ion. N,N-bis(2-hydroxyethyl)-2-aminoethanesulfonic acid (BES) and carbonate buffers (10 mM) containing 0.1 M $NaNO_3$ were used in the pH 6.4 - 10.6 range, while HNO_3 or NaOH solutions adjusted to a constant ionic strength of 0.1 M with $NaNO_3$ extended to pH interval down to 1 and up to 13. A 1.00 mM solution of 2 in 0.1 M $NaNO_3$ was mixed with the identical volume of the pH-controlling solution, both thermostated at 25.0 °C, and the absorbance was quickly determined in a 1-cm quartz cell. One determination was carried out in 3.2 M NaOH in order to better define the limiting absorbance at high pH. Hydrogen ion concentrations were derived from pH readings (Brinkmann pH-104 meter) as previously described.[24] The ionization constants K_{a1}, K_{a2} and extinction coefficients of unionized (ε_0), singly- (ε_1) and doubly-ionized (ε_2) diol species were extracted from a non-linear least squares fit (method of steepest descent) of the A_{367} versus $[H^+]$ data to expression (1), where C_o represents the total dimer concentration ($[Cr(OH)_2Cr^{4+}]$ + $[Cr(OH)(O)Cr^{3+}]$ + $[Cr(O)_2Cr^{2+}]$).

$$A_{367} = \varepsilon_0 [Cr(OH)_2Cr^{4+}] + \varepsilon_1 [Cr(OH)(O)Cr^{3+}] + \varepsilon_2 [Cr(O)_2Cr^{2+}] \quad (1)$$

$$[Cr(OH)_2Cr^{4+}] = C_o / (1 + Ka1/[H^+] + K_{a1}K_{a2}/[H^+]^2)$$

$$[Cr(OH)(O)Cr^{3+}] = C_o / (1 + [H^+]/K_{a1} + K_{a2}/[H^+])$$

$$[Cr(O)_2Cr^{2+}] = C_o / (1 + [H^+]/K_{a2} + [H^+]^2/K_{a1}K_{a2}).$$

In order to determine the acid ionization constants of $[(tmpa)LCr(OH)CrL(tmpa)]^{3+}$ complexes, spectrophotometric titrations (25.0 °C, I = 0.1 M ($NaNO_3$)) were carried out on buffered (10 mM) aqueous solutions over the pH 1-10 range, monitoring absorbance at

the most intense near-ultraviolet transition (near 350 nm) and performing non-linear least squares fits of the absorbance, $[H^+]$ data to the single step ionization expression (2), where C_o represents the total dimer concentration and ε_0 and ε_1 represent the molar extinction coefficients of the singly hydroxy-bridged and oxo-bridged dimers, respectively.

$$A = \varepsilon_0 [Cr(OH)Cr^{3+}] + \varepsilon_1 [CrOCr^{2+}] \quad (2)$$

$$[Cr(OH)Cr^{3+}] = C_o / (1 + Ka/[H^+])$$

$$[CrOCr^{2+}] = C_o / (1 + [H^+]/K_a).$$

Cyclic Voltammetric Measurements

Electrochemical measurements were made utilizing a Bioanalytical Systems CV-1B triangular wave generator. The electrode configuration consisted of a Pt working electrode, an Au auxiliary electrode, and a saturated calomel reference electrode. All solutions were prepared with reagent grade acetonitrile, using mM concentrations of the species under investigation, and 0.100M TBAP (tetrabutyl ammonium perchlorate) as the supporting electrolyte. A three-compartment cell was utilized, with the reference electrode in 0.100 M $NaNO_3$ in the first compartment, buffering 0.100 M TBAP in acetonitrile solution in the middle compartment (to prevent water contamination of the working compartment), and the reactant solution, working and auxiliary electrodes in the third compartment. Junction potential compensation and correction to SHE (standard hydrogen electrode) was evaluated by standardizing versus HEF (hydroxyethyl ferrocene, E^o = 402 mV versus SHE).[25]

Kinetic Measurements

The kinetics of $[(tmpa)Cr(O)_2Cr(tmpa)]^{2+}$ base hydrolysis was monitored at 368 nm in 1-cm cells thermostated at six temperatures in the range 20.6 to 45.0 ^oC. The hydroxide ion concentration dependence of the rate was investigated in solutions containing 0.1-1.0 M NaOH and sufficient NaBr to maintain a constant ionic strength of 1.0 M; NaBr was shown to have no effect on the rate or product distribution of the base hydrolysis reaction

and was used in place of $NaClO_4$ because of the insolubility of the tmpa diol species in perchlorate media. The chromium reactant was generated in situ by injecting sufficient $[(tmpa)Cr(OH)_2Cr(tmpa)]Br_4$ to give an initial dioxo dimer concentration of 0.375 mM. Pseudo-first-order rate constants for the fast (k_{fast}) and slow (k_{slow}) components of biphasic $\ln(A_t-A_\infty)$ versus time traces were extracted from a consecutive first order analysis.[26] Least squares fits of the kinetic data to this consecutive first order scheme were found to be excellent over the entire hydroxide concentration and temperature ranges examined. Reported rate parameters are the mean of at least three determinations.

The kinetics of $[(tmpa)(L)CrOCr(L)(tmpa)]^{2+}$ (L = SCN^-, OCN^-, CN^-) and $(tmpa)Cr(NCS)_2^+$ base hydrolysis were monitored at 352, 347, 352, and 336 nm respectively. NaOH or KOH was used to vary $[OH^-]$, and appropriate amounts of $NaNO_3$, KNO_3, NaSCN or NaCl were added to maintain a constant ionic strength of 1.00 M. In all cases rate constants were obtained from the slope of linear first order plots of $\ln(A_t-A_\infty)$ versus time.

In the determination of thiocyanate formation during the course of base hydrolysis of the $(tmpa)(SCN)CrOCr(NCS)(tmpa)^{2+}$ cation, 0.1954g of 10 (2.000×10^{-4} mol) was dissolved into 190 mL of triply distilled H_2O and thermostated to 35.0 °C. 4.92 mL of 4.057 M NaOH (0.0200 mol) was added, and the total volume quickly brought to 200 mL. Aliquots of 10 mL were taken periodically, acidified to pH 3.0 by HNO_3 addition, and measured at 35.0 °C in 25 mL beakers. Readings were taken with a Metrohm/Brinkmann PH-104 digital meter after one minute (typical electrode response time was 30 seconds).

The kinetics of $[(tmpa)Cr(O)(CH_3COO)Cr(tmpa)]^{3+}$ formation was monitored in methanol at 336 nm in 1-cm cells thermostated to 25.0 °C. The acetate ion concentration dependence of the rate was investigated in solutions containing 0.0250 - 0.500 M $LiOAc{\cdot}2H_2O$ and sufficient LiBr to maintain a constant ionic strength of 0.500 M. LiBr was used because it does not react with the diol. Preliminary mixing experiments of the

diol with LiOAc in methanol resulted in the removal of one proton from a portion of the diol, giving a mixture of the doubly hydroxo-bridged and oxo-hydroxo-bridged species. Hence 4 was used in the reaction to assure that the starting material was in one form. Rate constants were obtained from linear first order analytical plots and are reported as the mean of at least three determinations.

Instrumentation

UV-visible and infrared spectra were acquired on Shimadzu UV-260 and Perkin Elmer 1600 series spectrophotometers, respectively. Kinetic measurements were carried out on a Perkin-Elmer Lambda 5 instrument.

Thiocyanate ion concentrations were determined with an Orion thiocyanate ion selective electrode (model 94-58) in conjunction with a Ag/AgCl reference electrode.

Magnetic susceptibility determinations were performed at ambient temperature on a Johnson-Matthey magnetic susceptibility balance, calibrated against $Hg[Co(SCN)_4]$. Reported magnetic moments are uncorrected for ligand and counterion diamagnetism. Magnetic susceptibility temperature dependence data were recorded with a S.H.E. Corporation VTS superconducting SQUID susceptometer. The sample bucket was fabricated from an Al-Si alloy obtained from S.H.E. Corp. The magnetic susceptibility of the sample bucket was measured independently over the temperature region of 6-300 K, and the magnetic data for all samples were then corrected for the bucket contribution. All of the samples were examined at a field of 5 kOe. Measurement and calibration procedures are described previously.[27] Magnetic susceptibilities corrected for diamagnetism by using Pascal's constants are expressed per dimer unit (i.e., 2 Cr ions per molecule) as a function of temperature. The model of an isolated Heisenberg dimer containing S = 3/2 ions with interaction Hamiltonian $H = -2JS_1 \cdot S_2$ was used to analyze the data for binuclear compounds 2, 4, 7, and 13. The susceptibility (χ') based on this model is:[27]

$$\chi' = \frac{Ng^2\mu_B{}^2}{kT} \cdot \frac{2e^{2J/kT} + 10e^{6J/kT} + 28e^{12J/kT}}{1 + 3e^{2J/kT} + 5e^{6J/kT} + 7e^{12J/kT}} . \quad (3)$$

where all of the parameters have their usual meaning. Taking into account the possibility of monomeric impurities that obey the Curie-Weiss expression, the magnetic data were fit to relationship (4) by a non-linear least squares procedure which weights the data so that the percent difference deviation is minimized; ρ and θ represent the impurity fraction and the Weiss constant, respectively.

$$\chi_m = \chi'(1-\rho) + Ng^2\mu_B{}^2S(S+1)\rho/3k(T-\theta) + TIP. \quad (4)$$

X-ray Diffraction Studies

The structure of $[(tmpa)Cr(OH)_2Cr(tmpa)]Br_4 \cdot 8H_2O$ was determined in collaboration with Dr. Charles F. Campana of Nicolet Instrument Corp. The structure was solved by direct methods on a Nicolet R3m/V diffractometer, utilizing 2428 unique reflections ($I > 3\,s(I)$). In full-matrix least squares refinements (SHELXTL PLUS), all non-hydrogen atoms were refined independently with anisotropic thermal parameters. The largest peak in a final difference map was 0.69 e/Å^3. Details of the crystal data, experimental conditions, and a summary of refinement details are given in Table 1. Bond lengths and angles presented here were selected from the refined data.

The structure of $[(tmpa)(SCN)CrOCr(NCS)(tmpa)]SCN_2$ was determined in collaboration with Dr. Harvey J. Schugar and Joseph A. Potenza of Rutgers University. The structure was solved by direct methods using 2231 unique reflections ($I > 3s(I)$ on an Enraf-Nonius CAD-4 diffractometer. All H atoms were located on difference maps but were not refined. The largest peak in a final difference map was 0.25 e/Å^3. Details of the crystal data, experimental conditions, and a summary of refinement details are given in Table 2. Bond lengths and angles were selected from the refined data.

Table 1
Crystallographic Data for $[(tmpa)Cr(OH)_2Cr(tmpa)]Br_4 \cdot 8H_2O$ [a]

formula	$C_{36}H_{54}N_8O_{10}Cr_2Br_4$
formula weight, g mol^{-1}	1182.49
space group	monoclinic, C 2/c
cell constants	a, Å 13.739(5)
	b, Å 14.858(5)
	c, Å 23.146(9)
	β, deg 94.72(3)
cell volume, $Å^3$	4709(3)
molecules/unit cell	4
ρ(calcd), g cm^{-3}	1.67
temp, °C	22
μ, cm^{-1}	38.7
radiation	Mo K_α; λ = 0.71073 Å
R_1	0.0658
R_2	0.0649

[a] Uncertainties in the last significant digit are shown in parentheses.

Table 2
Crystallographic Data for [(tmpa)(SCN)CrOCr(NCS)(tmpa)]SCN_2 [a]

formula	$Cr_2S_4ON_{12}C_{40}H_{36}$
formula weight, g mol^{-1}	933.04
space group	monoclinic, $P2_1/c$
cell constants	a, Å 11.3212(8)
	b, Å 14.805(1)
	c, Å c = 12.658(1)
	β, deg 7.82(1)
cell volume, $Å^3$	2101.8(5)
molecules/unit cell	4
ρ(calcd), g cm^{-3}	1.474
temp, °C	19(1)
radiation	Mo K_α; λ = 0.71073 Å
R_F	0.038
R_{wF}	0.052
G.O.F.	1.64

[a] Uncertainties in the last significant digit are shown in parentheses.

CHAPTER III

RESULTS

Doubly-Bridged Cr(III) Dimers

Synthesis

The syntheses of $[(tmpa)Cr(OH)_2Cr(tmpa)](ClO_4)_4 \cdot 4H_2O$ and the corresponding bromide salt in high yields were easily accomplished through the aerobic oxidation of (tmpa)Cr(II). Analogous preparations of $[(bpy)_2Cr(OH)_2Cr(bpy)_2](ClO_4)_4 \cdot 2H_2O$ and $[(phen)_2Cr(OH)_2Cr(phen)_2](ClO_4)_4 \cdot 3H_2O$ reproduced the compounds reported previously[28] from the direct reactions of chromium(III) with the aromatic amine ligands in refluxing $HClO_4$ over extended time periods. We also note that Hodgson and co-workers recently reported the synthesis of $[(tmpa)Cr(OH)_2Cr(tmpa)](ClO_4)_4 \cdot 4H_2O$ in 30% yield from the gradual addition of LiOH to a refluxing mixture of $[H_3tmpa](ClO_4)_3$ with chromium(III) nitrate, requiring a total reaction time of 5 hours.[29] Like the bipyridine and phenanthroline diols, $[(tmpa)Cr(OH)_2Cr(tmpa)]^{4+}$ ionizes to give oxo(hydroxo) and dioxo dimers, but only the former could be isolated pure in the solid state. The generality of oxidative chromium(III) diol synthesis in the presence of aromatic amine ligands is further indicated by the preparation of $[(dmpa)Cr(SO_4)(OH)_2Cr(dmpa)](S_2O_6) \cdot 3H_2O$[30] (dmpa = bis(2-pyridylmethyl)amine) from the aerobic oxidation of a $CrSO_4$-dmpa mixture.

X-ray Diffraction Analysis

X-ray diffraction analysis of $[(tmpa)Cr(OH)_2Cr(tmpa)]Br_4 \cdot 8H_2O$ (Figure 2) revealed a centrosymmetric dimer possessing a highly distorted octahedral N_4O_2 coordination sphere about Cr. The Cr-O-Cr (101.0^o) and O-Cr-O (78.9^o) angles defined by the $Cr(OH)_2Cr$ core closely resemble those reported for $[(H_2O)_4Cr(OH)_2Cr(H_2O)_4]^{4+}$ (101.8^o and 78.2^o, respectively)[31] and an extensive family of $N_4Cr(OH)_2CrN_4$

dimers.[32] While the present work was in progress, Hodgson and co-workers reported the structure of $[(tmpa)Cr(OH)_2Cr(tmpa)](ClO_4)_4 \cdot 4H_2O$, noting that two possible isomers are distinguished by having the two bridgehead N atoms either cis or trans relative to the Cr_2O_2 core.[29] Our investigation of $[(tmpa)Cr(OH)_2Cr(tmpa)]Br_4 \cdot 8H_2O$ confirms their prediction (on steric grounds) and finding that the trans, centrosymmetric form should be preferred over the cis isomer.[29] Vital structural parameters characteristic of the perchlorate salt,[29] including both bond lengths and angles from Cr to ligated N and O atoms, agree well with those reported here.

Spectrocopic Analysis

The diol UV-visible spectrum exhibits only three prominent features, including d-d bands at 18,500 (= 10Dq) and 26,000 cm^{-1}; the intense 38,300 cm^{-1} band is assigned to a tmpa ligand-centered π-π^* transition, by comparison with the spectrum of $[H_3tmpa](ClO_4)_3$. The electronic spectrum of $[(tmpa)Cr(OH)_2Cr(tmpa)]^{4+}$ reported here is in reasonable agreement with the literature.[29]

Ionization Constant Determinations

Ionization constants (25.0 °C, I = 0.1 M) of the $[(tmpa)Cr(OH)_2Cr(tmpa)]^{4+}$ ($pK_{a1} = 7.50 \pm 0.05$) and $[(tmpa)Cr(O)(OH)Cr(tmpa)]^{3+}$ ($pK_{a2} = 12.4 \pm 0.1$) ions, derived from a 367 nm spectrophotometric titration (Figure 3) of diol 2, are quite similar to the literature values[28] for the corresponding bpy ($pK_{a1} = 7.60$, $pK_{a2} = 11.9$) and phen ($pK_{a1} = 7.40$, $pK_{a2} = 11.8$) dimers. Non-linear least squares extinction coefficients (eq 1, expressed per mole of dimer) are: $\varepsilon_0 = 188 \pm 12$; $\varepsilon_1 = 1750 \pm 10$; $\varepsilon_2 = 3090 \pm 20$ $M^{-1}cm^{-1}$. The latter two values are in excellent agreement with the 367 nm extinction coefficients measured directly (per mole of dimer) for $[(tmpa)Cr(O)(OH)Cr(tmpa)]^{3+}$ (1760 $M^{-1}cm^{-1}$) and $[(tmpa)Cr(O)_2Cr(tmpa)]^{2+}$ (3060 $M^{-1}cm^{-1}$) at pH 10.0 and 14.5, respectively. Although $[(tmpa)Cr(O)_2Cr(tmpa)]^{2+}$ is considerably more susceptible to decomposition in

basic solution than the bpy and phen dioxo dimers[28], the two-step ionization of $[(tmpa)Cr(OH)_2Cr(tmpa)]^{4+}$ was shown to be quite reversible when the $Cr(O)_2Cr$ complex was not allowed to stand at 25.0 °C for longer than 15 seconds.

Magnetic Properties

The magnetic characteristics of $[(tmpa)Cr(OH)_2Cr(tmpa)]^{4+}$ are consistent with expectations for a weakly antiferromagnetically-coupled dimer. The magnetic susceptibility (295.15 K) of 2 was found to be $(9.10 \pm 0.10)\times10^{-6}$ cgs units, equivalent to a μ_{eff} of 3.57 $\pm$ 0.05 μ_B per chromium atom; Hodgson and co-workers report[29] a singlet-triplet energy gap (-2J) of 30.58 cm^{-1}. The magnetic suceptibility (295.15 K) of oxo(hydroxo) dimer 4 is $(6.05 \pm 0.10) \times10^{-6}$ cgs units, giving a μ_{eff} value of 2.72 $\pm$ 0.05 μ_B (or approximately 2 unpaired electrons) per chromium atom. Monomer 20 exhibits a magnetic susceptibility (296.95 K) of $(11.0 \pm 0.10)\times10^{-6}$ cgs units, corresponding to an effective magnetic moment (3.82 $\pm$ 0.05 μ_B) close to the spin-only value for three unpaired electrons per Cr atom (3.87 μ_B).

Parameters derived from least squares fits of χ', T points to equation (4) for compounds 2 and 4 are summarized in Table 3. Comparisons of experimental points with calculated lines for the dependences of 2 and 4 magnetic susceptibilties on temperature are shown in Figures 4 and 5, respectively. In each case, the Heisenberg exchange model provides a mechanism for a quantitative fitting of the data.

Base Hydrolysis of the Di-μ-Oxo Tmpa Dimer

Product Identification

The base hydrolysis reaction of $[(tmpa)Cr(O)_2Cr(tmpa)]^{2+}$ proceeds according to the stoichiometry of equation (5), and gives no chromium byproducts detectable by cation exchange chromatography.

$$[(tmpa)Cr(O)_2Cr(tmpa)]^{2+} + 2\,H_2O \longrightarrow 2\,[Cr(tmpa)(OH)_2]^{+}. \qquad (5)$$

In support of this stoichiometry, it was demonstrated that 2.00 ± 0.01 mol of OH^- is consumed per mol of unionized diol reactant consumed. 2 (0.841 mmol) was added to 200 mL of distilled water originally at pH 7.75, and the temperature was raised to the boiling point, giving a clear, deep purple solution. Upon the addition of 1.68 mmol of NaOH, the color changed immediately to dark green and transformed to dark blue after continued heating for 10 minutes. The pH of the cooled product solution was found to be 8.30, and a single blue band (complex 22) was eluted from a SP-Sephadex C-25 cation exchange column (0.1 M $LiClO_4$ eluant at pH 10.0).

Attempts to isolate the blue diol base hydrolysis product in crystalline form were unsuccessful with several counterions (ClO_4^-, $S_2O_6^{2-}$, SO_4^{2-}) owing to the very high solubility of 22 and its tendency to lose tmpa upon long-standing in alkaline media, analogous to the behaviors of the bpy and phen diol systems.[28] Taken together, stoichiometric, spectrophotometric, and derivative preparation results provide a convincing basis for attributing the formula $[Cr(tmpa)(OH)_2]^+$ to 22, which exhibits d-d absorptions at 401 (e 68 $M^{-1}cm^{-1}$) and 578 nm (e 53 $M^{-1}cm^{-1}$). Upon acidification, 22 is reversibly protonated (in the pH 2-4 range) to a red complex (23) (λ_{max} 375 nm (ε 71 $M^{-1}cm^{-1}$), 501 (91)), which is thought to be $[Cr(tmpa)(H_2O)_2]^{3+}$. The relative positions of the lowest energy (= 10Dq) spin-allowed bands of 22, $[(tmpa)Cr(OH)_2Cr(tmpa)]^{4+}$, and 23 at 17,300, 18,500 and 20,000 cm^{-1}, respectively, are consistent with the spectrochemical series OH^- < bridging OH^- < H_2O. Like $[Cr(tmpa)(OH)_2]^+$, $[Cr(tmpa)(H_2O)_2]^{3+}$ is highly soluble and could not be precipitated in pure form; $LiClO_4$ crystallized before 23 in perchlorate media. For this reason, 23 was converted to $[Cr(tmpa)(NCS)_2](ClO_4)$ in the presence of excess thiocyanate to provide evidence for a monomeric precursor with two replacable ligands derived from the solvent. The elemental analysis, magnetic susceptibility, infrared and UV-visible spectra of complex 20 indicate a simple Cr(III) monomer with a N_6 ligand field. It should also be noted that 20 could be obtained from

diol 2 upon extended heating in the presence of excess NaSCN, under conditions where the acid hydrolysis of 2 was shown to be negligible. The red species attributed to $[Cr(tmpa)(H_2O)_2]^{3+}$ did not give the characteristic spectrum of $[(tmpa)Cr(O)(OH)Cr(tmpa)]^{3+}$ when the pH was raised to 10, indicating the absence of $[(tmpa)Cr(OH)_2Cr(tmpa)]^{4+}$ in re-acidified solutions of the diol base hydrolysis product.

Kinetic Analysis

Biphasic plots of $\ln(A_t-A_\infty)$ versus time observed in kinetic studies of reaction (5) ($[OH^-]$ = 0.1 to 1.0 M) were successfully fit to the integrated rate expression for consecutive first order reactions, as exemplified by Figure 6. Repetitive spectra (300-700 nm) recorded over the entire period of the base hydrolysis reaction demonstrated that absorbance decreases at the monitoring wavelength of 368 nm are typical of those observed throughout the entire wavelength interval. Rate measurements at pH < 12 demonstrated that the base hydrolysis reactivity of $[(tmpa)Cr(O)(OH)Cr(tmpa)]^{3+}$ is negligible as compared with that of $[(tmpa)Cr(O)_2Cr(tmpa)]^{2+}$. Observed pseudo-first-order rate constants for fast and slow components at six temperatures in the range 20.6 - 45.0 °C are displayed in Table 5. Plots of k_{fast} and k_{slow} versus $[OH^-]$ (Figure 7) indicate that the species responsible for fast and slow 368 nm absorbance changes both decay via two parallel pathways, zeroth and first order in hydroxide ion (equations 6 and 7).

$$k_{fast} = k_o + k_{OH}[OH^-]. \quad (6)$$

$$k_{slow} = k_o^s + k_{OH}^s[OH^-]. \quad (7)$$

Rate parameters derived from linear least squares analyses of k_{slow} and k_{fast} versus $[OH^-]$ correlations are summarized in Table 5, and $\Delta H^{\ddagger}$, $\Delta S^{\ddagger}$ values corresponding to the rate constants k_o, k_{OH} , k_o^s and k_{OH}^s (from linear Eyring plots of ln(k/T) versus 1/T) are given in Table 6. Unfortunately, kinetic data for the considerably slower[28] bpy and phen diol base hydrolysis reactions are not available for comparison with the present results.

Base Hydrolysis Intermediate Identification

Since biphasic kinetics may reflect either consecutive or parallel first order reaction sequences,[26] the isolation and characterization of an intermediate derived from the partial base hydrolysis of $[(tmpa)Cr(O)_2Cr(tmpa)]^{2+}$ would greatly strengthen our interpretation of the rate data. Such an intermediate was, in fact, identified through chromatographic separations (5 °C) of base hydrolysis reaction mixtures quenched before full conversion of chromium to $[Cr(tmpa)(OH)_2]^+$ was achieved. A solution containing 0.0594 g of 2 (0.05 mmol) dissolved in 24 mL of water was thermostated at 40.0 °C and mixed with 0.625 mL of 4.00 M NaOH. This reaction mixture was diluted to 25 mL and then partially quenched after five minutes by pouring into 25 mL of distilled water ice. Upon adsorption of the mixture onto a 20x2.5 cm cation exchange column equilibrated with 0.05 M NaOH, a leading blue band emerged and was separated cleanly from a dark green trailing fraction by elution with 0.05 M NaOH. When the eluant was changed to 0.20 M NaBr/0.05 M NaOH, the remaining chromium-containing species separated sharply into a leading deep green band, followed by a lighter green component. The 300-700 nm electronic spectra of all three bands were acquired immediately following elution, and Cr analyses were carried out so that extinction coefficients could be determined. The first and third fractions were identified as $[Cr(tmpa)(OH)_2]^+$ and residual reactant (as $[(tmpa)Cr(O)(OH)Cr(tmpa)]^{3+}$), respectively. The middle, deep green component (24), which exhibited peaks at 580 (ε 85 $M^{-1}cm^{-1}$) and 364 nm (ε 415 $M^{-1}cm^{-1}$), may be classified as an intermediate since irreversible decay to the ultimate product, $[Cr(tmpa)(OH)_2]^+$, was observed when 24 was allowed to stand in 0.05 M NaOH at room temperature. The intermediacy of 24 is further demonstrated by the observation that the percentage of ΔA_{368nm} corresponding to the fast phase in kinetic studies (89 %) is independent of $[OH^-]$ and agrees well with that predicted (90 %) from the extinction coefficients of $[(tmpa)Cr(O)_2Cr(tmpa)]^{2+}$ and 24 at 368 nm. Species 24 evidently is dimeric, since acidification of the dark green fraction (to pH 1)

immediately following elution gave $[(tmpa)Cr(OH)_2Cr(tmpa)]^{4+}$, identified from its electronic spectrum and that of ionization product 4 (measured after neutralizing the acidified solution with NaOH and adjusting the pH to 10). As was noted above, the tmpa diol is not regenerated by the acidification of final product 22 .

In separations of $[(tmpa)Cr(O)_2Cr(tmpa)]^{2+}$ hydrolysis products carried out at pH 10.0 and 11.0, three well-separated components were isolated as before, and fractions 1 and 3 once again contained 22 and 4, respectively. The middle fraction attributed to the reaction intermediate was deep blue instead of dark green, however, and exhibited absorption maxima (pH 10) at 574 (90 $M^{-1}cm^{-1}$) and 372 nm (180 $M^{-1}cm^{-1}$). Addition of NaOH to this middle blue component (25) caused a reversible (with dilute $HClO_4$) color change to green above pH 12. This green species, an apparent ionization product of 25, was shown to be identical to intermediate 24 on the basis of its UV-visible spectrum. Attempts to isolate solids from the chromatographic fractions containing 24 and 25 were futile, resulting only in quantitative conversions to monomer 22.

Knowing k_{fast} and k_{slow} for the hydrolysis of $[(tmpa)Cr(O)_2Cr(tmpa)]^{2+}$ in 0.1 M NaOH at 40.0 °C, it is possible to estimate the time at which the intermediate concentration is maximal (5 minutes) from the relationship $t_{max} = \ln(k_{fast} / k_{slow})/(k_{fast} - k_{slow})$[26]. An attempt was made to quantitate the actual amounts of 22, 24 and unreacted dioxo dimer present at t_{max}, for comparison with the theoretical values calculated from k_{fast} and k_{slow} under the reaction conditions. A solution of 2 (0.0397 g, 33.4 μmol) in 24 mL of H_2O was rapidly mixed with 0.625 mL of 4.00 M NaOH and diluted to 25 mL in a volumetric flask thermostated at 40.0 °C. After 5 minutes, the reaction mixture was poured into 25 mL of ice and immediately adsorbed onto a 20x2.5 cm cation exchange column equilibrated with 0.05 M NaOH. Upon elution of the column with 0.05 M NaOH and 0.05 M NaOH/0.2 M NaBr, the three bands were collected as described above and quantitatively diluted in preparation for chromium analyses. Observed and calculated yields (as Cr μmols) of

$[Cr(tmpa)(OH)_2]^+$ (obsd, 22.4; calcd, 5.2), intermediate 24 (obsd, 31.0; calcd, 35.7), and $[(tmpa)Cr(O)(OH)Cr(tmpa)]^{3+}$ (obsd, 13.1; calcd, 25.8) are in fair agreement, with actual yields deviating as would be expected for incomplete quenching of the hydrolysis reaction after 5 minutes. Nevertheless, the relatively close correspondence between actual and theoretical yields of 24 is a good indication that this complex is an authentic hydrolysis intermediate. Total recovery of Cr from the cation exchange column was 99.6% (66.5 μmol).

μ-Oxo Dimers

Synthesis

The preparations of $[(tmpa)LCrOCrL(tmpa)]^{2+}$ ($L = SCN^-, NCO^-, CN^-, N_3^-, Cl^-$) by displacement of a single hydroxo bridge from $[(tmpa)Cr(OH)_2Cr(tmpa)]^{4+}$ according to reaction (8) proceed with excellent yields.

$$[(tmpa)Cr(OH)_2Cr(tmpa)]^{4+} + 2\,L^- \longrightarrow [(tmpa)LCrOCrL(tmpa)]^{2+} + H_2O. \qquad (8)$$

Although the thiocyanate complex was prepared in a boiling aqueous solution, better yields are generally obtained from refluxing acetonitrile, even though Na^+ or K^+ salts of the L^- ligands are only slightly soluble in this medium. The dimers with $L = N_3^-$ and Cl^- cannot be isolated from aqueous solutions at all, owing to dimer cleavage (N_3^-) or diol regeneration (Cl^-) side reactions. Indeed, the success of the aqueous synthetic route depends on the precipitation of the oxo dimer prior to the onset of decomposition side reactions.

Not all anions examined gave linear, oxo-bridged products when refluxed with 2 in CH_3CN. Indeed the reactions of both the pyrazolate and imidizolate anions afforded only the single deptrotonation product 4, while Br^- and I^- both did not react with the diol at all. Interestingly, all attempts to prepare $[(tmpa)LCrOCrL(tmpa)]^{4+}$ species from reactions of the diol with neutral monodentate ligands such as ammonia, pyridine, and N,N-

dimethylformamide have failed, in both aqueous and acetonitrile solutions. In addition, acetonitrile solutions of the diol are unchanged upon refluxing for 12 hours in the presence of a 10-fold excess of dmf or equimolar pyridine and pyridinium perchlorate.

X-ray Diffraction Analysis

X-ray diffraction analysis of $[\{Cr(tmpa)(NCS)\}_2O](NCS)_2$ revealed the cation (Figure 8) to be a centrosymmetric dimer having a linear Cr-O-Cr bridge and distorted octahedral N_5O coordination about Cr. Owing to the limited bite of the tmpa ligand, the trans N-Cr-N' angles (range 160.8(1)-173.65(7)°) and some of the cis N-Cr-N' angles (range 79.75(9)-101.1(2)°) deviate substantially from the ideal values. The Cr-N(3) distance (2.12 Å) is significantly longer than the average of the other four Cr-N distances (2.07 Å)[6], consistent with a trans effect arising from the tightly bound oxo group. Unambiguous trans effects were not observed in the parent basic rhodo ion[20] and $[Cr(TPyEA)(NCS)]_2O^{2+}$ ion[21] within the reported esd's of the Cr-N distances. The Cr-O distance in 7 (1.800 Å) is slightly shorter than those reported for the $[(NH_3)_5Cr]_2O^{4+}$ (1.821 Å)[20] and $[Cr(TPyEA)(NCS)]_2O^{2+}$ (1.815 Å)[21] ions.

As compared with the doubly-bridged $[(tmpa)Cr(OH)_2Cr(tmpa)]^{4+}$ dimer, the Cr-O bond length in the oxo dimer is considerably shorter (1.800 versus 1.937 Å) while the Cr-pyridyl N distances are somewhat longer (averages of 2.090 Å versus 2.048 Å). Overall, the conformations of the tmpa pyridine rings in the oxo- and dihydroxo-bridged dimers are quite similar.

An important structural distinction should be noted, however, with implications for the mechanism of hydroxo bridge displacement by SCN^- in the conversion of $[(tmpa)Cr(OH)_2Cr(tmpa)]^{4+}$ to $[(tmpa)(SCN)CrOCr(NCS)(tmpa)]^{2+}$, which occurs readily in both acetonitrile and aqueous solutions. Whereas the apical tmpa nitrogen atoms of the diol are trans to hydroxo bridge O(1) and O(2) atoms, the apical nitrogens of the oxo-bridged dimer are both trans to thiocyanate ligands. It is not immediately obvious how

the substitution of one OH^- bridge by two non-bridging nucleophiles induces the rearrangement of the two tetradentate tmpa ligands such that neither of the nitrogen atoms originally trans to oxygen retains that orientation in the Cr-O-Cr product.

Spectrocopic Analysis

Electronic spectra of dimers 7, 11-14 in acetonitrile solution (Table 7, the example spectrum of 7 shown in Figure 9) exhibit a common intense ($\varepsilon \approx 10^4\ M^{-1}cm^{-1}$), sharp band in the 349-355 nm interval coupled with a second, poorly-resolved feature near 420 nm ($\varepsilon \approx 3x10^3\ M^{-1}cm^{-1}$). Unfortunately, these dominant bands prevent the resolution of d-d transitions, which appear as shoulders between 440 and 460 nm and plateaus with shallow maxima in the vicinity of 570 nm. Both of the dominant near-ultraviolet bands exhibit apparent splittings into components separated by approximately $1\text{-}2x10^3\ cm^{-1}$. In the case of the dimer with the least symmetric ligand field, $[tmpa)ClCrOCrCl(tmpa)]^{2+}$, maxima were resolved at {23,800; 25,700} and {27,800; 28,600} cm^{-1} for all four components of the split principal transitions.

Assignment of the Principal Oxo-Dimer Transition

In order to probe the possibility that the strongest near-ultraviolet band of $[(tmpa)LCrOCrL(tmpa)]^{2+}$ dimers corresponds to a metal-to-bridging oxygen charge transfer transition, the transition energy for $[(tmpa)(SCN)CrOCr(NCS)(tmpa)]^{2+}$ was determined in thirteen solvents and plotted as a function of $(1\text{-}D_{op})/(2D_{op}+1)$ according to the method of Meyer and co-workers;[33] D_{op} represents the optical dielectric constant of the solvent, computed as (refractive index) from sources tabulated in reference 33. Spectra were found to be invariant with time, demonstrating that 7 is inert to NCS^- substitution and bridge cleavage reactions in all solvents considered. Given that the ground state of the oxo-bridged dimer does not have a permanent dipole moment and assuming that the 355 nm (CH_3CN) band is, in fact, a MLCT transition, a plot of band energy versus (1-

$D_{op})/(2D_{op}+1)$ is expected to be linear with slope of μ^2/b^3, where μ and b are the dipole moment of the excited state and the radius of the chromophore, treated as a non-polarizable sphere, respectively.[33] The alternative assignment of this band as a LMCT or MLCT transition involving the tmpa ligand may be dismissed in view of its absence in the spectra of $[Cr(tmpa)Cl_2]^+$ and related monomeric (tmpa)Cr(III) complexes.

As is shown in Figure 10, the plot of band energy versus $(1-D_{op})/(2D_{op}+1)$ for 7 is reasonably linear, with slope of 4460 ± 410 cm^{-1} and correlation coefficient of 0.995, confirming the MLCT assignment of the transition. Considering only the N and O donor atoms to be contained within the chromophore sphere (excluding the full pyridyl rings), b is estimated at 3.9 Å from the sum of Cr-O and average Cr-N bond lengths. On this basis, the excited state dipole moment and dipole length are estimated at 7.3 ± 0.5 D and 1.5 ± 0.2 Å, respectively. Considering the highly approximate nature of this calculation[33], the close agreement between the Cr-O bond length of 1.8 Å and dipole length computed from the solvent dependence of the absorption spectrum supports the assignment of the dominant near-ultraviolet bands of dimers 7, 11-14 to a transition exhibiting substantial Cr(III)-to-bridging O MLCT character.

Electrochemical Measurements

The cyclic voltammograms of all five $[(tmpa)LCrOCrL(tmpa)]^{2+}$ complexes in acetonitrile solution (0.1 M $(n\text{-}Bu)_4NClO_4$ supporting electrolyte) exhibit a reversible one-electron oxidation wave in the 0.96 to 1.17 V interval (Table 7) with peak-to-peak separations of 70-75 mV at a sweep rate of 50 mV/second and anodic to cathodic peak current ratios within experimental error of 1.0. A coulometric determination at a constant working electrode potential 0.3 V more positive than $E_{1/2}$ showed that $n = 0.93 \pm 0.05$ for 7. Although these $[(tmpa)LCrOCrL(tmpa)]^{2+}$ oxidation waves are fully reversible on the cyclic voltammetric time scale of 10 to 60 seconds, it was not possible to isolate the

presumed mixed-valence Cr(III)-O-Cr(IV) oxidation product of 7 subsequent to a bulk electrolysis experiment which required greater than 1 hour to complete.

μ-Hydroxo Dimer Acid Dissociation Constants

Spectrophotometric titrations of 7, 11-13 (Figure 11) revealed that the oxo-bridged dimers accept one proton to give purple $[(tmpa)LCr(OH)CrL(tmpa)]^{3+}$ conjugate acids which exhibit pK_a values that are highly sensitive to the nature of the L group (Table 7), reminiscent of rhodo erythro cation acid-base characteristics.[2] The electronic spectra of these protonation products (Table 7) lack the intense near-ultraviolet bands of the oxo-bridged precursors, exhibiting only comparatively weak d-d bands and a SCN^--to-Cr(III) LMCT band at 327 nm similar to that reported for $[Cr(tmpa)(NCS)_2]^{+}$[7] in the case of the thiocyanate complex. All of the hydroxo-bridged (tmpa)Cr(III) dimers are stronger acids than $[(NH_3)_5Cr(OH)Cr(NH_3)_5]^{5+}$ (acid rhodo ion, $pK_a = 7.63$)[2] by 3-7 orders of magnitude, which is contrary to expectations on the basis of charge separation considerations alone.

Magnetic Properties

Parameters derived from least squares fits of χ', T points to eq (4) for compounds 7, and 12 are summarized in Table 3. Comparisons of experimental points with calculated lines for the dependency of 7 magnetic susceptibilty on temperature is shown in Figure 12. The Heisenberg exchange model used for 2 and 4 was also used successfully in the fitting of the data for these two oxo dimers. The presence of strong antiferromagnetic coupling between the Cr atoms of linear, oxo-bridged dimers 7 and 12, mediated by $d\pi(Cr)$-$p\pi(O)$ orbital overlaps, is reflected in considerably larger singlet-triplet gaps of 509 and 580 cm^{-1}, respectively, on the same order as that reported for the the basic rhodo ion (450 cm^{-1}).[6] Perchlorate, bromide and nitrate salts of $[(tmpa)(SCN)CrOCr(NCS)(tmpa)]^{2+}$ all exhibited 300 K μ_{eff} values of $0.8 \pm 0.1\ \mu_B$,

corresponding to approximately 0.3 unpaired electrons per chromium atom. No signal could be detected in epr measurements (Varian E-109 spectrometer) on 7 in CH_3CN at ambient and liquid nitrogen temperatures.

Base Hydrolysis of $(tmpa)(SCN)CrOCr(NCS)(tmpa)^{2+}$

Product Identification

To determine the ultimate products of the base hydrolysis of the $[(tmpa)(SCN)CrOCr(NCS)(tmpa)]^{2+}$ cation, a 2.00 mM solution of 7 was prepared by dissolving 0.0104 g into 50 mL of 0.050 M NaOH, and thermostated to 50.0 °C. The color of the solution changed from deep golden brown to light blue within one hour. After two hours (to insure full reaction) the spectrum of the solution was taken from 700 to 300 nm, revealing two broad bands at 578 and 400 nm, and a sharp band at 262 nm. The blue species was found to elute as one band with 0.100M $LiClO_4$ at pH 10 from a SP-Sephadex C-25-120 cation exchange column. This single product's spectral features and elution behavior identify it as the $(tmpa)Cr(OH)_2^{+}$ cation (22), the same species found in the base hydrolysis of the $(tmpa)Cr(O)_2Cr(tmpa)^{2+}$ cation. As further evidence for the assignment of this product to $(tmpa)Cr(OH)_2^{+}$, an acidified solution changes color to red, with a shift in band positions from 578 to 501 nm, and 400 to 375 nm, as found previously for conversion to the $(tmpa)Cr(H_2O)_2^{3+}$ cation (23). From these results, the balanced base hydrolysis reaction equation can be written as

$$[(tmpa)(NCS)Cr_2O]^{2+} + 2\,OH^- + H_2O \rightarrow 2\,(tmpa)Cr(OH)_2^{+} + 2\,SCN^-. \qquad (9)$$

Repetitive scans (700-300 nm) of the monomeric $(tmpa)Cr(NCS)_2^{+}$ cation in 0.100 M NaOH showed convergence on the spectrum of the $(tmpa)Cr(OH)_2^{+}$ cation, with loss of absorbance at 336 (peak) and 313 nm (shoulder). During hydrolysis, the 313 nm feature was resolved as a peak, due to a more rapid decay at 336 nm. Kinetic determinations were performed at 336 nm on the assumption that the rapid loss in absorbance at this wavelength

corresponds to departure of the first SCN^-. From these observations, the reaction monitored at 336 nm is

$$(tmpa)Cr(NCS)_2^+ + OH^- \longrightarrow (tmpa)Cr(NCS)(OH)^+ + SCN^-, \quad (10)$$

with very little contribution of $(tmpa)Cr(NCS)(OH)^+$ to the absorbance.

Determination of Reaction Intermediates

To probe the existence of an isolable intermediate during the base hydrolysis of 9, SP C-25-120 Sephadex cation exchange separations were performed on quenched basic solutions of 9 under varying conditions. Typical results for at least two trials under each set of conditions are summarized as follows:

(a) Separation of Monomeric and Dimeric Products

A total of 0.0326 g of 2 (3.16×10^{-5} mol) was dissolved into 24 mL of triply distilled H_2O in a 25 mL volumetric flask and thermostated to 45.0 °C. After 15 minutes 0.318 mL of 3.92 M standard NaOH (1.25×10^{-3} mol) was added and the volume brought quickly to 25 mL. 9 was allowed to react at 45.0 °C for the calculated $t_{1/2}$ of 14.4 minutes. The flask was then quickly placed in a water/ice mixture for rapid cooling, and the contents quickly adsorbed on a 15x2.5 cm column that had been equilibrated with 5.00 mM NaOH for at least one hour at 5 °C. Upon complete product adsorption the top of the column was an intense brown/green color, with slow emergence of a leading blue band. When the eluent was changed to 5.00 mM NaOH / 0.300 M NaBr, two bands were resolved, with the first blue band separated cleanly from the trailing brown/green band, which moved much more slowly down the column. The first blue band was collected and identified by its UV-visible spectrum as 22. To speed elution of the remaining band, the eluent was changed to 5.00 mM NaOH / 0.500 M NaBr. The brown/green band showed hints of further resolution, but never clearly separated into more than one component and was collected as one fraction. This fraction was found by its 200-700nm spectrum to contain

unreacted 9. Both fractions and the recovered Sephadex were subjected to chromium analysis, yielding a total chromium recovery of >98%, with 30% recovered as the monomer and 70% as the second fraction.

(b) Dimeric Intermediate Isolation

In an attempt to resolve the components of the second fraction in the previous separation, eluents containing ClO_4^- were used with the expectation of achieving separation on the basis of solubility differences. The reaction conditions of 0.050 M NaOH at 45.0 °C and 14.4 minutes were repeated, and the quickly cooled solution was again adsorbed on an 5.00 mM NaOH-equilibrated Sephadex column at 5 °C. Upon complete adsorption the top of the column was the same intense brown/green color, with a blue leading edge as before. When the eluent was changed to 5.00 mM NaOH / 0.100 M $LiClO_4$, the top brown/green band quickly precipitated, leaving a fine brown solid dispersed throughout the top 1 cm of Sephadex. The blue band separated cleanly, and moved down the column at a moderate pace. Upon switching to the eluent 5.00 mM NaOH / 0.300 M $LiClO_4$ a green band cleanly separated from the brown precipitate. and moved slowly down the column. The leading blue band was collected and determined to be the product 22 as before. The eluent was then changed to 5.00 mM NaOH / 0.500 M $LiClO_4$, and the green fraction (26) was collected for spectral and chromium analysis. This intermediate exhibited peaks at 566 nm (ε 85 M^{-1} cm^{-1}) and 364nm (ε 450 M^{-1} cm^{-1}), and when acidified converts instantaneously to the $(tmpa)Cr(OH)_2Cr(tmpa)^{4+}$ cation (2), identified by its peaks at 540 and 385 nm. Both fractions and the recovered Sephadex were treated with basic peroxide, and their chromium contents were determined as before. Total recovery was at least 98%, with 30% belonging to the monomeric fraction, 10% to the green base hydrolysis intermediate, and the remaining 60% to the precipitated solid recovered from the column. A SCN^- analysis performed on the intermediate, after conversion to 2 by acidifying to pH 3

and adjusting to an ionic strength of 0.100 M with $NaNO_3$, indicated less than 0.1 mol SCN^- per mole of dimer, indicating loss of both SCN^- ligands.

The comparison between this green intermediate and the intermediate 24 found in the base hydrolysis of the $(tmpa)Cr(O)_2(tmpa)^{2+}$ cation is striking. Both are unstable in basic solution at room temperature, and hydrolyze partially even on the time scale of spectral measurement. Hence it is very difficult to obtain the intermediate in the absence of at least some 22. Nevertheless, good agreement between peak positions and molar extinction coefficients { 364 nm (ε 450) versus 364 nm (ε 415), 566 nm (ε 85) versus 580 nm (ε 85) }, lack of SCN^-, elution as a 2+ species, and ring closure to 2 in acid provides convincing evidence for a common assignment to $[(tmpa)(OH)CrOCr(OH)(tmpa)]^{+2}$ (24).

(c) Diol Isolation From Acid-quenched Mixtures

The reaction conditions of 0.050 M NaOH at 45.0 °C and 14.4 minutes were repeated, but this time the quickly cooled solution was acidified to 1.0 mM H^+ by addition of 0.63 mL of standard 2.02 M HBr. This solution was then adsorbed on an 1.00 mM HBr-equilibrated Sephadex column at 5 °C. Upon elution with 1.0 mM HBr/0.100 M NaBr, there was no movement of any Cr-containing species. When the eluent was changed to 1.0 mM HBr/0.300 M NaBr, a clean separation was achieved over the course of 15 minutes resolving a leading brown band, a red middle band, and a purple top band, thought to be 2+, 3+, and 4+ species, respectively. When the eluent was changed to 1.0 mM HBr/0.500 M NaBr, the initial brown and second red fractions were collected. To hasten the elution of the third purple fraction, the eluent was changed to 1.0 mM HBr/1.00 M NaBr. The first brown fraction was identified from its spectral features as unreacted starting material, the second fraction was identified as 23, the protonation product of 22, and the third as diol 2. The two characteristic diol peaks were found at 385 nm (ε 110 M^{-1} cm^{-1}) and 540 nm (ε 130 M^{-1} cm^{-1}). Total chromium recovered was found to be an average 99%, with 24% recovered as monomer, 32% as diol, and 44% as unreacted dimer.

A summary of the separation results and proposed product distribution for the three separation types is presented in Table 8. In (a) separations employing NaBr/NaOH eluents, the ability to separate only 30% as the leading blue monomeric band and 70% as the trailing brown dimeric band is expected on the basis of charge alone. The 6% difference between the proposed 24% and isolated 30% of monomer is attributed to furthur hydrolysis of 24 during separation. In (b) separations employing $LiClO_4$/NaOH eluents, intermediate 24 was isolated with 60% precipitation consistent with 16% intermediate $[(tmpa)(SCN)CrOCr(OH)(tmpa)]^{2+}$ (26) and 44% unreacted $[(tmpa)(SCN)CrOCr(NCS)(tmpa)]^{2+}$. In (c) separations employing NaBr/HBr eluents, the 32% diol yield implies ring closure of 16% 26 and 16% 24. The 24% found in monomeric form 23 is 6% less than NaOH eluent separations due to complete conversion of 16% 26 to the stable diol before separation.

Although intermediate 26 was never isolated and identified separately, the presence of a dimeric 2+ intermediate that ring-closes to diol with acid and has low solubility in ClO_4^- solutions is inferred from the separation results. The $[(tmpa)(SCN)CrOCr(OH)(tmpa)]^{2+}$ formulation proposed for 26 has appeal when one considers that stepwise loss of two equivalents of SCN^- is strongly suggested by the isolation of 24.

Kinetics

In sharp contrast with the consecutive first order base hydrolysis kinetics observed with the $[(tmpa)Cr(O)_2Cr(tmpa)]^{2+}$ cation, oxo dimers 7, 12, and 13 exhibited excellent pseudo first order decay curves. Rate constants derived from the slopes of linear least squares fits of $\ln(A_t-A_\infty)$ versus time plots were remarkably consistent over a series of trials, with correlation coefficients greater than 0.999 being typical over at least 95% of the total absorbance change.

However, unlike the base hydrolysis of the $[(tmpa)Cr(O)_2Cr(tmpa)]^{2+}$ cation, all three oxo dimers showed rate saturation in hydroxide ion, with the observed rate constants taking the form shown in equation (11).

$$k_{obs} = \frac{(AB)\,[OH^-]}{1 + B\,[OH^-]}. \qquad (11)$$

A summary of the rates found at various hydroxide ion concentrations and several temperatures can be found in Table 9. These rates were determined at an ionic strength of 1.00 M, employing NaOH and $NaNO_3$ to maintain constant ionic strength. Upon examination of the saturation curve seen in the k_{obs} versus $[OH^-]$ plot for 7, there arose some doubt as to whether the effect is truly saturation in hydroxide or rather rate retardation by nitrate ion. In order to answer this question, the hydroxide dependence was repeated using NaOH and NaCl solutions. The same saturation curve was observed, with rates varying only slightly from those determined in $NaNO_3$ solutions. A summary of these rates can be found in Table 10. To demonstrate cation independence as well, K^+ was exchanged with Na^+ in the base hydrolysis of 13 (Table 10). To determine if thiocyanate departure is involved in steps preceding the rate determining step, the base hydrolysis reaction of 7 was performed at a constant $[OH^-]$ of 0.100 M and varying $[SCN^-]$. The rate was found to be essentially independent of $[SCN^-]$ over the 0.025 M to 0.500 M range, as shown in Table 11.

To evaluate the A and B parameters of the saturation equation, a linear least squares fit of k_{obs}^{-1} versus $[OH^-]^{-1}$ was performed. Correlation coefficients from these fits were typically in the range of 0.997 to 0.999. Surprisingly, A values were found to be almost identical for each of the three oxo-bridged dimers, signifying that differences in k_{obs} arising mostly from B. A summary of these parameters can be found in Table 12. The enthalpy and entropy of activation for A were determined by linear least squares fit of the

Eyring plot to be 21.3 ± 0.5 kcal/mol and -5 ± 1 eu respectively. The slope and intercept of the Van Hoff plot ($ln(Q_p)$ versus 1/T) gave ΔH^o and ΔS^o values of 4.6 ± 2 kcal/mol and 21 ± 5 eu respectively (vide infra).

One might suggest that rate saturation is due to the interaction of hydroxide with the tmpa ligand on chromium, rather than attributing it to bridge reactivity. To address this question, the hydroxide dependence of the rate of 20 base hydrolysis was performed, and is summarized at the end of Table 9. The plot of k_{obs} versus $[OH^-]$ for 20 showed essentially no hydroxide effect over the range of 0.050 to 1.00 M. The absence of hydroxide saturation behavior in this monomeric tmpa complex is further evidence for saturation being a distinctive characteristic of oxo-bridged dimers.

Figure 13 shows the decay curve for 9 at 352.0 nm overlaid with the formation curve for free SCN^- (35.0 °C, 0.100 M NaOH). It should be noted that the formation of thiocyanate begins at essentially a concentration of zero, and follows loss of absorbance at 352 nm. Essentially two equivalents of free SCN^- per dimer unit are seen towards reaction completion, as expected with a $(tmpa)Cr(OH)_2^+$ final product. It should also be noted that since the samples were acidified to a pH of 3.0, an acid-induced release of SCN^- from an intermediate could result in a higher $[SCN^-]$ than exists in the basic solution at the time the sample was taken.

Oxo-, Carboxylato-Bridged Dimers

Synthesis

The preparations of $[(tmpa)Cr(O)(RCOO)Cr(tmpa)]^{3+}$ (R = CH_3 17, H 18, C_6H_5 19) in refluxing acetonitrile proceed according to equation (12) with excellent yields.

$$[(tmpa)Cr(OH)_2Cr(tmpa)]^{4+} + RCOO^- \longrightarrow [(tmpa)Cr(O)(RCOO)Cr(tmpa)]^{3+} + H_2O. \quad (12)$$

The reaction can also be performed easily in methanol at room temperature, but if attempted in H_2O the formation of $[(tmpa)Cr(O)(RCOO)Cr(tmpa)]^{3+}$ is only slightly favored over its decomposition. The time-dependent UV-visible spectrum of an aqueous solution of the diol in the presence of NaOAc shows that only a very small percent of the oxo-,carboxylato-bridged dimer is formed, which then decays slowly with time.

Electronic Spectral Analysis

Electronic spectra of dimers 17-19 in acetonitrile solution (Table 13) exhibit peaks at positions that are very nearly identical. The resemblance of the spectra of these complexes to those of the linear oxo-bridged dimers is striking. The major difference in spectra is that the very intense ($\varepsilon \approx 10^4\ M^{-1}cm^{-1}$) sharp band in the 349-355 nm region seen in the linear oxo-dimers is replaced by two components in the carboxylate-bridged dimers at 336 and 371 nm ($\varepsilon \approx 3000\ M^{-1}cm^{-1}$ and $5000\ M^{-1}cm^{-1}$, respectively).

Infrared Spectral Analysis

The infrared spectra of 17-19 exhibit in addition to the usual tmpa bands seen in both the diol and all oxo-dimers, two strong features in the range of 1527-1561 cm^{-1} and 1369-1443 cm^{-1} (Table 14). It should be noted that lower energy band in 17 overlaps with a tmpa feature, and hence the energy can only be estimated to within $\pm$ 10 cm^{-1}. Two features with similar energies have been previously reported for Δ,Λ-$[(en)_2Cr(HCOO)(OH)Cr(en)_2](ClO_4)_4$ (1569, 1379 cm^{-1}) and Δ,Λ-$[(en)_2Cr(CH_3COO)(OH)Cr(en)_2](ClO_4)_4 \cdot 2H_20$ (1552, 1418 cm^{-1}) and were assigned to antisymmetric and symmetric OCO stretches, respectively.[34] The formulation of 17-19 with the carboxylate anion playing a bridging role is consistent with these aliphatic amine dimers by infrared band energy and (ν_{as}-ν_s) similarities.

Electrochemical Measurements

The cyclic voltammograms of all three $[(tmpa)Cr(O)(RCOO)Cr(tmpa)]^{3+}$ complexes in acetonitrile (0.1 M $(n\text{-}Bu)_4NClO_4$ supporting electrolyte) exhibit a reversible one-electron oxidation wave in the 1.17 to 1.22 V interval (Table 13) with peak-to-peak separations of 70-75 mV at a sweep rate of 50 mV/second and anodic to cathodic peak current ratios within experimental error of 1.0.

μ-Hydroxo-μ-Carboxylato Dimer Acid Dissociation Constants

Spectrophotometric titrations of 17-19 (Figure 14) revealed that these oxo-, carboxylato-bridged dimers accept one proton to give reddish $[(tmpa)Cr(OH)(RCOO)Cr(tmpa)]^{4+}$ conjugate acids which exhibit pK_a values (Table 13) that vary only moderately with differing carboxylate bridge. These hydroxo-, carboxylato-bridged dimers are stronger acids than both $\Delta,\Lambda\text{-}[(en)_2Cr(HCOO)(OH)Cr(en)_2]^{4+}$ and $\Delta,\Lambda\text{-}[(en)_2Cr(CH_3COO)(OH)Cr(en)_2]^{4+}$ ($pK_a \approx 12$)[34] by ten orders of magnitude. The electronic spectra of these protonation products (Table 13) lack the features at 336, 371, and 419 nm seen in their oxo-bridged forms.

Formation Kinetics

Reaction of $LiCH_3COO$ with 4 in methanol (25.0 °C, I=0.500 M) was found to be first order in both 4 and CH_3COO^-. The rate constants for this reaction are reported in Table 15. The second order rate constant k in the rate expression

$$\text{Rate} = k\,(\text{OAc-})\,([(tmpa)Cr(OH)(O)Cr(tmpa)]^{4+}) \qquad (13)$$

was evaluated at $1.00 \pm 0.05\ 10^{-3}\ M^{-1}\ s^{-1}$ from the slope of the linear least squares plot of k_{obs} versus $[CH_3COO^-]$.

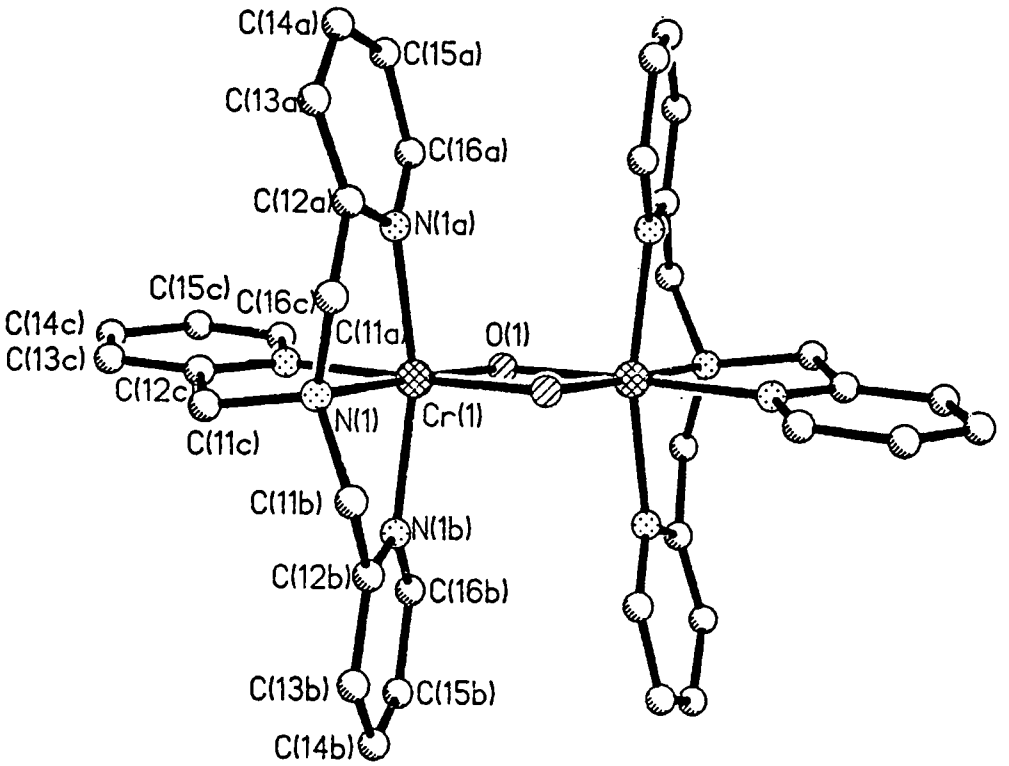

Figure 2. View of the $[(tmpa)Cr(OH)_2Cr(tmpa)]^{4+}$ cation (complex 3, H atoms excluded). Selected interatomic distances and angles are: Cr(1)-O(1), 1.937(8); -N(1), 2.041(11); -N(1a), 2.052(11); -N(1b), 2.041(12); -N(1c), 2.052(11) Å. N(1)-Cr(1)-O(1), 176.0(4); N(1a)-Cr(1)-O(1), 99.7(4); N(1a)-Cr(1)-N(1), 81.2(5); N(1b)-Cr(1)-O(1), 99.0(4); N(1b)-Cr(1)-N(1), 80.3(5); N(1b)-Cr(1)-N(1a), 161.2(4); N(1c)-Cr(1)-O(1), 100.1(4); N(1c)-Cr(1)-N(1), 83.9(4); N(1c)-Cr(1)-N(1a), 84.2(4); N(Ic)-Cr(1)-N(1b), 90.5(4) deg. Uncertainties in the last significant digit are shown in parentheses.

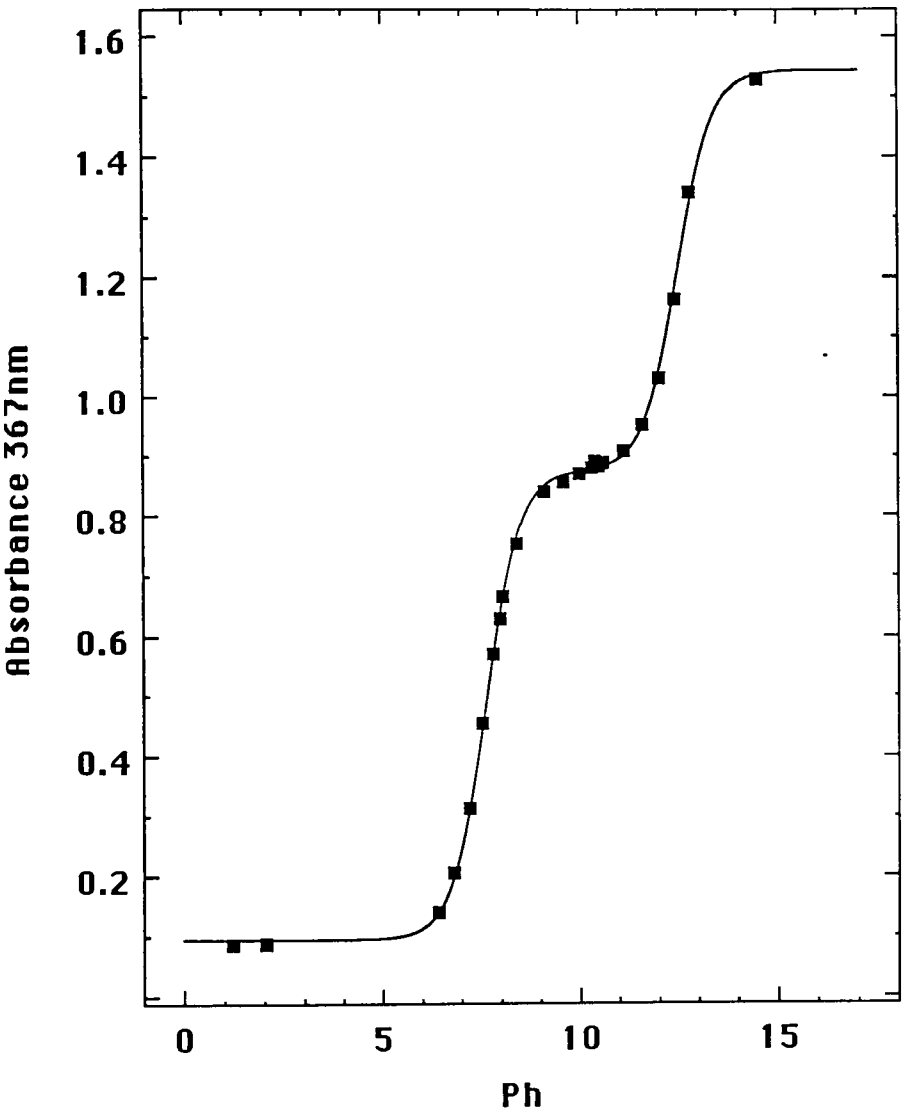

Figure 3. Spectrophotometric titration of $[(tmpa)Cr(OH)_2Cr(tmpa)]^{4+}$ at 367 nm. 25.0 °C, I=0.1 M ($NaNO_3$), 1-cm path length, C_o = 0.5 mM.

Table 3

Magnetic Characteristics of Binuclear (tmpa)Cr(III) Compounds [a,b]

compound code	2	4	7	13
g	1.93	2.16	2.15	2.12
J, cm^{-1}	-15.7	-68.5	-255	-290
zJ' [c], cm^{-1}	3.5	7.2	0	0
TIP, cgs units	0	$3.8x10^{-4}$	$1.7x10^{-5}$	$4.0x10^{-4}$
% impurity with Curie-Weiss behavior	0	0.15	0.09	0.99
θ	0	-0.936	-0.008	0.252

[a] See Experimental Section for identification of compound codes.

[b] Molecular field corrections for 7 and 13; TIP, % impurity and θ for 2 fixed to 0.

[c] Molecular field correction.

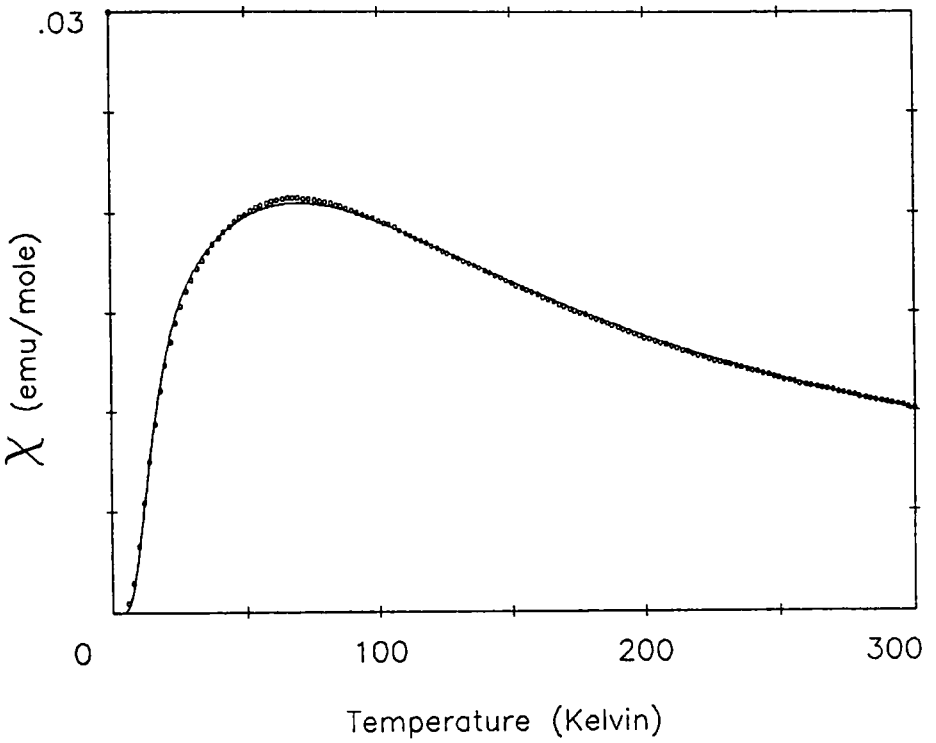

Figure 4. $[(tmpa)Cr(OH)_2Cr(tmpa)](ClO_4)_4 \cdot 4H_2O$ (2) magnetic susceptibility temperature dependence.

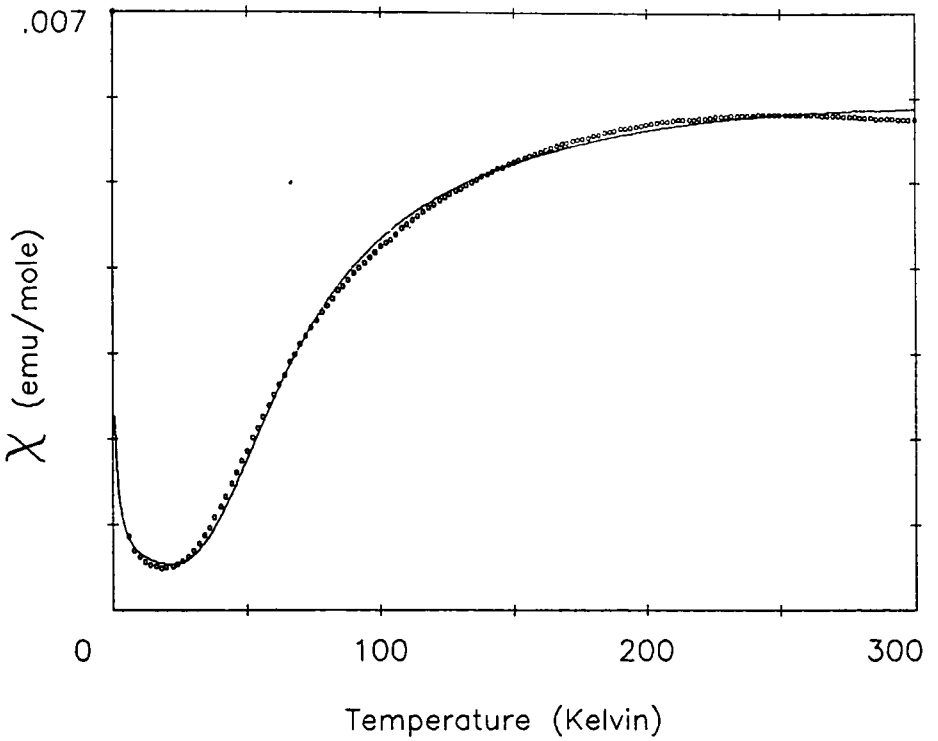

Figure 5. [(tmpa)Cr(OH)(O)Cr(tmpa)]$(ClO_4)_3 \cdot H_2O$ (4) magnetic susceptibility temperature dependence.

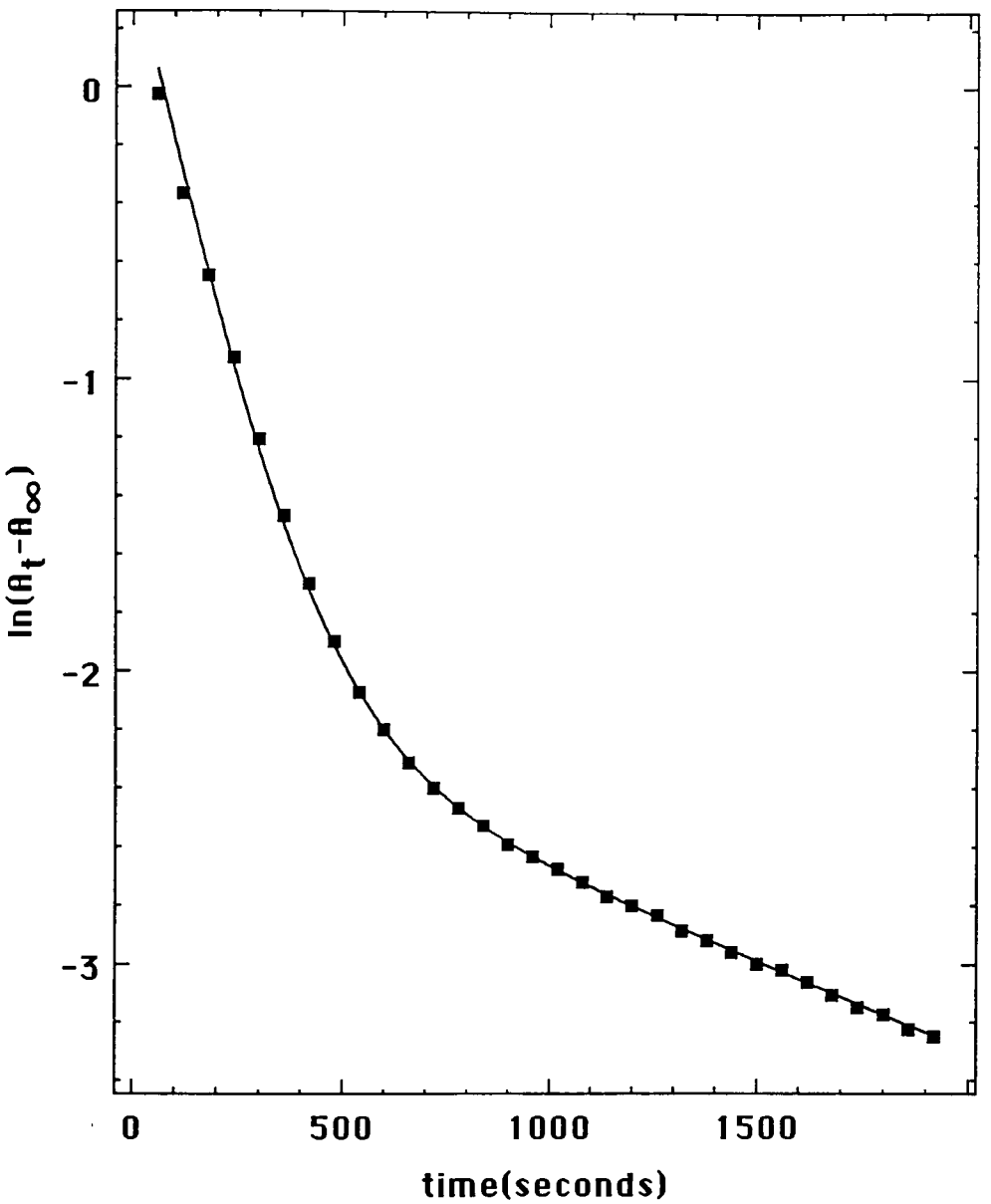

Figure 6. Typical $\ln(A_t-A_\infty)$ (368 nm) versus time plot for the biphasic hydrolysis reaction of $[(tmpa)Cr(O)_2Cr(tmpa)]^{2+}$, 40.0 °C, I = $[OH^-]$ = 1.0 M. The solid curve was drawn from the least squares consecutive first order rate parameters.

Table 4
Rate Constants for Base Hydrolysis of $[(tmpa)Cr(O)_2Cr(tmpa)]^{2+}$ a

temp, °C	$[OH^-]$, M	$10^3\ k_{fast}$, s^{-1}	$10^4\ k_{slow}$, s^{-1}
20.6	0.200	0.283	0.248
	0.500	0.401	0.274
	0.700	0.459	0.291
	1.00	0.574	0.315
26.1	0.200	0.547	0.435
	0.500	0.748	0.526
	0.700	0.924	0.606
	1.00	1.16	0.700
29.9	0.200	0.856	0.848
	0.500	1.24	1.06
	0.700	1.61	1.31
	1.00	2.00	1.39
35.0	0.200	1.23	1.10
	0.500	1.86	1.48
	0.700	2.60	1.83
	1.00	3.17	2.10

Table 4 (continued).

temp, °C	$[OH^-]$, M	$10^3\ k_{fast}$, s^{-1}	$10^4\ k_{slow}$, s^{-1}
40.0	0.100	2.68	
	0.200	3.14	5.04
	0.300	3.87	
	0.400	4.06	
	0.500	4.80	5.94
	0.600	5.20	
	0.700	5.46	5.82
	0.800	5.91	
	0.900	6.42	
	1.00	6.84	6.33
45.0	0.200	4.21	4.48
	0.500	6.34	6.76
	0.700	8.23	7.66
	1.00	9.99	8.80

[a] I = 1.0 M (NaOH/NaBr). Rate constants of the fast (k_{fast}) and slow (k_{slow}) phases of the consecutive first order decomposition reaction were derived as described in the text. Uncertainties in k_{fast} and k_{slow} are estimated at ± 3% and ± 6%, respectively.

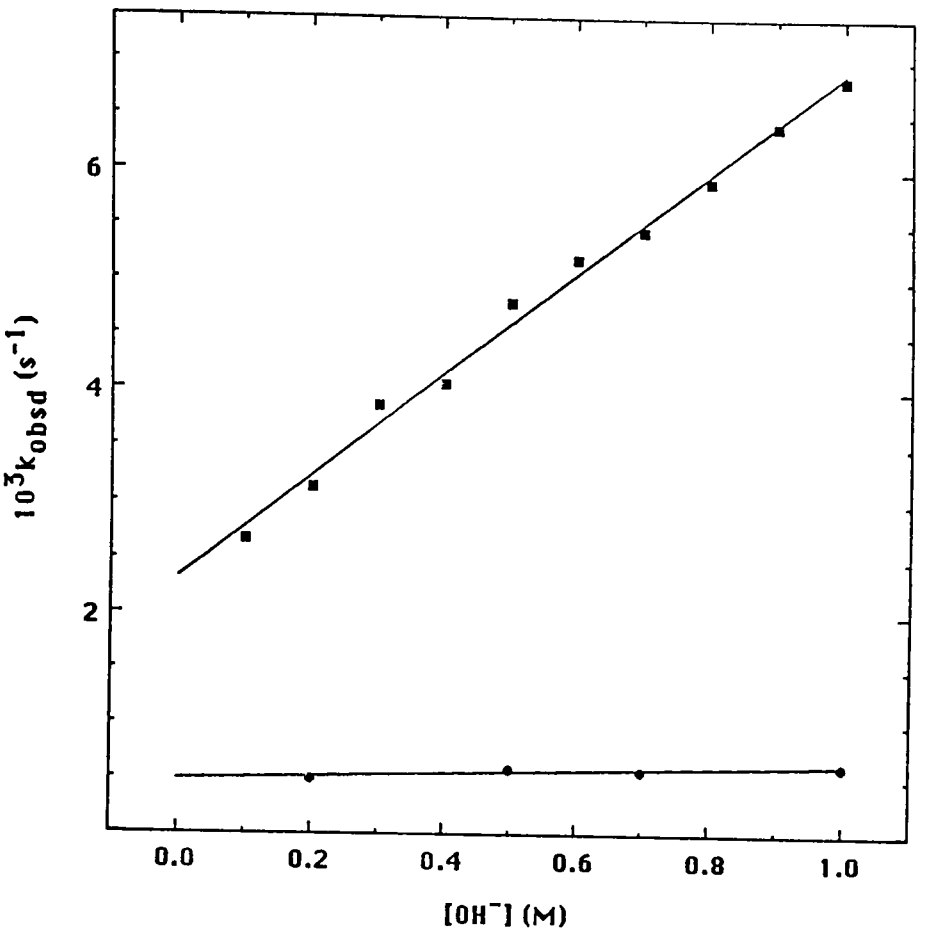

Figure 7. Plots of k_{fast} (■) and k_{slow} (●) versus [OH^-] indicating the presence of both zeroth and first order terms in OH^- for the hydrolysis of $[(tmpa)Cr(O)_2Cr(tmpa)]^{2+}$ (fast phase) and intermediate 24 (slow phase). 40.0 °C, I = 1.0 M (NaOH/NaBr).

Table 5

Rate Parameters for Base Hydrolysis of $[(tmpa)Cr(O)_2Cr(tmpa)]^{2+}$ [a]

temp, °C	$10^3 k_o$, s^{-1}	$10^3 k_{OH}$, $M^{-1}s^{-1}$	$10^4 k_o^s$, s^{-1}	$10^4 k_{OH}^s$, $M^{-1}s^{-1}$
20.6	0.214(0.008)	0.359(0.012)	0.232(0.001)	0.0838(0.0012)
26.1	0.381(0.019)	0.773(0.028)	0.366(0.008)	0.335(0.012)
29.9	0.554(0.047)	1.45(0.07)	0.725(0.083)	0.711(0.012)
35.0	0.715(0.140)	2.50(0.22)	0.860(0.071)	1.28(0.11)
40.0	2.33(0.09)	4.56(0.14)	4.89(0.29)	1.48(0.44)
45.0	2.78(0.29)	7.36(0.43)	3.72(0.47)	5.35(0.71)

[a] I = 1.0 M (NaOH/NaBr). Rate parameters are defined in equations (6) and (7). Standard deviations are shown in parentheses.

Table 6

Activation Parameters for the Biphasic Base Decomposition Reaction of $[(tmpa)Cr(O)_2Cr(tmpa)]^{2+}$ [a]

rate constant	k (25 °C)	$\Delta H^{\ddagger}$, kcal mol^{-1}	$\Delta S^{\ddagger}$, eu
k_O^S, s^{-1}	4.7×10^{-5}	23 (4)	-1 (11)
k_{OH}^S, $M^{-1}s^{-1}$	2.7×10^{-5}	28 (3)	+14 (10)
k_O, s^{-1}	3.0×10^{-4}	19.9 (2.2)	-8 (7)
k_{OH}, $M^{-1}s^{-1}$	5.8×10^{-4}	22.5 (0.8)	+2 (3)

[a] I = 1.0 M (NaOH/NaBr). Standard deviations are shown in parentheses.

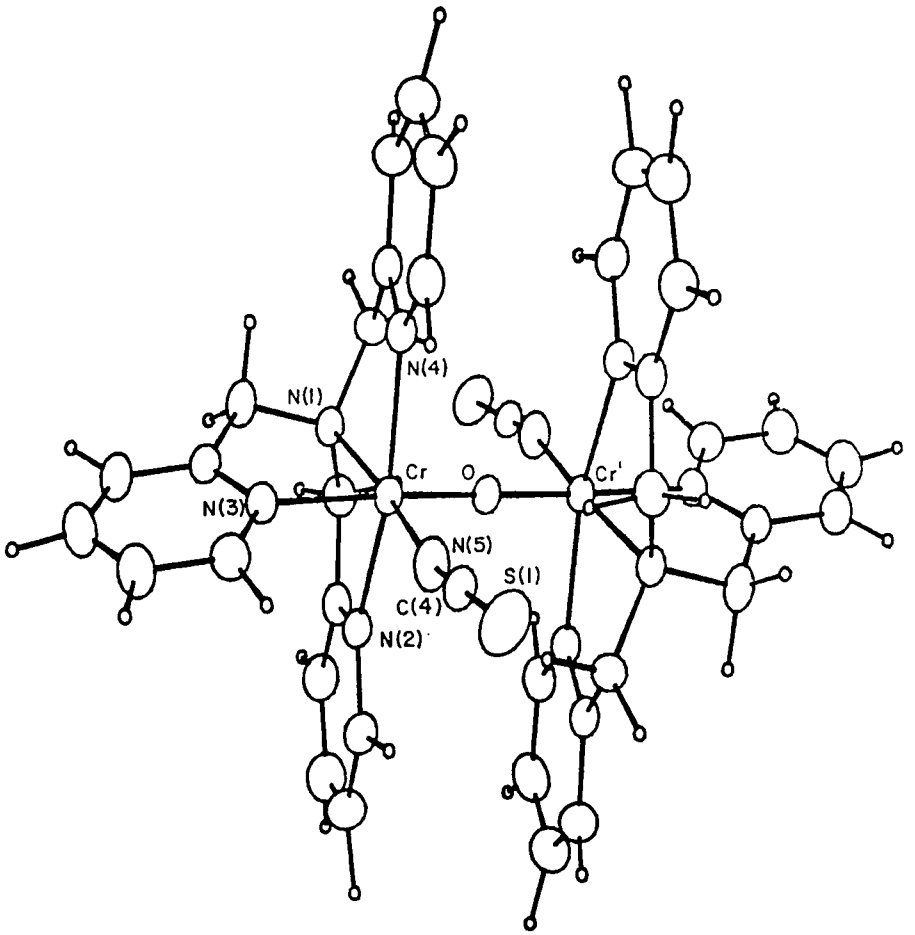

Figure 8. View of the $[\{Cr(tmpa)(NCS)\}_2O]^{2+}$ cation. Selected interatomic distances and angles are: Cr-O, 1.8001(4); -N(1), 2.072(2); -N(2), 2.070(2); -N(3), 2.121(2); -N(4), 2.078(2); -N(5), 2.004(3) Å. Cr-O-Cr', 180; N(1)-Cr-N(2), 81.01(9); -Cr-N(3), 81.02(9); -Cr-N(4), 79.75(9); -Cr-N(5), 169.9(1); N(2)-Cr-N(3), 85.02(9); Cr-N(4), 160.8(1); -Cr-N(5), 101.1(2); N(3)-Cr-N(4), 92.40(9); -Cr-N(5), 89.3(1); N(4)-Cr-N(5), 97.9(2); Cr-N(5)-C(4), 168.3(3); N(5)-C(4)-S(1), 178.6(3); O-Cr-N(5), 95.54(7) deg.

Table 7

Physical Properties of $[(tmpa)LCrOCrL(tmpa)]^{2+}$

L	UV-visible λ_{max}, nm (ε_{max}, $M^{-1}cm^{-1}$)[a]		pK_a[b]	$E_{1/2}$, V versus SHE[c]
	CrOCr dimer[d]	Cr(OH)Cr dimer[e]		
NCS^-	313 (10,800)	327 (8700)	2.05	1.170
	355 (14,100)	524 (410)		
	368, sh (11,200)			
	398, sh (2750)			
	417 (2740)			
	457, sh (1780)			
	567, pl (250)			
NCO^-	308, sh (6750)	403 (180)	4.09	1.02
	349 (10,500)	533 (340)		
	362, sh (8500)			
	393 (2980)			
	420 (3200)			
	450, sh (2100)			
	572, pl (200)			
CN^-	313, sh (6750)	510 (230)	0.64	1.17
	355 (12,800)			
	367 (11,400)			
	398 (3050)			
	414 (2900)			

Table 7 (continued).

	450, sh (1950) 570, pl (230)			
N_3^-	294, sh (6900) 354 (8600) 364, sh (7650) 416, sh (2350) 448, sh (1730) 572, pl (260)	412 (240) 545 (430)	4.25	0.96
Cl^-	310, sh (5700) 350 (9000) 360 (7950) 389 (2600) 420 (2700) 440, sh (2010) 570 (160)		unstable in water	1.03

a Spectra recorded at ambient temperature. Extinction coefficients are expressed per mole of dimer. Intense characteristic tmpa pyridyl π-π^* transition in the 250 to 260 nm interval is not tabulated.

b pK_a of conjugate acid $[(tmpa)LCr(OH)LCr(tmpa)]^{3+}$ in water at 25.0 °C, I = 0.1 M. Uncertainty estimated at ± 0.05.

c Half-wave potential for the $[(tmpa)LCrOCrL(tmpa)]^{2+/3+}$ oxidation couple in CH_3CN at 25.0 °C, I = 0.1 M TBAP. Uncertainty estimated at ± 0.01 V.

d $[(tmpa)LCrOCrL(tmpa)]^{2+}$ spectrum in CH_3CN solution.

e $[(tmpa)LCr(OH)CrL(tmpa)]^{3+}$ spectrum in 1.0 M aqueous $HClO_4$ except in the case of L = N_3^- (1.0 M $HClO_4$ in 50:50 H_2O/CH_3CN).

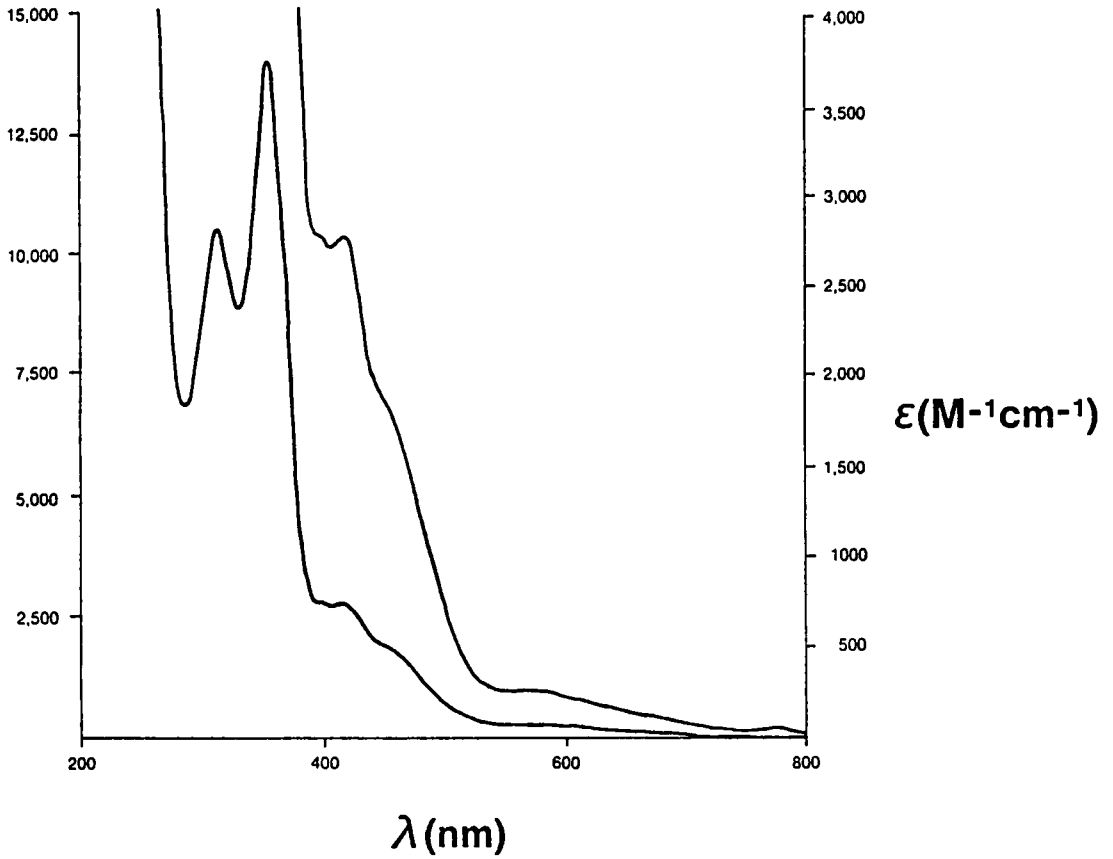

Figure 9. UV-visible spectrum of $[(tmpa)(SCN)CrOCr(NCS)(tmpa)]^{2+}$ in CH_3CN.

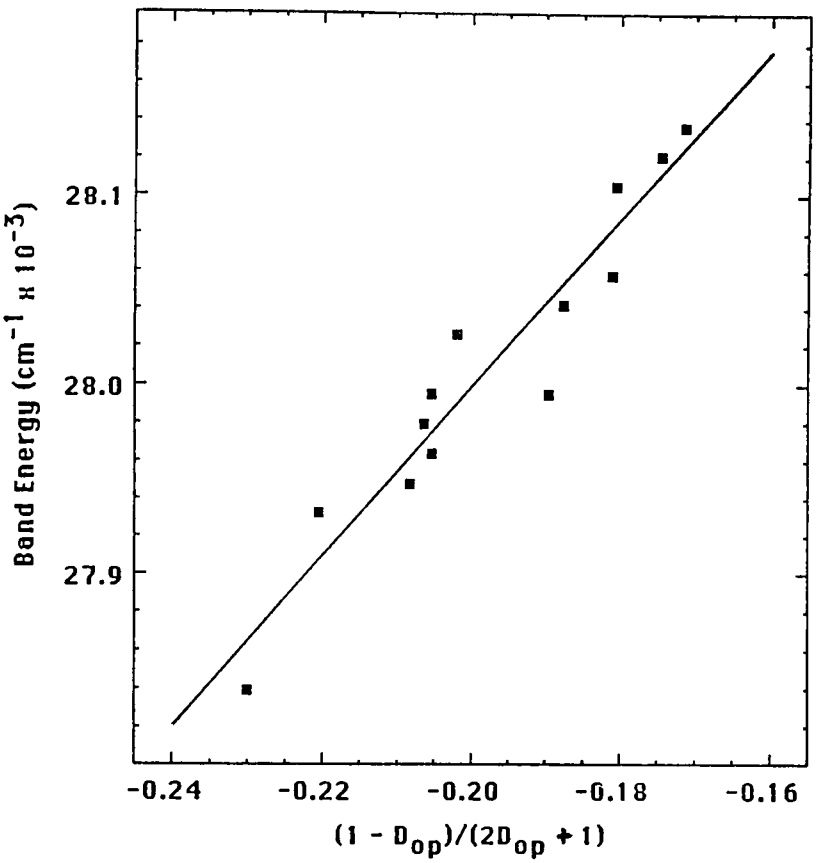

Figure 10. Linear least squares correlation of $[(tmpa)(NCS)CrOCr(NCS)(tmpa)]^{2+}$ e_g-e_u* transition energy with solvent optical dielectric constant function at ambient temperature. Solvents [band energy x 10^{-3} cm^{-1}, $(1-D_{op})/(2D_{op} + 1)$]: methanol (28.14, -0.1714); acetonitrile (28.12, -0.1746); N-methylformamide (27.98, -0.2063); dimethylsulfoxide (27.93, -0.2205); ethanol (28.06, -0.1811); N,N-dimethylformamide (28.00, -0.2053); N,N-dimethylacetamide (27.95, -0.2082); propylene carbonate (28.03, -0.2019); acetone (28.11,-0.1806); N-methylacetamide (27.96, -0.2053); pyridine (27.84, -0.2300); methyl ethyl ketone (28.04, -0.1876); n-butyronitrile (28.00, -0.1895).

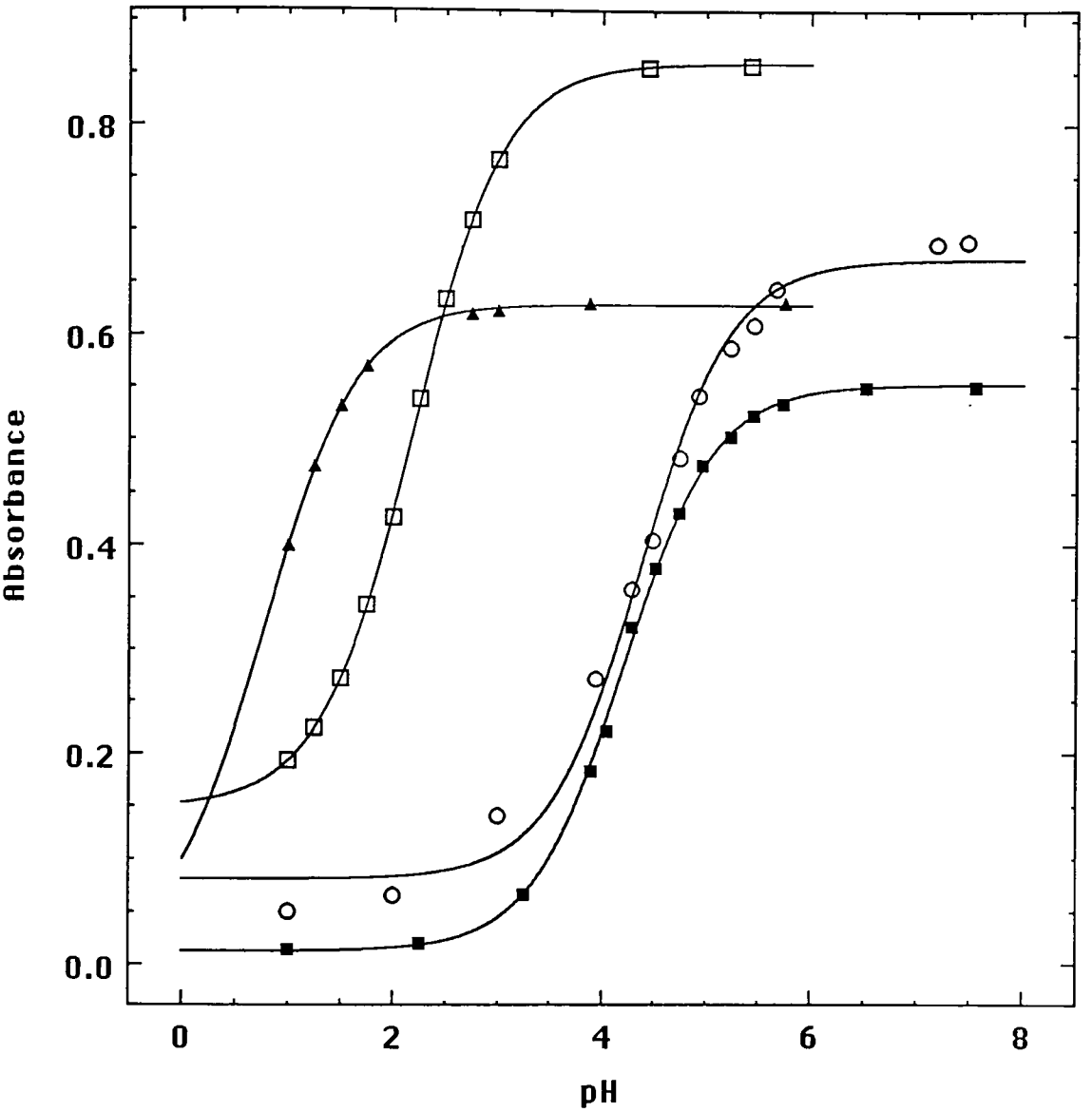

Figure 11. Spectrophotometric titrations of $[(tmpa)LCrOCrL(tmpa)]^{2+}$ complexes with L = CN^- (▲, 0.0493 mM, 354 nm); NCS^- (□, 0.121 mM, 352 nm); NCO^- (■, 0.0493 mM, 347 nm); N_3^- (○, 0.0667 mM, 351 nm). 25.0 °C, I = 0.1 M ($NaNO_3$), 1 cm path length. Solid curves and pK_a were calculated on the basis of non-linear least squares fits.

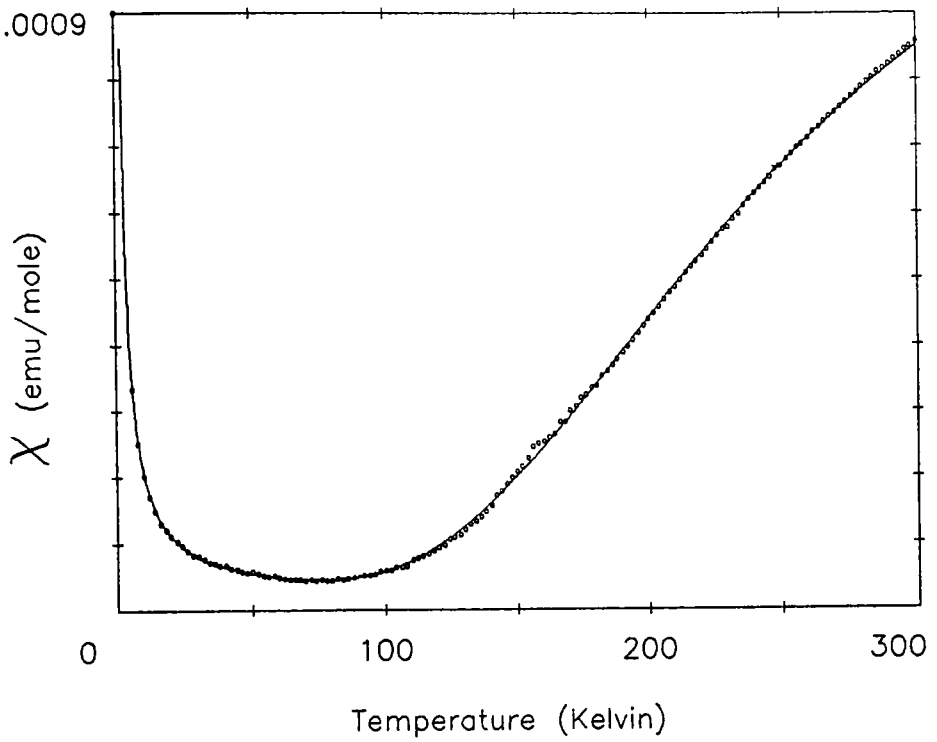

Figure 12. [(tmpa)(SCN)CrOCr(NCS)(tmpa)]$(ClO_4)_2 \cdot 0.5H_2O$ (7) magnetic susceptibility temperature dependence.

Table 8

Quenched (tmpa)(SCN)CrOCr(NCS)(tmpa)$^{2+}$

Base Hydrolysis Separation Summary

Cations that exists in solution under reaction conditions	Proposed Distribution	NaBr/NaOH (a)	$LiClO_4$/NaOH (b)	NaBr/HBr (c)
$[(tmpa)(SCN)Cr]_2O^{2+}$	44%	44%	44%	44%
OH^-			60%	
$[(tmpa)(SCN)CrOCr(OH)(tmpa)]^{2+}$	16%	16% 70%	16%	32% diol
OH^-				
$[(tmpa)(OH)Cr]_2O^{2+}$	16%	10%	10%	
H_2O		6%	6%	
$[(tmpa)(OH)_2Cr]^+$	24%	30%	30%	24%

Table 9

Base Hydrolysis Rate Constants of Selected Cr(III) Cations in $NaOH/NaNO_3$ Solutions [a]

L[b]	temp, °C	$[OH^-]$, M	$10^4 k_{obs}$, s^{-1}
NCS^-	35.0	0.010	0.813
		0.020	1.36
		0.050	2.32
		0.100	2.97
		0.500	3.89
		1.00	4.53
	40.0	0.010	1.86
		0.050	4.43
		0.075	5.19
		0.100	5.97
		0.200	6.70
		0.300	7.04
		0.400	7.36
		0.500	7.49
		0.600	7.61
		0.700	7.80
		0.800	7.87
		0.900	8.00

Table 9 (continued).

	45.0	0.010	3.11
		0.020	4.82
		0.050	8.02
		0.100	9.78
		0.500	12.3
		1.00	14.1
	50.0	0.010	6.34
		0.020	9.65
		0.050	16.1
		0.100	18.4
		0.500	21.1
		1.00	24.3
	55.3	0.010	11.1
		0.020	16.6
		0.050	25.8
		0.100	32.5
		0.500	37.6
		1.00	41.5
NCO^-	40.0	0.020	0.410
		0.050	0.897
		0.100	1.53

Table 9 (continued).

		0.150	2.14
		0.200	2.66
		0.300	3.68
		0.500	5.70
		1.00	11.1
CN^-	40.0	0.150	1.14
		0.200	1.45
		0.300	2.07
		0.500	2.98
		1.00	4.75
SCN^- [c]	40.0	0.005	5.16
		0.025	5.26
		0.050	5.88
		0.100	5.72
		0.500	5.59
		0.800	5.98
		1.00	6.49

[a] I = 1.00 M. Uncertainty in k_{obs} is estimated at 3%.

[b] Denotes ligand L in $[(tmpa)LCrOCrL(tmpa)]^{2+}$.

[c] Denotes SCN^- in $(tmpa)Cr(NCS)_2^+$.

Table 10

Base Hydrolysis Rate Constants of Selected Cr(III) Cations in Differing Ionic Strength Media [a]

L[b]	Media	temp, °C	$[OH^-]$, M	$10^4 k_{obs}$, s^{-1}
SCN^-	NaOH/NaCl	40.0	0.010	2.12
			0.020	3.23
			0.050	5.24
			0.100	6.65
			0.500	7.93
			1.000	8.33
CN^-	KOH/KNO_3	40.0	0.100	0.906
			z0.200	1.71
			0.300	2.33
			0.400	2.79
			0.500	3.15
			0.600	3.46
			0.700	3.67
			0.800	3.91
			0.900	4.12
			1.00	4.41

[a] I = 1.00 M. Uncertainty in k_{obs} is estimated at 3%.

[b] Denotes ligand L in $[(tmpa)LCrOCrL(tmpa)]^{2+}$.

Table 11

Base Hydrolysis Rate Constants of $[(tmpa)(SCN)CrOCr(NCS)(tmpa)]^{2+}$ at Varying $[SCN^-]$ [a]

temp, °C	$[NaSCN^-]$, M	$[NaNO_3^-]$, M	$[NaOH^-]$, M	$10^4\ k_{obs}$, s^{-1}
40.0	0.025	0.875	0.100	5.85
	0.050	0.850	0.100	5.75
	0.100	0.800	0.100	5.75
	0.250	0.650	0.100	5.42
	0.400	0.500	0.100	5.43
	0.500	0.400	0.100	5.30

[a] I = 1.00 M. Uncertainty in k_{obs} is estimated at 3%.

Table 12

Rate Parameters for the General Saturation Equation [a]

L[b]	Media	temp, °C	10^4 A, s^{-1}	B
NCS^-	$NaOH/NaNO_3$	35.0	4.37	23
		40.0	7.86	31
		45.0	13.3	30
		50.0	23.6	36
		55.3	40.3	37
	NaOH/NaCl	40.0	8.42	33
NCO^-	$NaOH/NaNO_3$	40.0	8.20	2.6
CN^-	$NaOH/NaNO_3$	40.0	10.4	1.2
	KOH/KNO_3	40.0	7.94	1.3

a I = 1.00M, Uncertainty in A is Estimated at 5% with B Estimated at 10%.

b Denotes ligand L in $[(tmpa)LCrOCrL(tmpa)]^{2+}$.

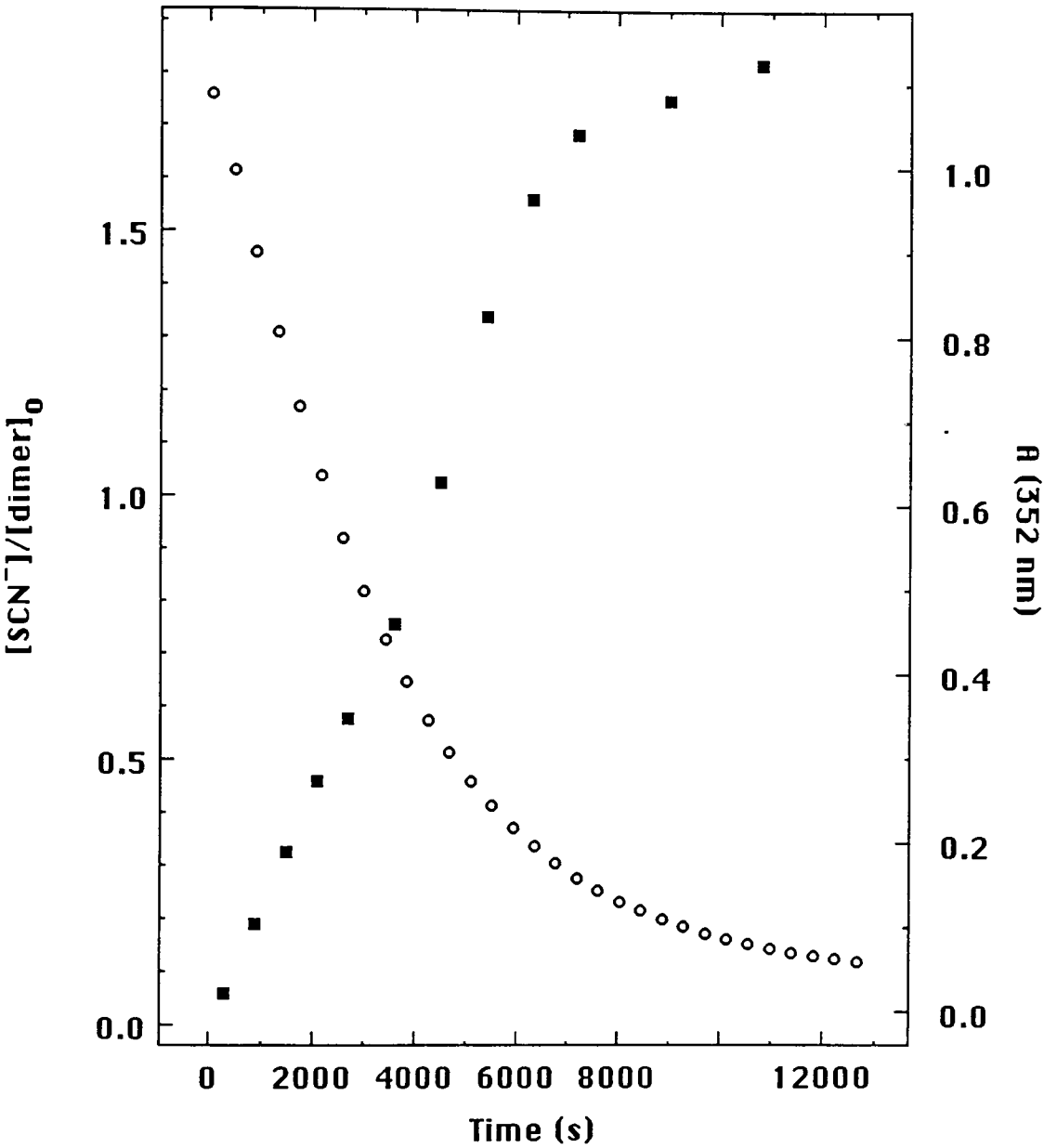

Figure 13. Experimental points for 352.0 nm absorbance decay (o, right axis) and $[SCN^-]/[dimer]_0$ (■, left axis) versus time for $(tmpa)(SCN)CrOCr(NCS)(tmpa)^{2+}$ (35.0 °C, 0.100 M NaOH).

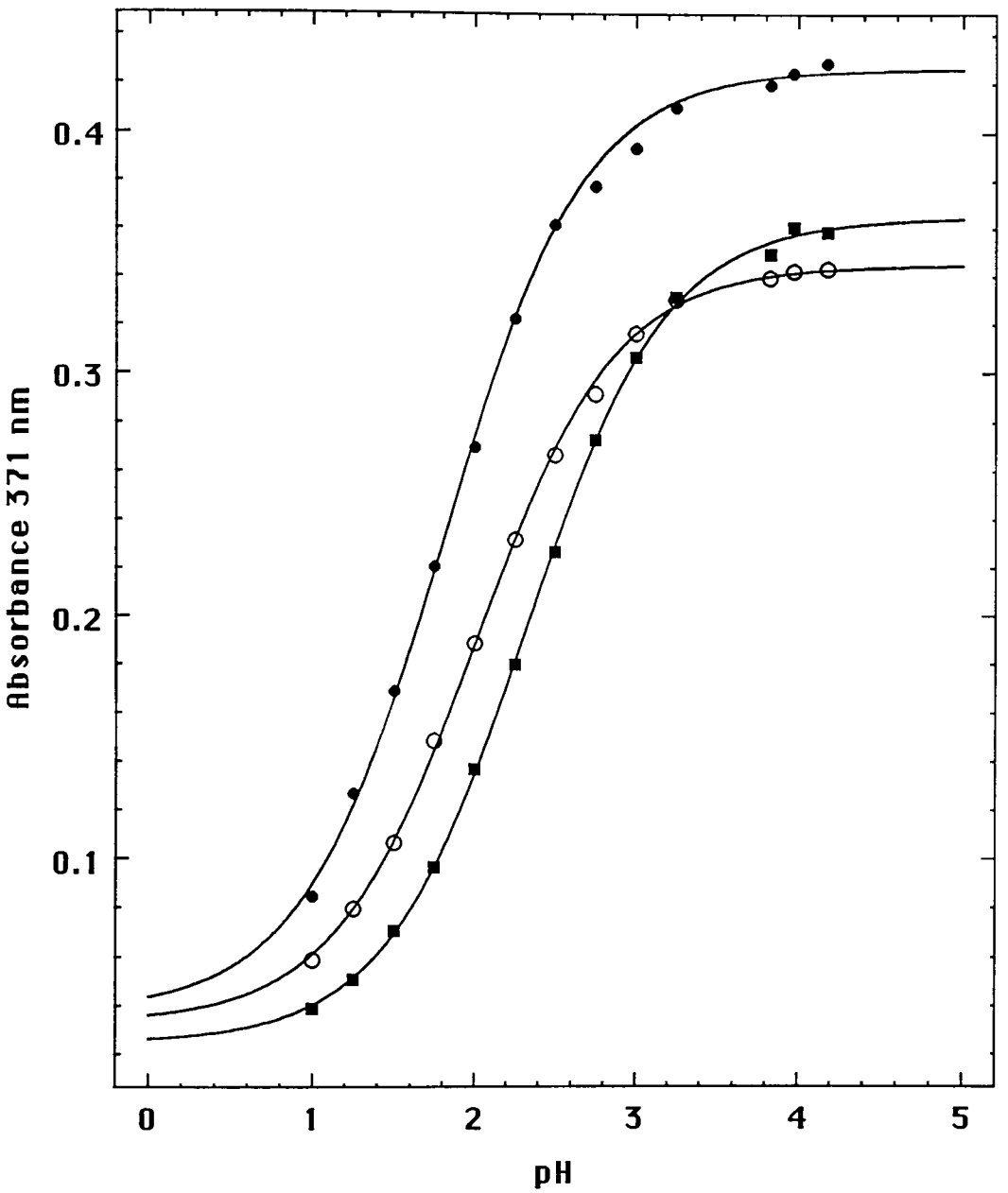

Figure 14. Spectrophotometric titrations of $[(tmpa)CrO(RCOO)Cr(tmpa)]^{3+}$ complexes with R= H (•), C_6H_5 (o) and CH_3 (▪) (1-cm path length). Solid curves and pK_a values were calculated on the basis of non-linear least squares fits.

Table 13
UV-visible Spectral Features, $E_{1/2}$, and Bridging OH pK_a for the Oxo-, Carboxylato-Bridged Cr(III) Dimers

Bridging Groups	UV-vis λ_{max}, nm (ε, $M^{-1}cm^{-1}$)	$E_{1/2}$ V	pK_a
O^{2-}/CH_3COO^-	562 (200)	1.17 ± 0.05	
	419 (1,780)		
	388 (2,070) (sh)		
	372 (2,890)		
	336 (4,090)		
	256 (20,600)		
OH^-/CH_3COO^-	510 (300)		2.20 ± 0.02
	386 (224)		
	264 (18,000)		
$O^{2-}/HCOO^-$	563 (217)	1.21 ± 0.05	
	419 (2,050)		
	388 (2,240) (sh)		
	372 (3,600)		
	336 (5,460)		
	256 (21,900)		
$OH^-/HCOO^-$	508 (310)		1.69 ± 0.02
	386 (230)		
	264 (17,000)		
$O^{2-}/C_6H_5COO^-$	566 (225)	1.22 ± 0.05	
	419 (2,330)		
	388 (2,540) (sh)		
	371 (3,450)		
	337 (5,440)		
	251 (35,200)		
$OH^-/C_6H_5COO^-$	512 (335)		1.88 ± 0.02
	382 (266)		
	263 (29,000)		

Table 14

Infrared Symmetric and Antisymmetric OCO Stretching Frequencies for the Oxo-, Carboxylato-Bridged Cr(III) Dimers and Na^+ Salts of the Free Ligands

Compound	ν_{as}(OCO) cm^{-1}	ν_s(OCO) cm^{-1}
$[(tmpa)Cr(O)(C_6H_5COO)Cr(tmpa)](ClO_4)_3 \cdot 2H_20$	1527	1413
$[(tmpa)Cr(O)(CH_3COO)Cr(tmpa)](ClO_4)_3$	1549	1443 [a]
$[(tmpa)Cr(O)(HCOO)Cr(tmpa)](ClO_4)_3$	1561	1369
C_6H_5COONa	1551	1413
CH_3COONa [b]	1578	1425
HCOONa [b]	1590	1355

[a] Overlaps with tmpa mode, estimated uncertainty is 10 cm^{-1}.

[b] Values from reference 34.

Table 15
Rate Parameters for $[(tmpa)Cr(O)(CH_3COO)Cr(tmpa)]^{3+}$
Formation in Methanol [a]

[OAc-], M	$10^4 k_{obs}$, s^{-1}
0.0250	0.381
0.0375	0.582
0.0500	0.833
0.100	1.34
0.200	2.50
0.300	3.08
0.400	4.49
0.500	5.10

[a] 25.0 °C, I =0 .500 M, LiOAc/LiBr Media.

CHAPTER IV

DISCUSSION

Oxo and Hydroxo Doubly-Bridged Dimers

Magnetic Properties

In the interpretation of the temperature dependence of the magnetic succeptibility of 2 and 4, the Heisenberg exchange model provides an adequate basis for a quantitative understanding. The singlet-triplet separation for diol 2 implied by our findings (-2J = 31.4 cm^{-1}) agrees well with that published by Hodgson and co-workers (30.58 cm^{-1})[28] while the present work was in progress. This value is similar to those reported for other diols with aromatic amine ligands,[35] $[(bpy)_2Cr(OH)_2Cr(bpy)_2](ClO_4)_4 \cdot 3H_2O$ (37.41 cm^{-1}) and $[(phen)_2Cr(OH)_2Cr(phen)_2](ClO_4)_4 \cdot 2H_2O$ (44.87 cm^{-1}), but is characteristically larger than singlet-triplet gaps for dihydroxo-bridged dimers with aliphatic amine donor sets.[31] Although the singlet-triplet separation in the tmpa chromium diol is somewhat smaller than those of the analogous phen and bpy systems, the -2J value of 137 cm^{-1} for 4 is substantially larger than the splittings of $[(bpy)_2Cr(OH)OCr(bpy)_2](ClO_4)_3 \cdot 4H_2O$ (60 cm^{-1}) and $[(phen)_2Cr(OH)OCr(phen)_2](ClO_4)_3 \cdot 2H_2O$ (90 cm^{-1}).[35]

Di-μ-Oxo Dimer Base Hydrolysis Rate Considerations

Although the conjugate base hydrolysis mechanism (D_{cb}) is well-established for Co(III) complexes with ionizable amine ligands, Cr(III) species in general are considerably less sensitive to base hydrolysis[36] and may opt for direct nucleophilic displacement of the leaving group by hydroxide ion in pathways characterized by a first order OH^- dependence. We propose that the k_o and k_{OH} terms in the fast phase of $[(tmpa)Cr(O)_2Cr(tmpa)]^{2+}$ decomposition correspond to H_2O and OH^- assisted bridge opening to give the intermediate 24, thought to be $[(tmpa)(OH)CrOCr(OH)(tmpa)]^{2+}$, which then decays to

$Cr(tmpa)(OH)_2^{+}$ through analogous H_2O or OH^- assisted oxo-bridge cleavage steps (equation 14).

$$[(tmpa)Cr(O)_2Cr(tmpa)]^{2+} + H_2O \longrightarrow [(tmpa)(OH)CrOCr(OH)(tmpa)]^{2+} \quad (\underline{24})$$

$$[(tmpa)Cr(O)_2Cr(tmpa)]^{2+} + OH^- \xrightarrow{k_{OH}} [(tmpa)(O)CrOCr(OH)(tmpa)]^{+} \xrightarrow[+H_2O]{\text{fast}} \underline{24} + OH^-$$

$$\underline{24} + H_2O \xrightarrow{k_o^S} 2\,[Cr(tmpa)(OH)_2]^{+} \qquad (14)$$

$$\underline{24} + OH^- \xrightarrow{k_{OH}^S} [Cr(tmpa)(OH)_2]^{+} + [Cr(tmpa)(OH)(O)]^{+} \xrightarrow[+H_2O]{\text{fast}} [Cr(tmpa)(OH)_2]^{+} + OH^-$$

The elution behavior of 24, which separates cleanly from leading 1+ (22) and trailing 3+ (4) components on SP-Sephadex C-25 resin, is consistent with the postulated 2+ charge, and the rapid regeneration of the tmpa diol observed upon acidification of 24 confirms that the hydrolysis intermediate is binuclear. Although the blue protonation product of 24 observed in pH 10 and 11 chromatographic separations did not survive long enough to permit a full characterization, the similarity of lowest energy d-d band positions in 22 (17,300 cm^{-1}) and 25 (17,400 cm^{-1}) suggests that the latter is $[(tmpa)(OH)Cr(OH)Cr(OH)(tmpa)]^{3+}$.

Although the rate expression: $k_{obsd} = k_o + k_{OH}[OH^-]$ is common for base hydrolysis reactions of mononuclear Co and Cr complexes with ionizable amine ligands[36], the finding of this rate law for both fast and slow phases of the $[(tmpa)Cr(O)_2Cr(tmpa)]^{2+}$ alkaline

decay reaction does not necessarily imply a corresponding mechanistic similarity, especially considering the absence of ionizable amine protons in the dioxo dimer. Indeed, k_{OH} and k_{OH}^{S} values extrapolated to 25 °C (Table 4) are two to four orders of magnitude smaller than the majority of room temperature Cr(III) complex k_{OH} terms,[36-47] for which more favorable activation entropies on the order of +15-30 eu have been reported.[37,38,43] For example, Cr-O bond-breaking leading to $[(NH_3)_5CrOH]^{2+}$ in the base hydrolysis reaction of $[(NH_3)_5CrONO_2]^{2+}$ at 25 °C is characterized by k_o and k_{OH} values of 2.5×10^{-3} s^{-1} and 1.1×10^{-2} $M^{-1}s^{-1}$ ($\Delta H^{\ddagger}$ = 25.2 kcal/mol, $\Delta S^{\ddagger}$ = +17.0 eu), respectively.[39] With the possible exception of the k_{OH}^{S} term, $\Delta G^{\ddagger}$ values for both OH^--dependent and independent pathways in the decomposition reactions of $[(tmpa)Cr(O)_2Cr(tmpa)]^{2+}$ and 24 are governed predominantly by $\Delta H^{\ddagger}$. Also notable are the relatively minor roles played by the OH^--dependent terms in the base hydrolyses of both the dioxo tmpa dimer and 24, as measured by the ratios k_{OH}/k_o (1.9) and k_{OH}^{S}/k_o^{S} (0.6). By comparison, k_{OH}/k_o values for $[(NH_3)_5CrX]^{2+}$ complexes are much larger and highly sensitive to the leaving group; X = NO_3^- (15) < Cl^- (196) < Br^- (690) < I^- (6900), extrapolated to zero ionic strength.[36]

Rate parameters reported here for the transformation of the tmpa dioxo dimer to $[(tmpa)Cr(OH)CrOCr(OH)(tmpa)]^{2+}$ (k_o path) are strikingly similar to those for the ring opening reactions[48-50] of $[(en)_2Cr(OH)_2Cr(en)_2]^{4+}$ and $[(NH_3)_4Cr(OH)_2Cr(NH_3)_4]^{4+}$ in acidic solution, giving the aqua(hydroxo) mono-ols $[(en)_2(OH)Cr(OH)Cr(H_2O)(en)_2]^{4+}$ and $[(NH_3)_4(OH)Cr(OH)Cr(H_2O)(NH_3)_4]^{4+}$, respectively. Thus, the latter reaction[50] proceeds with a rate constant k_1 (25 °C) of 1.21×10^{-4} s^{-1}($\Delta H^{\ddagger}$ = 20.7 kcal/mol; $\Delta S^{\ddagger}$ = -7 eu), but is reversible ($k_{-1} = 3.80\times10^{-4}$ s^{-1}), unlike tmpa dioxo dimer cleavage in basic solution. Similar rate constants and activation parameters pertain to the analogous reactions of meso[48] and racemic[49] $[(en)_2Cr(OH)_2Cr(en)_2]^{4+}$. Thermodynamic driving force in these diol to aqua(hydroxo) mono-ol conversions is thought to be strongly influenced by hydrogen bonding between

OH^- and H_2O ligands in the bent (Cr-O-Cr) products.[48-50] Although the formula of intermediate 24 is not known with certainty, hydrogen bonding between hydroxo substituents of a similarly bent, oxo-bridged complex ($[(tmpa)(OH)CrOCr(OH)(tmpa)]^{2+}$) could provide part of the thermodynamic motivation for decomposition of the dioxo dimer and the enhanced kinetic stability of the intermediate relative to that of the doubly-bridged reactant. In any case, the vast difference between the UV-visible spectra of 24 and the well-characterized $[(tmpa)(SCN)CrOCr(NCS)(tmpa)]^{2+}$ ion rules out the classification of the base hydrolysis intermediate as a linear, μ-oxo dimer.

μ-Oxo Dimers

Synthesis

Although not completely general, our approach to the synthesis of oxo-bridged chromium(III) dimers through the nucleophilic displacement of a single bridging OH^- group from a diol with aromatic amine ligands has thus far been successful in generating five $[(tmpa)LCrOCrL(tmpa)]^{2+}$ complexes and two dimers derived from the bpy diols.

The stereochemistry of reactant 2 and product 7 provides an important clue to the mechanism of reaction (8). A rearrangement of tmpa pyridyl N donor arms or migration of the bridging oxo function must take place in order for the apical N atoms of 2 that are each trans to a bridging OH^- group to both adopt positions trans to thiocyanate ligands in 7. Figure 15 illustrates the sequence of steps that is thought to occur in the conversion of the tmpa diol to an oxo-bridged product in the presence of thiocyanate ion. The initial Cr-OH bond-breaking step, induced by the first L^- incoming group, is analogous to the well-documented ring opening/closing equilibria of ammonia and ethylenediamine diols.[50,48] In order to achieve the observed product geometry, the remaining bridging oxygen atom must migrate to a cis coordination position concurrent with or prior to nucleophilic attack by the second L^- unit. It is anticipated that rate studies of reaction (8) with various incoming groups will clarify the precise role of this second L^- ion, if any, in promoting the

bridging group migration step and release of H_2O. The mechanistic alternative to oxygen bridge migration, cleavage and re-formation of all four Cr-N bonds on one chromium center, is considered to be highly unlikely.

Stereochemical Considerations

Although X-ray crystallographic structural confirmation is not yet available for any of the other compounds described here, the presence of a linear Cr-O-Cr bridge in 7, 11-16 is clearly revealed by distinctive strong asymmetric Cr-O-Cr stretching[51,52] infrared bands near 850 cm^{-1} in all cases and the close correspondence between calculated and observed elemental analyses. The strong resemblance of UV-visible spectra, protonation characteristics and electrochemical profiles among compounds 7, 11, 12, 13, and 14 (vide infra) further supports their assignment to a common structural class, particularly considering that doubly-bridged and monomeric (tmpa)Cr(III) species exhibit very different physical properties. It should be noted, however, that the physical characterization offered here is not sufficient to prove that all of the L^- donors adopt the trans stereochemistry relative to the Cr-O-Cr axis that is preferred by NCS^-.

Molecular Orbital Model Perspective and Interpretation

The need to formulate the linear MOM unit as an electronically unique moiety, with distinctive properties unexpected for weakly-coupled monomers, is apparent from physical measurements on a variety of binuclear transition metal complexes.[7,10,11,21,53-59] Considering only π-bonding of the M(dπ)-O(pπ)-M(dπ) type, the one-electron molecular orbital scheme proposed originally by Dunitz and Orgel[5] and subsequently applied to the basic rhodo ion by Schmidtke[12] (Figure 1) is a useful starting point in correlating the spectral, magnetic, electrochemical and acid-base properties of oxo-bridged chromium(III) dimers. Considering the Cr-O-Cr unit to define the z coordinate axis in the D_{4h} point group of a $N_5CrOCrN_5$ species, e_u^b and e_u^* bonding and antibonding molecular orbitals,

respectively, are derived from p_x, p_y (O); d_{xz}, d_{yz} (Cr) atomic orbitals. The ordering of approximately non-bonding b_{2g}, b_{1u} (derived from d_{xy}) and e_g ($d_{xz,yz}(1) + d_{xz,yx}(2)$ combinations) levels is not easily defined, being dependent on the magnitudes of the tetragonal crystal field component, M-M d-bonding and π-interactions with non-bridging ligands.[5,12,60,61] Alternative electronic structures[12,62] suggested for $[(NH_3)_5CrOCr(NH_3)_5]^{4+}$ include $(e_u{}^b)^4(e_g)^4(b_{2g})^1(b_{1u})^1$ and $(e_u{}^b)^4(b_{2g})^2(b_{1u})^2(e_g)^2$.

Magnetism and Electronic Spectroscopy

The properties of $[(tmpa)LCrOCrL(tmpa)]^{2+}$ complexes are entirely consistent with the π-molecular orbital model, provided that the predominant electronic structures are $(e_u{}^b)^4(e_g)^4(b_{2g})^2$ (ground state) and $(e_u{}^b)^4(e_g)^4(b_{2g})^1(b_{1u})^1$ (first excited state). The exceptionally large singlet-triplet gaps calculated from the magnetic susceptibilities of 7 and 13 clearly point to diamagnetic ground states for both dimers. By comparison with the most intense electronic spectral features of other MOM complexes,[58,59] the strong, sharp bands of $[(tmpa)LCrOCrL(tmpa)]^{2+}$ ions near 350 nm are most logically assigned to the fully allowed e_g-e_u* ($^1A_{2u} \leftarrow {}^1A_{1g}$) transition, which has the elements of both a Cr-to-Cr and a Cr-to-O charge transfer process. Indeed, the solvent dependence of the 7 electronic spectrum supports the attribution of this most intense feature to a MLCT band linked to the central Cr-O-Cr chromophore. The appearance of a shoulder towards lower energy on the ~350 nm bands is as expected from the lower (approximately C_{2h}) symmetry of the complexes under consideration, which would lift the degeneracy of both the e_g ($b_g + b_g$) and e_u ($b_u + b_u$) molecular orbitals and give rise to several closely-spaced spectral components. The second, less intense band at lower energy in the spectra of 7, 11-14 (398, 417 nm features of 7; peaks or shoulders in the 416-420 and 389-398 nm intervals of all complexes) most likely is the b_{2g}-e_u* ($^1E_u \leftarrow {}^1A_{1g}$) electronic transition.[58,59] In agreement with this perspective on band assignments is the observation that the splittings of

both low and high energy electronic transitions are best resolved, as distinct peaks at 350, 360, 389 and 420 nm, for the dimer which exhibits the largest deviation from D_{4h} symmetry, $[Cl(tmpa)CrOCr(tmpa)Cl]^{2+}$. Finally, it should be noted that the remarkable constancy of the e_g-e_u* band energy among the five $[(tmpa)LCrOCrL(tmpa)]^{2+}$ complexes (28,400 ± 200 cm^{-1} average) agrees with Schmidtke's angular overlap analysis,[12] which expresses the difference in one-electron energies of the e_g and e_u* molecular orbitals ($\Delta E(e_g\text{-}e_u^*)$) according to eq (15), where $e^M{}_{\pi Op}$ and $e_{\pi M}$ represent the M-O-M and M-M π-bonding energies

$$\Delta E(e_g\text{-}e_u^*) = e^M{}_{\pi Op} - 2\,e_{\pi M}, \qquad (15)$$

respectively. Variations in M-O-M π-bonding energy with changing L group should be paralleled by the M-M π-overlap energy, such that $\Delta E(e_g\text{-}e_u^*)$, which is sensitive to the difference between the two π-bonding energies, will be relatively invariant.

Aqua-Dimer Comparisons

In contrast to the electrochemistry of $[(H_2O)_5CrOCr(H_2O)_5]^{4+}$, which exhibits an irreversible, one-electron reduction wave ($E_{1/2}$ = 0.52 versus SHE) and a susceptibility to reductant-catalyzed acid hydrolysis,[19] the $[(tmpa)LCrOCrL(tmpa)]^{2+}$ complexes are characterized by fully reversible, one-electron oxidation waves between 0.96 and 1.17 V versus SHE. In spite of its drastically different ligand field, the aqua dimer nevertheless exhibits prominent near-ultraviolet absorption bands close to those observed for the tmpa oxo-bridged dimers (347 nm, ε 1.0x10^4 $M^{-1}cm^{-1}$/dimer; 413 nm, ε 4.6x10^3 $M^{-1}cm^{-1}$/dimer) plus an additional strong transition at 443 nm (ε 6.0x10^3 $M^{-1}cm^{-1}$/dimer) that is not seen in the tmpa Cr-O-Cr system.[16] In order to reconcile these observations, we propose that the aqua dimer electronic configuration is $(e_u{}^b)^4(b_{2g})^2(b_{1u})^2(e_g)^2$, such that the HOMO's of the tmpa and aqua dimers would be b_{2g} and e_g, respectively. On this

basis, a one-electron reduction of the aqua dimer would generate an e_g^3 configuration that would be subject to Jahn-Teller configurational instability, while one-electron oxidations of the tmpa dimers would leave an $(e_u^b)^4(e_g)^4(b_{2g})^1$ electronic configuration that would not trigger such a distortion. Both complexes should exhibit e_g-e_u* and b_{2g}-e_u* electronic transitions but only the aqua dimer could also have a e_u^b-e_g band, suggesting a possible assignment of its 443 nm feature.

10 Dq, pK_a and $E_{1/2}$ Correlations

As anticipated from a comparison of basic rhodo and acid rhodo chromium dimer spectra[4], the presumably bent[63] $[(tmpa)LCr(OH)CrL(tmpa)]^{3+}$ protonation products of complexes 7, 11-14 are characterized by uv-visible spectra containing only relatively weak d-d bands and, in the case of L = SCN^-, a thiocyanate LMCT transition. Because the d-d bands of the oxo-bridged dimers are not well-resolved, the lowest energy visible transitions of the corresponding hydroxo-bridged complexes may be used to estimate the crystal field parameter 10 Dq. Since π-bonding strength within the Cr-O-Cr structural unit is expected to increase with decreasing ΔE(d-p), the energy difference between overlapping Cr 3d and O 2p orbitals, $e^M_{\pi Op}$ should also become larger with increasing 10 Dq, given that the d_{xz} and d_{yz} orbitals derived from the octahedral t_{2g} set are specifically implicated in Cr-O-Cr π-bonding. Considering that π-bonding strength within a linear, oxo-bridged binuclear complex is not easily assessed by direct measurement, we have probed this important characteristic indirectly through measurements of Cr(OH)Cr complex acid ionization constants. Assuming that the inductive influences of the various L substituents on pK_a are small and that the solvation free energies of the hydroxo-bridged dimers are comparable, pK_a is expected to increase with decreasing π-bonding strength within a $[(tmpa)LCrOCrL(tmpa)]^{2+}$ complex. Looked at from another perspective, a Cr-O-Cr dimer with strong π-bonding will resist protonation, leading to a bent hydroxo-bridged product in which such π-bonding is much weaker or totally absent.

Figure 16 displays correlations of Cr(OH)Cr dimer acid ionization constants and $[(tmpa)LCrOCrL(tmpa)]^{2+/3+}$ oxidation half-wave potentials with 10 Dq, estimated as the energy of the Cr(OH)Cr dimer $^4T_{2g} \leftarrow {}^4A_{2g}$ (O_h) transition. Consistent with expectations from the π molecular orbital model, pK_a values fall off sharply with increasing 10 Dq while $E_{1/2}$ generally follows an increasing trend as the L^- substituent moves from weaker to stronger field within the spectrochemical series. The latter observation follows from the expected enhancement of $E_{1/2}$ with decreasing energy of the redox electron,[64] which is ionized from the b_{2g} (essentially non-bonding d_{xy} (t_{2g})) molecular orbital according to our model. Thus, the relationship of electrochemical potentials to t_{2g} orbital and valence state ionization energies is well-established for monomeric transition metal redox couples.[64] From this perspective, $E_{1/2}$ values of the $[(tmpa)LCrOCrL(tmpa)]^{2+}$ complexes are not expected to correlate with the π-bonding energy of the Cr-O-Cr unit but rather more simply with 10 Dq, which may be expressed in crystal field terms as the energy difference between $d_{x^2-y^2}$ and d_{xy} orbitals (in point group D_{4h}).[12]

It should be noted that the least squares lines in Figure 16 are not intended to imply that linear relationships between pK_a or $E_{1/2}$ values and 10 Dq are anticipated on theoretical grounds. Rather, we are content to establish that quantitative dependences of the dimer physical parameters on 10 Dq do in fact exist and are reasonable on the basis of a molecular orbital description of the Cr-O-Cr bonding. In order to better understand the physical properties of oxo-bridged Cr(III) dimers, it will be necessary to introduce systematic perturbations into the energies of the e_g, b_{2g}, and b_{1u} molecular orbitals, which are not actually non-bonding but may interact with the low-lying π^* levels of phen and bpy aromatic amine ligands, both of which are far better π-acids than the non-conjugated tmpa pyridyl groups.

Base Hydrolysis Mechanism

The isolation of (tmpa)Cr(OH)$_2$Cr(tmpa)$^{4+}$ from acid-quenched solutions of partially base-hydrolyzed (tmpa)(SCN)CrOCr(NCS)(tmpa)$^{2+}$ has significant implications for the mechanism. The excellent agreement between both the peak positions and the molar extinction coefficients for the diol isolated from the acid quenched base hydrolysis reaction with the independently prepared diol 2 makes a strong case for identical geometry (Figure 2). This implies that an oxo-migration similar to that seen in the synthesis of 7 (Figure 15) must take place during the course of base hydrolysis, prior to or during formation of intermediate 24.

The general form for the rate expression (equation 9) found for the base hydrolysis of the three oxo dimers studied is relatively uncommon in the area of chromium(III) base hydrolysis.[36] The vast majority of base hydrolysis processes at chromium and cobalt exhibit simple first order behavior in OH^-. Saturation of k_{obs} with $[OH^-]$ in conjunction with a lack of aliphatic amine protons in (tmpa)LCrOCrL(tmpa)$^{2+}$ cations points to a pathway other than the common conjugate base (D_{cb}) mechanism.[36] The viable pathways that result in this form of the rate law have been summarized previously[65] as dead-end, activated intermediate and intermediate complex. A short summary of the correspondence between fitted parameters from k_{obs}^{-1} versus $[OH^-]^{-1}$ plots and each of these pathways can be found in Table 16. While all three mechanisms are consistent with the saturation behavior of k_{obs} with $[OH^-]$, careful examination of available experimental evidence can provide a degree of discernment among these possibilities.

The Dead-End Complex Mechanism

The dead-end complex mechanism interpretation suffers on many fronts. Indeed, we have found only one instance of a successful defense of this mechanism in the transition metal mechanistic literature.[66] Wilkins[67] has stated that the vast majority of intermediate

complexes in inorganic substitution reactions are active participants in the pathways leading to the final products. Indeed, the concept of a complex containing hydroxide bound to the oxo-dimer in which reactivity is somehow nullified is very difficult to grasp, as L displacement by hydroxide is necessary for the formation of the intermediate $(tmpa)(OH)CrOCr(OH)(tmpa)^{2+}$ (24) found by cation exchange.

In addition, if a dead-end complex were formed with hydroxide, then one might expect other nucleophiles to be capable of forming similar deactivated complexes. However, the nucleophiles SCN^- and Cl^- both appear to have no role other than contributing to the overall ionic strength of the media.

The Activated Intermediate Mechanism

This mechanism involves a reversible activation that results in a species that is succeptible to attack by hydroxide ion. The reaction scheme illustrated below does initially seem to account for the saturation behavior observed.

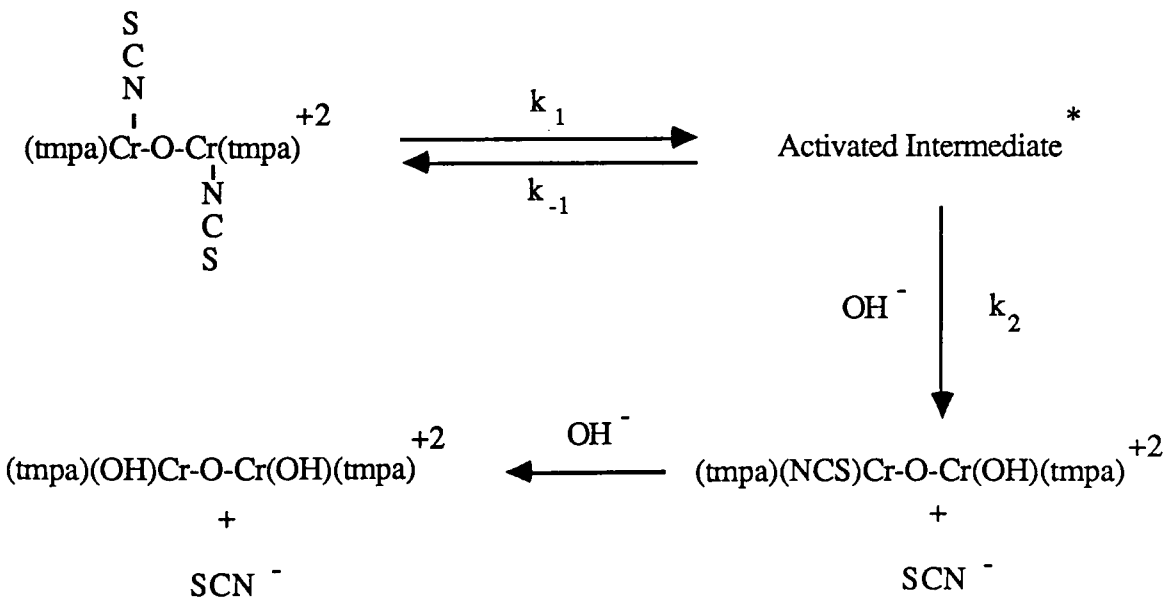

In this scheme, the absorbance from the e_g-e_u* transition is presumed lost with SCN^- displacement in the k_2 step. The asymmetrically substituted dimer would then react with OH^- and subsequently lose SCN^- to give intermediate 24. The A and B parameters in equation (11) correspond to k_1 and k_2/k_{-1} respectively. The invariance in the base hydrolysis rate with [SCN^-] (Table 11) is consistent with an activated intermediate in which thiocyanate departure does not occur. However, an interpretation employing this mechanism does have one major flaw: the lack of a plausible activation step. The difficulty in proposing a mode of activation that would result in a more reactive form is considerable. The incentive for some sort of rearrangement of the tmpa ligand, or an interchange of oxo and thiocyanate coordination positions is not obvious.

The Intermediate Complex Mechanism

In the case of the intermediate complex mechanism, the B parameter of equation (11) corresponds to Q_p, the formation constant of the dimer with hydroxide ion, and the A parameter corresponds to the k_2 term, as illustrated in the following diagram.

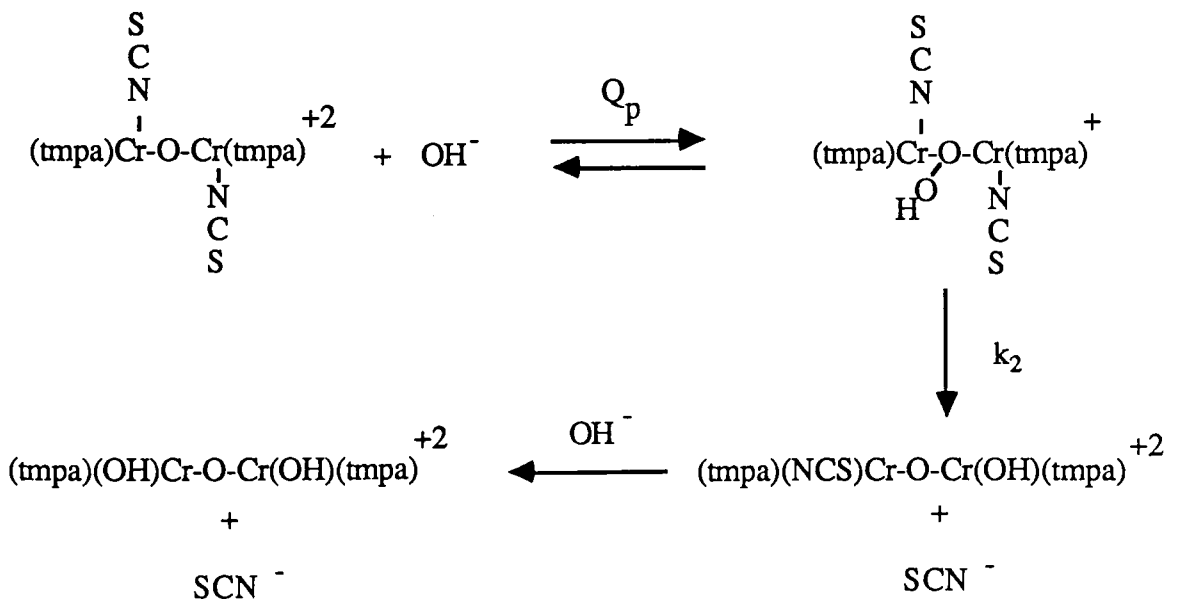

As with the activated intermediate mechanism, the absorbance from the e_g-e_u* transition is presumed lost in the k_2 step. The lack of a significant dependence of the base hydrolysis rate on [SCN^-] suggests an intermediate complex that contains both thiocyanate and weakly bound OH^- ions. However, unlike the activated intermediate mechanism, there exists a very plausible explanation for intermediate complex formation. Hydroxide ion could interact with the oxo-dimer b_{1u} LUMO (Figure 1) through a lone pair on oxygen.

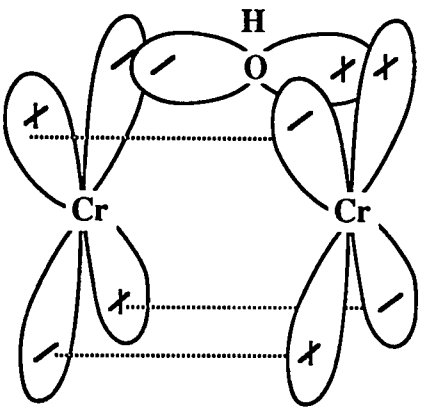

A series of steps consistent with the (tmpa)(SCN)CrOCr(NCS)(tmpa)$^{2+}$ quenched base hydrolysis product separation results, rate law and this mechanism are:

(a) Formation of the intermediate complex from the oxo dimer and OH^-.

(b) Reaction of weakly bound OH^- with the oxo bridge to cause both 90° bridge migration and displacement of one thiocyanate ligand in the k_2 step, forming an asymmetrically substituted oxo dimer (26).

(c) Reaction of 26 with OH^- to form the isolated intermediate 24.

(d) Reaction of intermediate 24 with water to form two equivalents of 22.

In addition, if proposed intermediate 26 ring-closes in acidic solution to give diol and free SCN^-, an explanation for 32% of the diol isolated in the acid quenched base hydrolysis reactions over the 10% expected from 24 is made clear. This would also imply that 26 is oxo-migrated with respect to the oxo dimer.

The similarities in k_2 (Table 12) for L = NCS^-, CN^-, and NCO^- is surprising. The differences in the actual rates are due almost entirely to Q_p. The invariance in k_2 can be attributed to rate-determining OH^--induced oxo-migration that displaces one L group in the intermediate complex, with rate differences due to a larger concentration (larger Q_p) of the reactive intermediate complex in solution. As further evidence for this pathway, the ΔH^o value of 4.6 ± 2 kcal/mol is reminiscent of the low standard enthalpy seen for displacement of H_2O by N_3^- in $Cu(dien)(H_2O)^{2+}$ (-2.2 kcal/mol) and $Cu(terpy)(H_2O)^{2+}$ (-2.9 kcal/mol).[68] However, the ΔS^o value of 21 ± 5 eu is much larger than those seen for these copper complexes ($\Delta S^o \approx 0$ eu).[68] The entropy driven nature of hydroxide binding to the oxo dimer is not surprising when one considers the extent of solvation of free hydroxide in water and the probable antibonding character of the b_{1u} molecular orbital.

The overall internal consistency of the intermediate complex pathway is even more appealing when one considers that the interaction inherent in step (a) results in the placement of hydroxide near the center of the dimer, where it is in striking distance of the oxo bridge. Indeed, the presence of an oxo-migration in the formation reaction (departure of hydroxide) and "reverse reaction" during base hydrolysis (attack of hydroxide) indicates that such an interaction may play a role in the fundamental steps of both processes.

Another mechanism that must be considered was postulated by Tobe[36] to account for a sizeable increase in the rate of base hydrolysis of some aromatic amine-containing cobalt complexes. In this mechanism, hydroxide does not attack chromium, but rather a carbon adjacent to the pyridine nitrogen, affording an amide nitrogen which labilizes the trans leaving group. We have isolated no product containing a phenolic group adjacent to the nitrogen from any reaction involving Cr(III)(tmpa) complexes in basic solution. Indeed, complex 20 was prepared both in acidic and basic solutions. Further evidence for interaction of a hydroxide lone pair with b_{1u} over this kind of modified D_{cb} mechanism is found when one considers that the $(tmpa)Cr(NCS)_2^+$ monomer does not exhibit saturation

behavior in hydroxide despite the availability of three pyridine rings, one of which must be trans to a thiocyanate ligand.

Oxo-, Carboxylate-Bridged Dimers

Molecular Orbital Derivation

If a relatively small degree of bending along the x axis is treated as a perturbation on the Schmidtke molecular orbital model[12], one can obtain the diagram (Figure 17) in which d-p-d π overlap still exists. Figure 18 illustrates the overlaps involved along with their symmetry. The anticipated energy increase in the a_{1g} and a_{2u} levels follows from the decrease in overlap that occurs after bending. The e_u splitting demanded by lowering to pseudo C_{2v} symmetry can be viewed as $a_1$overlap (yz plane) being reduced much more drastically than b_1 (xz plane). The very small splitting predicted in e_g, and lack of movement in the b_{2g}, b_{1u} sets is linked to their nonbonding nature. The slight energy lowering of a_{1g}* and a_{2u}*, lack of movement in b_{1g}, b_{2u} and splitting of e_u* follow by analogy.

Electronic Spectroscopy

In the UV-visible spectra of the three oxo-carboxylate-bridged dimers the appearance of two transitions at 29,800 cm^{-1} (336 nm) and 27,000 cm^{-1} (371 nm) rather than a single strong MLCT band at 28,400 cm^{-1} (an averaged band energy for 7,11-14) as seen for the linear oxo-dimers is more than circumstantial. The symmetry allowed transitions (Table 17) derived under C_{2v} show that both b_2-a_1 (lower energy) and a_2-b_1 (higher energy) transitions are y polarized. It is interesting to note that the energy difference between the b_2-a_1 and e_g-e_u* transitions is the same (1,400 cm^{-1}) as the energy difference between the a_2-$b_1$and e_g-e_u* transitions. Indeed, this is good evidence for symmetric splitting of the π-antibonding e_u* set in D_{4h} into b_1 and a_1 under C_{2v}. Although a similar splitting should be seen in the b_{2g}-e_u* transition, none is observed. However, in the model

proposed, no attempt was made to account for the energetics of electron pairing, which would play a larger role in electronic transitions originating from molecular orbitals with similar one-electron energies.

The UV-visible spectrum of the (tmpa)Cr(OH)(RCOO)Cr(tmpa)$^{4+}$ species show only two well resolved d-d transitions in the range of 508-512 and 382-386 nm, lacking the more intense features seen in the oxo forms. The d-d transition positions are reminiscent of (tmpa)Cr(H_2O)$_2^{3+}$, which has maxima at 375 and 501 nm. This similarity is consistent with the appearance of the carboxylates near water in the spectrochemical series.

pK_a Correlations

It was found empirically that a plot of pK_a for the free acid versus the pK_a of bridging hydroxide in the (tmpa)Cr(OH)(RCOO)Cr(tmpa)$^{4+}$ (R = H, CH_3, C_6H_5) cations (Figure 19) forms a very good line, showing that an increase in the basicity of the carboxylate anion is reflected in enhanced bridging oxo group basicity. An increase in bond strength between chromium and the oxygens of the more basic $RCOO^-$ group should occur at the sacrifice of bonding between chromium and bridging oxygen. This would result in a dimer with weaker d-p-d π bonding. The decrese in stability of the oxo form would manifest itself in a higher pK_a of the conjugate acid.

Electrochemistry

The reversible one-electron oxidation of complexes 17-19 seen in acetonitrile is consistent with the molecular orbital scheme proposed for these dimers (Figures 17,18). The energy of the b_{2g} and b_{1u} molecular orbitals (under D_{4h}) should not change drastically upon lowering the symmetry (b_1 and a_2 under C_{2v}) due to their nonbonding nature. The potential range (1.17-1.22 V) seen for these dimers is remarkably similar to the one-electron oxidation potentials of 7,11-14 under the same conditions. This is consistent with electron removal from the b_1 molecular orbital, the C_{2v} counterpart of b_{2g}

(D_{4h}). Apparently the ground state electronic configuration of these dimers is $(a_1)^2(b_2)^2(a_1)^2(b_1)^2(b_2)^2(a_2)^2(b_1)^2$, which parallels the electronic configuration $(a_{1g})^2(a_{2u})^2(e_u)^4(e_g)^4(b_{2g})^2$ proposed for the linear oxo-bridged dimers.

Formation Kinetics of $[(tmpa)Cr(O)(CH_3COO)Cr(tmpa)]^{3+}$

The simple first order relationship in both 4 and acetate implies a straight forward mechanism for the replacemnt of OH^- by CH_3COO^-. It is unlikely that an oxo-migration similar to that seen in the formation of the linear oxo-dimers applies here as well. Although structural confirmation of the arrangement of the tmpa ligands with respect to the bridges has not yet been achieved, the following observations provide a rationale for the stereochemistry. If the final product involved oxo-migration, and if the oxo-migration was the rate determining step, then the formation of 17 should have been zeroth order in acetate. Indeed, if cleavage of one Cr-OH bond by acetate is the first step in the mechanism, then one would expect that bridge closure to displace OH^- altogether from the complex would be the next logical step. It is difficult to envision a necessity for oxo migration when both the starting and ending dimers are doubly-bridged. Finally, the reaction proceeds faster (at room temperature in acetonitrile) than formation of 7 (at least one hour in boiling water). This indicates that the activation barriers are very different in these reactions.

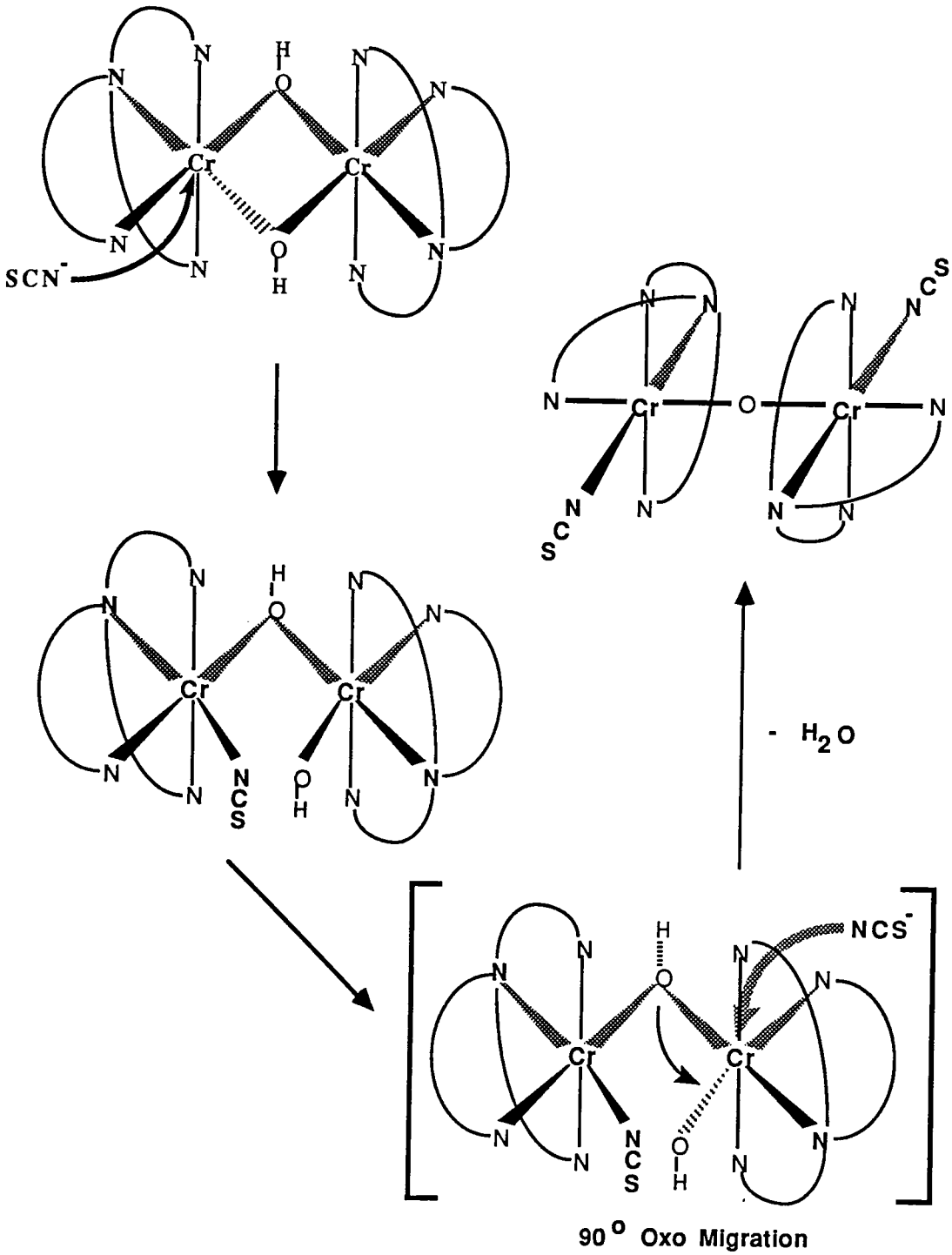

Figure 15. Proposed oxo-bridge migration mechanism for [(tmpa)(SCN)CrOCr-(NCS)(tmpa)]$^{2+}$ formation.

Table 16

Rate Parameters Obtained From k_{obs}^{-1} versus $[OH^-]^{-1}$ Plots for Several $[OH^-]$ Saturation Mechanisms

Mechanism	1 / Intercept (A)	Intercept / Slope (B)
Intermediate Complex	k_2	Q_p
Activated Intermediate	k_1	k_2 / k_{-1}
Dead End Complex	k_2 / Q_d	Q_d

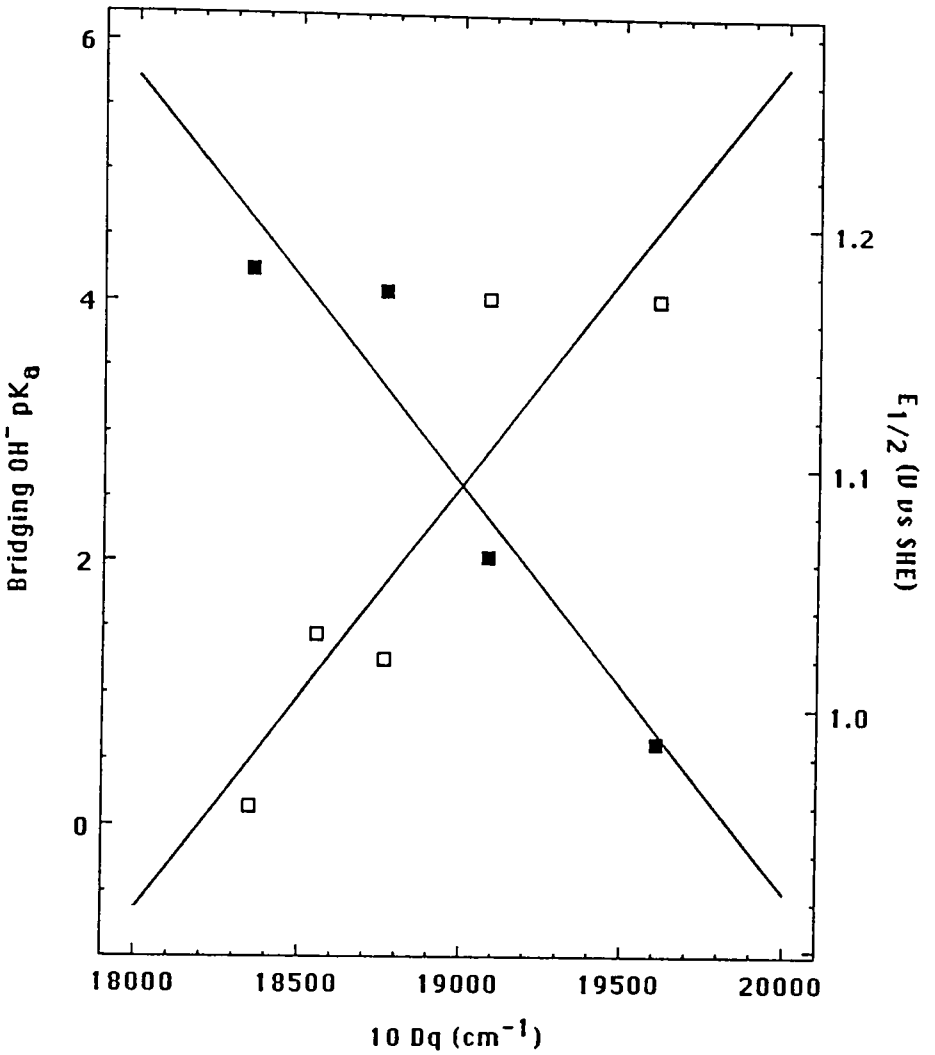

Figure 16. Correlation of $[(tmpa)LCr(OH)CrL(tmpa)]^{3+}$ pK_a values (■, left hand axis) and $[(tmpa)LCrOCrL(tmpa)]^{2+}$ oxidation $E_{1/2}$ values (□, right hand axis) with 10 Dq for the hydroxo-bridged dimers. Solid lines represent linear least squares fits. Since 10 Dq for $[(tmpa)ClCr(OH)CrCl(tmpa)]^{3+}$ could not be measured directly (decomposition to 2 in aqueous solution), the value for $[Cr(tmpa)Cl_2]^{+}$ (18,550 cm^{-1}) is used as an approximation in the $E_{1/2}$ correlation.

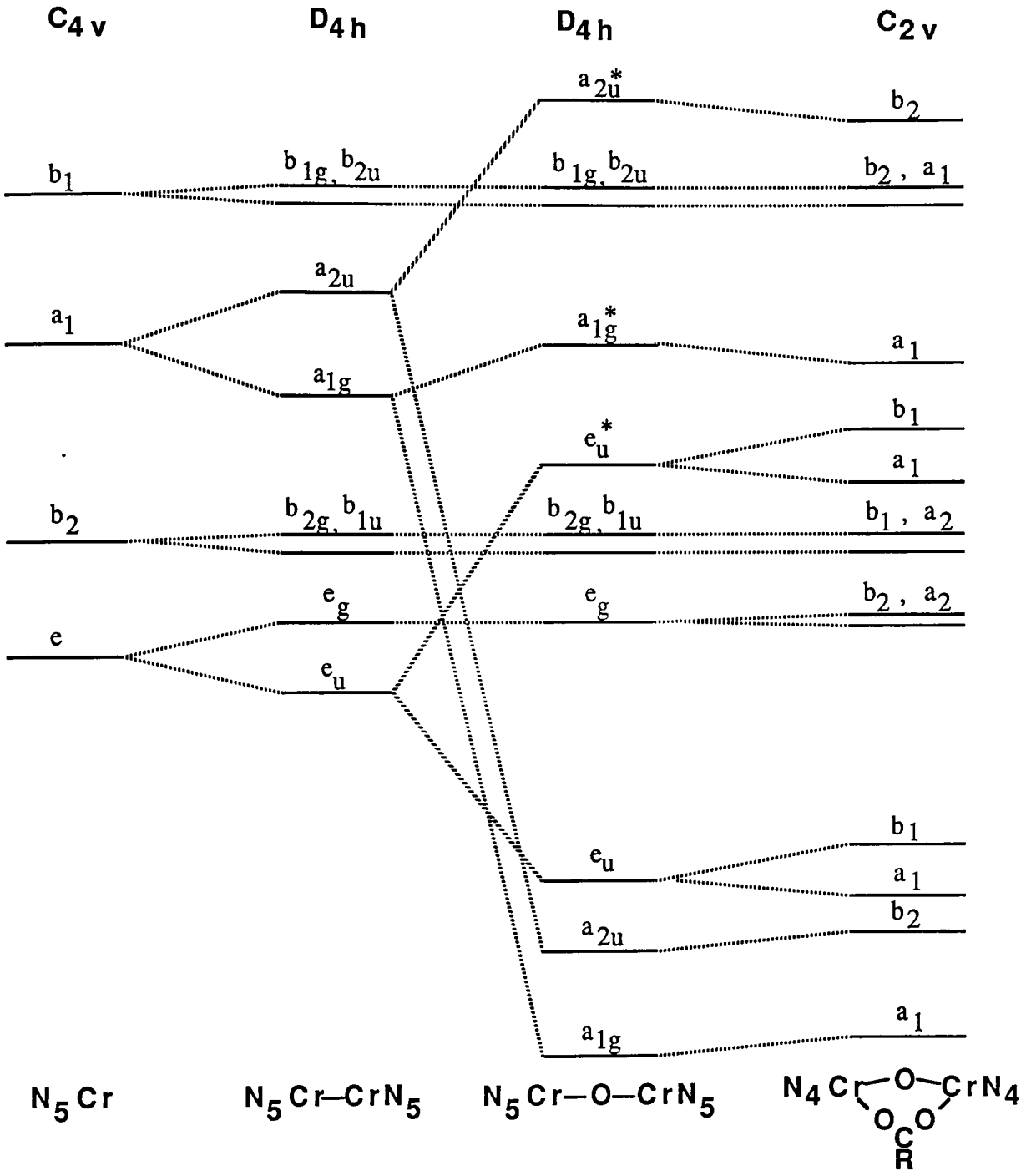

Figure 17. Molecular orbital diagram for the oxo-, carboxylato-bridged dimers with relation to the Schmidtke molecular orbital diagram[12].

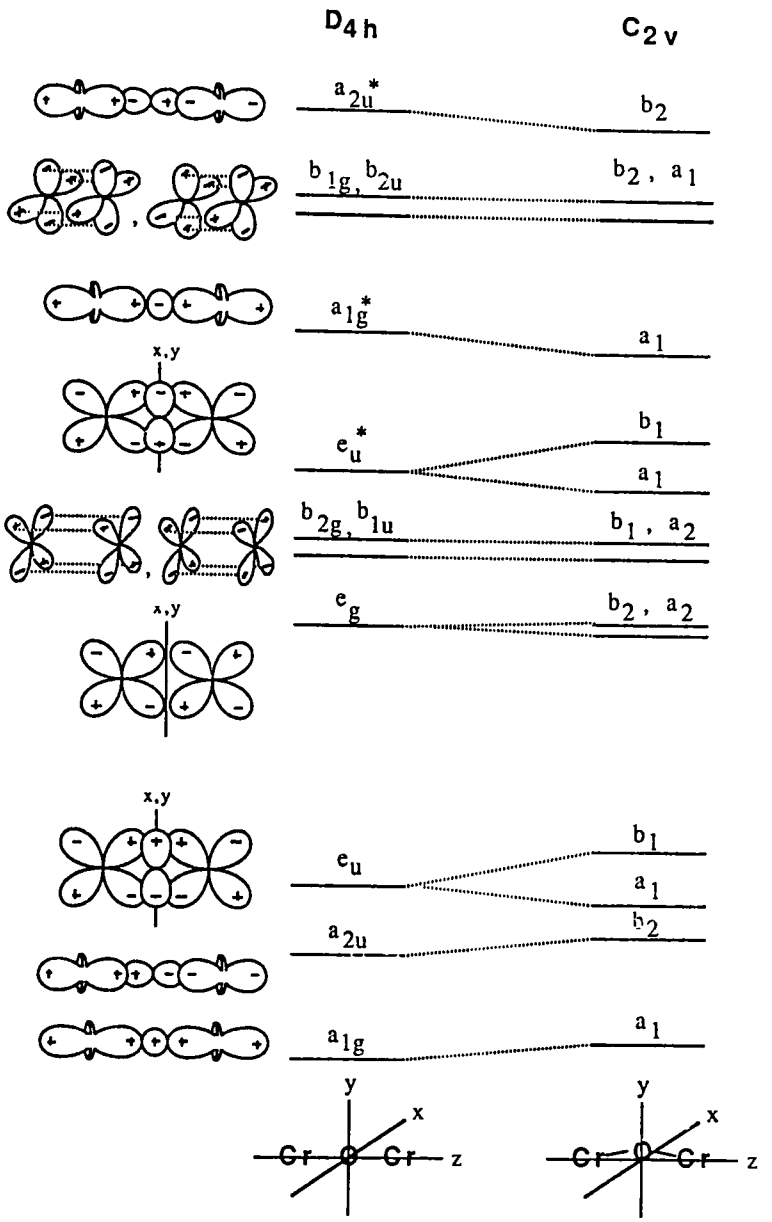

Figure 18. Oxo-,carboxylato-bridged dimer molecular orbital model with orbital overlap illustrations. Bending along the x axis removes the degeneracy of e_g and e_u.

Table 17

Symmetry Allowed Transitions for the Oxo-,Carboxylato-Bridged Dimers [a]

Point Group C_{2v}		
X Polarized	Y Polarized	Z Polarized
a_1-b_1	a_1-b_2	a_1-a_1
b_1-a_1	**a_2-b_1**	**a_2-a_2**
a_2-b_2	b_1-a_2	b_1-b_1
b_2-a_2	**b_2-a_1**	b_2-b_2

[a] Bolded entries show transitions from an occupied (essentially nonbonding) molecular orbital to an unoccupied (a_1, b_1 or a_2) molecular orbital (Figures 17,18).

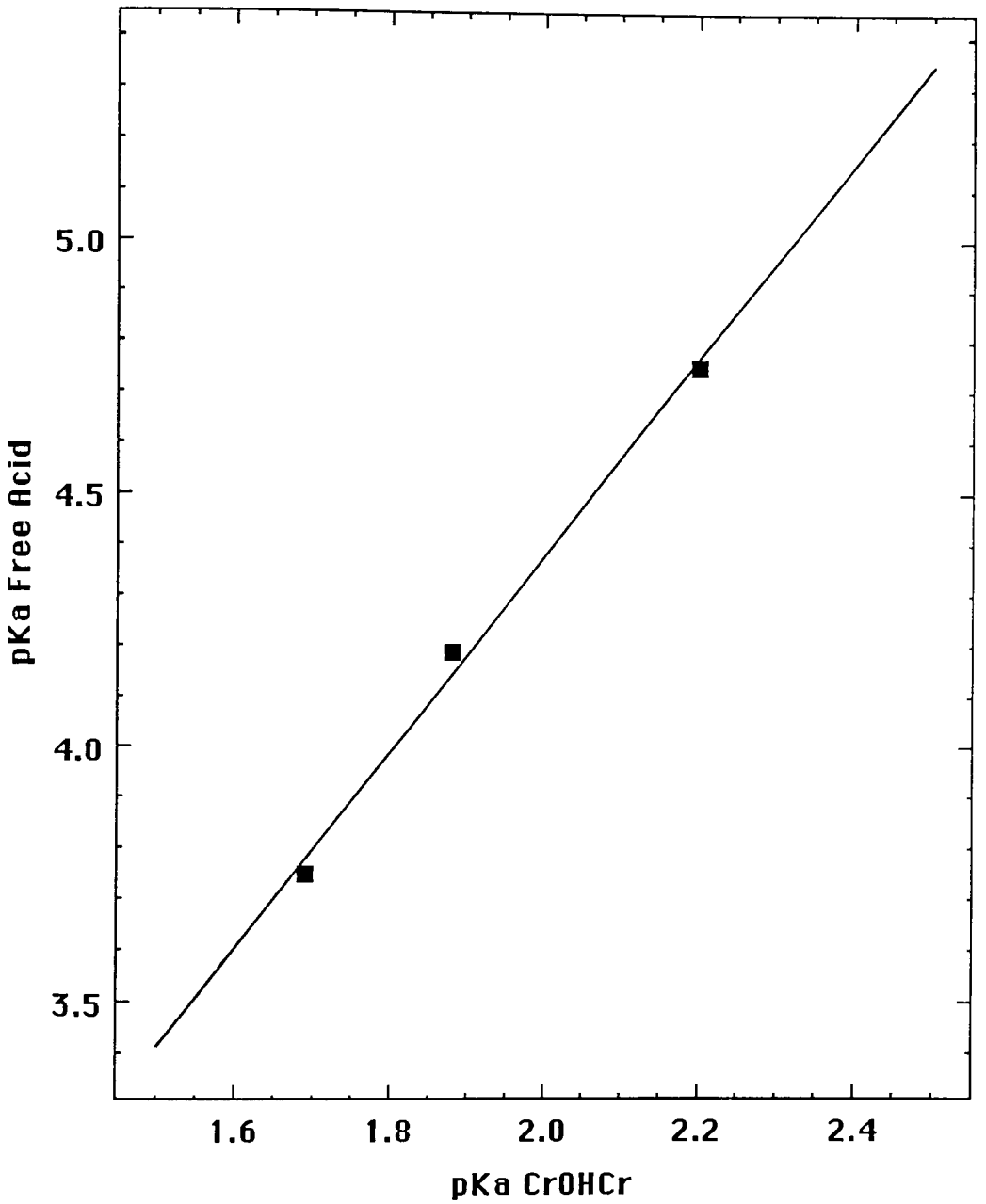

Figure 19. Plot of pK_a of bridging hydroxide in $[(tmpa)Cr(OH)(RCOO)Cr(tmpa)]^{4+}$ (R = H, C_6H_5 and CH_3) versus free acid pK_a.

REFERENCES

1 Jorgensen, S. J. *J. Prakt. Chem.* **1882**, *25*, 321.

2 Schwarzenbach, G.; Magyar, B. *Helv. Chim. Acta* **1962**, *45*, 1425.

3 Earley, J. E.; Cannon, R. D. *Transition Met. Chem* (N.Y.) **1965**, *1*, 33.

4 Dubicki, L.; Martin, R. L. Aust. J. Chem. **1970**, *23*, 215.

5 Dunitz, J. D.; Orgel, L. E. *J. Chem. Soc.* **1953**, 2594.

6 Pedersen, E. *Acta. Chem. Scand.* **1972**, *26*, 333.

7 Glerup, J. *Acta Chem. Scand.* **1972**, *26*, 3775.

8 Gudel, H. U.; Dubicki, L. *Chem. Phys.* **1974**, *6*, 272.

9 Kahn, O.; Briat, B. *J. Chem. Soc., Faraday Trans.* 2 **1976**, *72*, 268.

10 Baumann, J.; Meyer, T. J. *Inorg. Chem.* **1980**, *19*, 345.

11 Weaver, T. R.; Meyer, T. J.; Adeyami, S. A.; Brown, G. M.; Eckberg, R. P.; Hatfield, W.E.; Johnson, E. C.; Murray, R.W.; Unterecker, D. *J. Am. Chem. Soc.* **1975**, *97*, 3039.

12 Schmidtke, H. H. *Theor. Chim. Acta* **1971**, *20*, 92.

13 Wilmarth, W. K.; Graff, H.; Gustin, S. T. *J. Am. Chem. Soc* . **1956**, *78*, 2683.

14 Hoppenjans, D. W.; Hunt, J. B. *Inorg. Chem.* **1969**, *8*, 505.

15 Gafford, B. G.; Holwerda, R. A. *Inorg. Chem.* **1988**, *27*, 210.

16 Holwerda, R. A.; Petersen, J. S. *Inorg. Chem.* **1980**, *19*, 1775.

17 Johnston, R. J.; Holwerda, R. A. *Inorg. Chem.* **1983**, *22*, 2942.

18 Johnston, R. J.; Holwerda, R. A. *Inorg. Chem.* **1985**, *24*, 3181.

19 Johnston, R. J.; Holwerda, R. A. *Inorg. Chem.* **1985**, *24*, 3176.

20 Yevitz, M.; Stanko, J. A. *J. Am. Chem. Soc.* **1971**, *93*, 1512.

21 DiVaira, M.; Mani, F. *Inorg. Chem.* **1984**, *23*, 409.

22 Anderegg, G.; Wenk, F. *Helv. Chim. Acta* **1971**, *51*, 224.

23 Holwerda, R. A.; Clemmer, J. D. *Inorg. Chem.* **1982**, *21*, 2103.

24 Baek, H. B.; Holwerda, R. A. *Inorg. Chem.* **1983**, *22*, 3452.

25 Szentrimay, R.; Yeh, P.; Kuwana, T. In "Electrochemical Studies of Biological Systems"; Sawyer, D. T., Ed.; American Chemical Society: Washington, DC, **1977**; ACS Symp. Ser. No. 38, 143.

26 Espenson, J. H. *Chemical Kinetics and Reaction Mechanisms* ; McGraw-Hill: New York, **1981**.

27 O'Connor, C. J. *Prog. Inorg. Chem.* **1982**, *29*, 203.

28 Josephson, J.; Schaffer, E. *Acta Chem. Scand., Ser. A* **1970**, *24*, 2929.

29 Hodgson, D. J.; Zietlow, M. H.; Pedersen, E.; Toftlund, H. *Inorg. Chim. Acta* **1988**, *149*, 111.

30 Larsen, S.; Michelson, K.; Pedersen, E. *Acta Chem. Scand., Ser. A* **1986**, *40*, 63.

31 Spiccia, L.; Stoeckli-Evans, W.; Marty, W.; Giovanoli, R. *Inorg. Chem.* **1987**, *26*, 474.

32 Hodgson, D. In *Magneto-Structural Correlations in Exchange Coupled Systems* ; Willett, R. D., Ed.; Reidel:Dordrecht, **1985**, p. 497.

33 Kober, E. M.; Sullivan, B. P.; Meyer, T. J. *Inorg. Chem.* **1984**, *23*, 2098.

34 Springborg, J.; Toftlund, H. *Acta Chemica Scandinavica*, A, **1979**,*33*, 31.

35 Josephson, J.; Pedersen, E. *Inorg. Chem.* **1977**, *16*, 2534.

36 Tobe, M. L. *Adv. Inorg. Bioinorg. Mech.* **1983**, *2*, 1.

37 Parris, M.; Wallace, W. J. *Can. J. Chem.* **1969**, *47*, 2257.

38 Guastalla, G.; Swaddle, T. W. *Can. J. Chem.* **1974**, *52*, 527.

39 Campi, E.; Ferguson, J.; Tobe, M. L. *Inorg. Chem.* **1970**, *9*, 1781.

40 Lichtig, J.; Tobe, M. L. *Inorg. Chem.* **1978**, *17*, 2442.

41 Levine, M. A.; Jones, T. P.; Harris, W.E.; Wallace, W. J. *J. Am. Chem. Soc.* **1961**, *83*, 2453.

42 Pearson, R. G.; Munson, R. A.; Basolo, F. *J. Am. Chem. Soc.* **1958**, *80*, 504.

43 Yang, D.; House, D. A. *Inorg. Chem.* **1982**, *21*, 2999.

44 Dawson, B. S.; House, D. A. *Inorg. Chem.* **1977**, *16*, 1354.

45 House, D. A. *Coord. Chem. Rev.* **1977**, *23*, 223.

46 House, D. A. *Inorg. Chem.* **1988**, *27*, 2587.

47 Olsen, D. C.; Garner, C. S.*Inorg. Chem.* **1963**, *2*, 558.

48 Springborg, J.; Toftlund, H. *Acta Chem. Scand., Ser. A* **1976**, *30*, 171.

49 Christensson, F.; Springborg, J.; Toftlund, H. *Acta Chem. Scand., Ser. A* **1980**, *34*, 317.

50 Christensson, F.; Springborg, J. *Acta Chem. Scand., Ser. A* **1982**, *36*, 21.

51 Hewkin, D; Griffith, W. *J. Chem. Soc. A* **1966**, 472.

52 Nakamoto, K. *Infrared Spectra of Inorganic and Coordination Compounds*, 2nd ed.; Wiley: New York, **1970**.

53 Cotton, F. A.; Najjar, R. C. *Inorg. Chem.* **1981**, *20*, 1866.

54 Chakravarty, A. K.; Cotton, F. A. *Inorg. Chem.* **1984**, *23*, 409.

55 Gilbert, J. A.; Eggleston, D. S.; Murphy, W. R.; Geselowitz, D. A.; Gersten, S. W.; Hodgson, D. J.; Meyer, T. J. *J. Am. Chem. Soc.* **1985**, *107*, 3855.

56 Doppelt, P.; Meyer, T. J. *Inorg. Chem.* **1987**, *26*, 2027.

57 Schugar, H. J.; Rossman, G. R.; Barraclough, C. G.; Gray, H. B. *J. Am.Chem.Soc.* **1972**, *94*, 2683.

58 Campbell, J. R.; Clark, R. J. H. *Mol. Phys.* **1978**, *36*, 1133.

59 Campbell, J. R.; Clark, R. J. H. *J. Chem. Soc. Faraday II* **1980**, *76*, 1103.

60 Jezowska-Trzebiatowska, B. *Pure Appl. Chem.* **1971**, *27*, 89.

61 Mealli, C.; Sacconi, L. *Inorg. Chem.* **1982**, *21*, 2870.

62 Earnshaw, A.; Lewis, J. *J. Chem. Soc.* **1961**, 396.

63 Veal, J. T.; Jeter, D. Y.; Hempel, J. C.; Eckberg, R. P.; Hatfield, W. E.; Hodgson, D. J. *Inorg. Chem.* **1973**, *12*, 2928.

64 van Gaal, H. L. M.; van der Linden, J. G. M. *Coord. Chem. Rev.* **1982**, *47*, 41.

65 Yoneda, G.S.; Holwerda, R.A. *Bioinorg. Chem.* **1978**, *8*, 139.

66 Wilkins, R.G.; "The Study of Kinetics and Mechanism of Reactions of Transition Metal Complexes," Allyn and Bacon, Inc., Boston, **1974**, 181.

67 Haim, A.; *J. Am. Chem. Soc.* **1961**, *83*, 509.

68 Holwerda, R. A.; Stevens, G.; Anderson, C.; Wynn, M. *Biochemistry* **1982**, *21*, 4403.